Optique quantique avec des atomes artificiels semiconducteurs

Daniel Valente

UNIVERSITÉ DE GRENOBLE

THÈSE

Pour obtenir le grade de

DOCTEUR DE L'UNIVERSITÉ DE GRENOBLE

Spécialité : **Physique/Nanophysique**

Arrêté ministériel : 7 août 2006

Présentée par

Daniel VALENTE

Thèse dirigée par **Alexia AUFFÈVES**
et codirigée par **Jean-Philippe POIZAT**

préparée au sein de **l'Institut Néel, CNRS**
dans **l'École Doctorale de Physique**

Quantum Optics with Semiconducting Artificial Atoms

Thèse soutenue publiquement le **15 Octobre 2012**,
devant le jury composé de :

Pr. Frank HEKKING
Professeur a l'Université Joseph Fourier, Président
Pr. Dario GERACE
Chercheur au Dipartimento di Fisica «A. Volta» de l'Università degli Studi di Pavia, Rapporteur
Dr. Karim MURR
Chercheur au LENS de l'Università di Firenze, Rapporteur
Dr. Pascale SENELLART
Directrice de Recherche CNRS au Laboratoire de Physique des Nanostructures, Examinateur
Pr. Marcelo SANTOS
Professeur au Departamento de Física de l'Universidade Federal de Minas Gerais , Examinateur
Dr. Alexia AUFFÈVES
Chargé de Recherche CNRS à l'Institut Néel, Directrice de thèse
Dr. Jean-Philippe POIZAT
Directeur de Recherche CNRS à l'Institut Néel, Co-Directeur de thèse

Université Joseph Fourier / Université Pierre Mendès France /
Université Stendhal / Université de Savoie / Grenoble INP

Acknowledgements

Abstract

The thesis focuses on quantum optical effects in semiconducting artificial atoms. We first investigate theoretically a single emitter coupled to a one-dimensional waveguide. This system allows for light propagation while preserving sensitivity at the single-photon level, which has motivated proposals for quantum gates and single-photon transistors. A scheme to monitor stimulated emission at the single-photon level in this one-dimensional open space is proposed, using an excited emitter (e.g. a quantum dot) and a classical pump (laser). We show that light is emitted in the stimulating mode and that the atom performs classical Rabi oscillation. The fully quantum dynamics is also explored, where a single-photon packet interacts with an initially excited emitter. In contrast with the case of a classical pump, stimulation by a single photon is irreversible, i.e., no oscillation takes place. Stimulation is optimal for a packet three times shorter than the spontaneously emitted one. We show how this optimal irreversible stimulated emission can be applied to perform universal quantum cloning. The same device provides either optimal quantum cloning or maximally entangled photon pairs, depending only on the size of the incoming packet.

In the second part of the thesis, we investigate the spontaneous emission spectrum of a semiconducting quantum dot weakly coupled to a microcavity. In particular, we address the problem of cavity feeding, where the quantum dot spontaneously emits photons at the frequency of an off-resonance cavity. The influence of phonons in the cavity feeding mechanism is analysed. An important distortion of the apparent cavity peak induced by the presence of phonons is demonstrated. These effects are topical and can be implemented in state-of-the-art semiconducting devices.

Contents

Introduction

Photons and atoms

"I am incessantly busy with the question of radiation... This quantum question is so uncommonly important and difficult that it should concern everyone." (Letter from Einstein to Laub, 1908) [1].

The concept of light has radically changed since the beginning of the last century. This change starts with the revolutionary work by Planck [2] on the spectrum of blackbody radiation, where the concept of quantum of energy is introduced. Further development of this idea is made by Einstein, who derives from Planck's law the energy fluctuation of blackbody radiation [3], displaying the wave-particle duality, or complementarity, of light.

In his theory of light-matter interaction, Einstein rederives Planck's law from three basic components: spontaneous emission, absorption and stimulated emission of radiation [4]. A series of practical developments is made, based on the concept of amplification through stimulated emission. This culminates in the work by Maiman [5], which brings about a second revolution in the concept of light. Lasers work in a regime that is far from thermal equilibrium, so the statistical distribution it generates is markedly different from Planck's law. A proper theoretical framework to describe both the quantum statistics and the optical coherence of a laser field is developed mainly by Glauber, Sudarshan

[6, 7, 8, 9] and Mandel [10].

The modern perspective put forward by Glauber allowed the demonstration of non-classical behaviour of light in the resonant fluorescence of an atom. Two-photon correlation measurements evidenced the phenomenon of antibunching, where two successive photon clicks are separated by a time delay corresponding to the natural re-excitation period of the atom [11, 12, 13].

Single photon and single atom in a cavity

At the beginning of the 70's, quantum optics started challenging traditional ideas of quantum physicists, as pointed out by E. Schrödinger: "We never experiment with just one electron or atom or (small) molecule. In thought-experiments we sometimes assume that we do; this invariably entails ridiculous consequences...", British Journal of the Philosophy of Sciences, 3, 1952 [14].

Quantum optics is greatly developed within the field of cavity quantum electrodynamics, 'CQED'. The aim in this field is to study how the radiative properties of atoms are modified when they radiate close to boundaries. A pioneering work in CQED is made by Purcell [15], which shows a change in the spontaneous emission rate of a dipole due to the presence of a resonant cavity. CQED is also at the heart of the development of lasers [5, 16, 17, 18].

Research in CQED offers the possibility to perform experiments with a single atom and a single photon [14]. In the group of Serge Haroche, for instance, huge atomic dipoles are obtained by preparing the atoms in very excited Rydberg states. Mirrors of huge reflectivity are constructed. In the case of microwave light, for instance, mirrors are made of highly reflecting superconducting material. Innovative experiments reveal the field graininess and reproduce thought-experiments dating from the foundations of quantum mechanics.

Semiconducting artificial atom in a solid-state environment

Nowadays, quantum optics and condensed matter physics are converging, creating a field called "solid-state CQED". From the perspective of fundamental research, understanding the influence of the environment on a quantum system is still a timely task. In solid-state CQED, novel engineered electromagnetic environments are obtained. Besides, the solid-state reservoir itself can modify the dynamics of the emitter. It establishes connections with the field of open quantum systems, where the influence of the environment on energy dissipation and coherence loss of a quantum system is investigated [19, 20]. Open quantum systems can have their quantum correlations and coherences either suppressed or mediated by the environment [21, 22, 23, 24], properties that can be exploited for quantum information processing. From the perspective of applications, solid-state devices are promising systems for quantum information processing, as an appreciable ensemble of them can be fabricated on a chip [25, 26]. The control of the environment is a fundamental step towards practical realizations of quantum information protocols.

In nanophotonics, a quantum dot (QD) plays the role of single emitter. By confining charges in all three directions at the nanometer scale, it creates discrete bound states, providing sharp optical transitions. Quantum dots are thus recognized as artificial atoms. In Fig.1 (a) (resp b), InAs quantum dots are placed randomly (resp. organized) in a GaAs matrix. Fig.1 (c) shows photoluminescence of a single QD [27, 28].

Solid-state microcavities are of two types. Photonic crystal planar cavities, Fig.2, are built by construction of a hole pattern in the semiconducting material [27]. Micropillar cavities, Fig.3, are Bragg mirrors built from a series of layers of contrasting index refraction [27, 28, 29]. Recently, an outstanding application of microcavities has been obtained to perform subpicosecond optical switches [30, 31].

Recently, another engineered solid-state reservoir has been fabricated, namely, a photonic nanowire. A photonic wire is a waveguide that is made of a high refractive index material, and which is surrounded by a low index cladding (air or vacuum). The large contrast in refractive index between the material and the cladding leads to two effects:
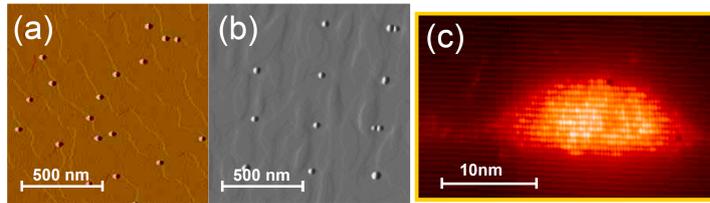
Figure 1: (a) InAs QDs placed randomly. (b) Organized pattern of InAs QDs. (c) Photoluminescence of a single QD.
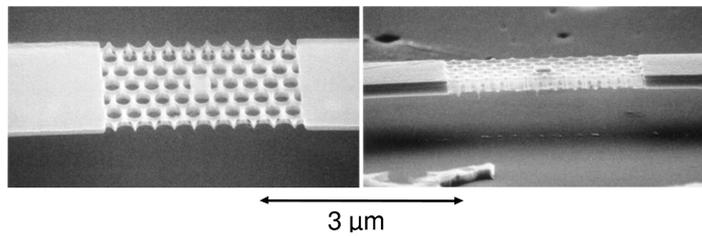
Figure 2: Planar photonic crystal cavity.
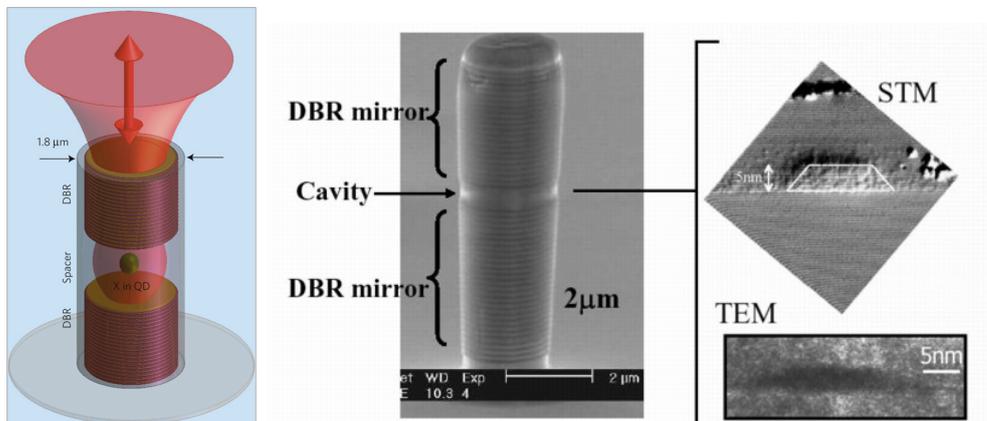
Figure 3: Micropillar cavity.

first, the guided mode is confined very tightly in the structure, allowing a good coupling to the embedded emitter. Second, a dielectric screening effect inhibits the coupling to the continuum of 'leaky' modes. These two effects result in an efficient control of sponta-

neous emission, that is maintained over a large operation bandwidth. These waveguides preserve the single-photon sensitivity of the single emitter, yet for propagating photons, opening novel perspectives. For instance, it is possible to control correlation in photon pairs and realize photon blockade effect [32].

Photonic wires have recently been used to realize an ultrabright on-demand single-photon source [33]. As shown in Fig.4, the upper tip features a conical shape, in order to obtain a directive far-field emission pattern. These results open a wealth of interesting perspectives for the realization of advanced quantum light sources [34].
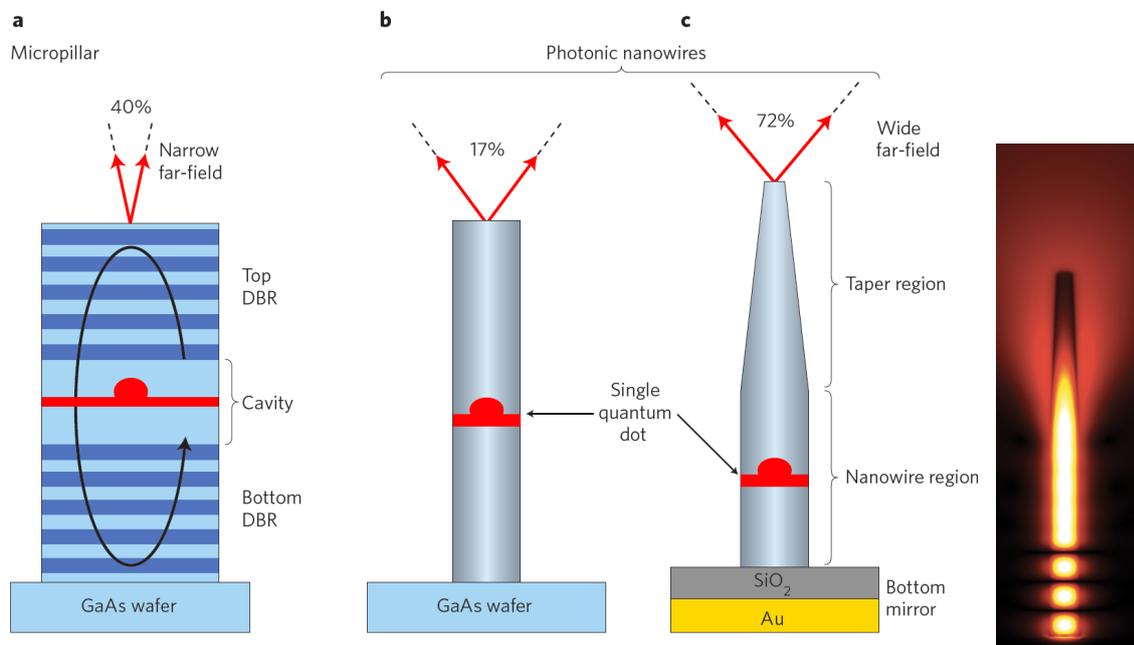
Figure 4: (a) State-of-the-art cavity-based single photon sources, 40% of efficiency. (b) Conventional nanowire. (c) Reflective tappered nanowire reaching 70% of efficiency.

Outline of the thesis

The present thesis explores theoretical perspectives opened by artificial atoms coupled to one-dimensional (1D) waveguides and microcavities.

In the first chapter, we revisit the giant optical nonlinearity at the single-photon level of an atom coupled to a 1D waveguide. We first show that it behaves as a perfectly reflecting medium when probed by a resonant laser at low powers. Then we explore this nonlinearity at the single-photon level when the atom is inverted in population. In that case, we revisit the effect of stimulated emission by a classical probe.

In the second chapter we explore the fully quantum dynamics of 1D atoms. In particular, we introduce the effect of stimulated emission by a single propagating photon packet. Under that condition, the novel phenomenon of optimal irreversible stimulated emission is demonstrated.

In the third chapter we apply optimal irreversible stimulated emission to quantum information. We present a protocol to realize either optimal universal quantum cloning or entanglement. The broadband aspect of the waveguide is an essential ingredient to the versatility of the device.

In the fourth chapter we model a quantum dot in a microcavity. We study the influence of phonons in the spontaneous emission. We finally show that an important distortion in the apparent cavity mode is provided by the influence of phonons.

Chapter 1

The one-dimensional atom: a semiclassical approach

In the beginning, there was nothing. God said: "Let there be light". And there was light.

There was still nothing, but you could see it a whole lot better.

Ellen DeGeneres.

A single photon interacting with a single emitter has been a major goal in quantum optics. So far, this has been successfully achieved in high-quality factor microwave [35] or optical cavities [36]. An efficient trapping of the photons is required to achieve high atom-field couplings. This limits, however, the potential of these systems to be explored for practical purposes. Alternatively, the emitter can be coupled to a one-dimensional (1D) electromagnetic environment. Termed *1D atom* since its pioneering realization [37], it has firstly been implemented in an atom coupled to a leaky directional cavity [38]. Nowadays, 1D atoms consist not only in single atoms [39] or molecules [40] in tightly focused beams, but also in solid-state artificial atoms coupled to solid-state 1D environments. The most prominent examples for the latter are quantum dots embedded in photonic wires [33] (Fig.1.1-a), in photonic crystals [41], or in plasmonic waveguides

[42], and superconducting qubits coupled to transmission lines in circuit QED [43, 44] (Fig1.1-b).

The natural directionality of 1D atoms allows a high mode matching to be reached between the resonant incoming and the scattered light. This provides saturation of the emitter with a single propagating photon [45] as well as an efficient interference between the two fields, motivating proposals for single-photon transistors [42] and two-photon gates [46].

The next three chapters are devoted to quantum optical properties of a single emitter coupled to this 1D environment. In the present chapter, we study the quasi-classical regime where the 1D atom is probed by a monochromatic laser. We revisit the effect of destructive interference that gives rise to total reflection of light [40, 41, 44, 45, 47]. Still in the quasi-classical regime, we explore this highly nonlinear behaviour when atomic population is inverted. This allows us to revisit the concept of stimulated emission at the single-photon level in 1D atoms.

1.1 Heisenberg equations

The model of the 1D atom consists in a few-level emitter coupled to a 1D continuum of modes of the electromagnetic field, as illustrated in Fig.1.1 (c). In this section, we describe the quantum time evolution of the system. We derive the Heisenberg operators firstly for the atom and then for the field.

1.1.1 Model

We consider a two-level system (TLS) having a transition frequency ν_A between the ground state $|g\rangle$ and the excited state $|e\rangle$. The electric dipole of the transition is $\vec{d} = e \langle g|\vec{R}|e\rangle$, where $\vec{R}$ is the electron position operator and e is its elementary charge. The dipole operator is $D = d \, (\hat{d} \, \sigma_- + \hat{d}^* \, \sigma_+)$, where $\sigma_- = |g\rangle\langle e|$, $\sigma_+ = \sigma_-^\dagger$ and $\vec{d} = d \, \hat{d}$,
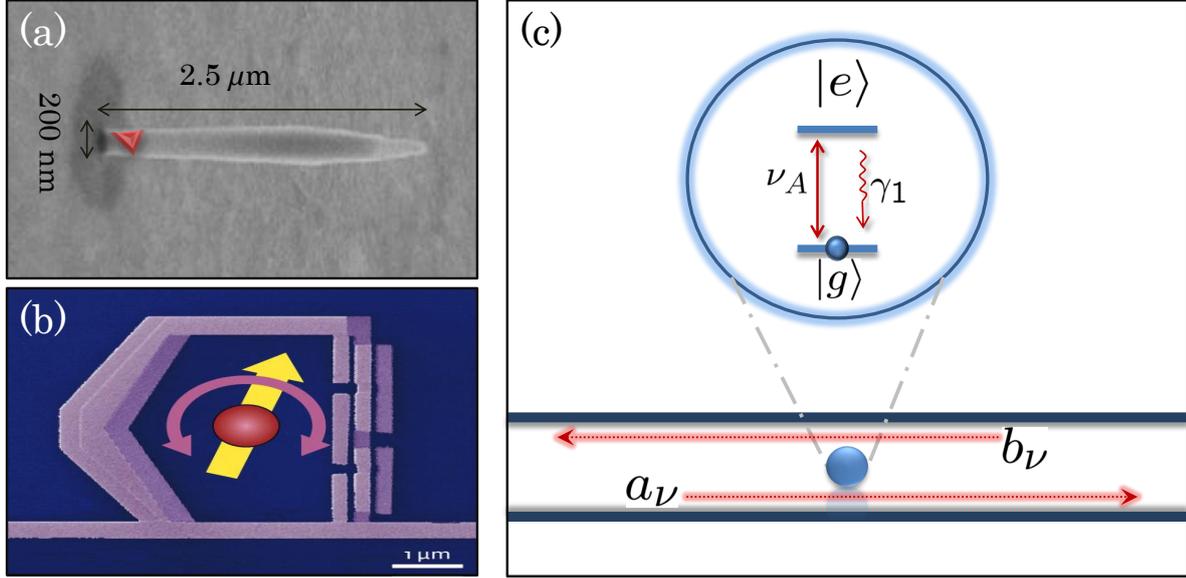
Figure 1.1: Illustrative examples of the 1D atom. (a) InAs quantum dot (red triangle) coupled to a GaAs photonic nanowire. (b) Superconducting artificial atom (flux qubit), based on Josephson junctions, coupled to a superconducting transmission line. (c) Model based on a generic two-level system coupled to an infinite 1D waveguide.

yielding the atom Hamiltonian [14, 19]

$$H_{\text{atom}} = \hbar \nu_A \, \sigma_+ \sigma_-. \tag{1.1}$$

The field normal modes are separated into a_ν and b_ν [48], respectively accounting for the forward and backward propagating fields of frequency ν. The free field Hamiltonian reads

$$H_{\text{field}} = \sum_\nu \hbar \nu \, (a_\nu^\dagger a_\nu + b_\nu^\dagger b_\nu). \tag{1.2}$$

The continuum limit is obtained by introducing the 1D density of modes ρ_{1D} so that $\sum_\nu \to \int d\nu \, \rho_{\text{1D}}$.

The emitter-field dipole interaction is described in the rotating-wave approximation [14, 19], valid for a coupling constant $g_\nu \ll \nu_A$. By setting the atom at position z_A, the

Hamiltonian writes

$$H_{\text{int}} = -i\hbar \sum_{\nu=0}^{\infty} g_\nu \left[\sigma_+ (a_\nu \, e^{i\nu z_A/c} + b_\nu \, e^{-i\nu z_A/c}) - \text{H.c.} \right].$$

(1.3)

In the following we assume the reference frame where $z_A = 0$. The total hamiltonian is finally given by

$$H = H_{\text{atom}} + H_{\text{int}} + H_{\text{field}}.$$

(1.4)

1.1.2 Evolution of the atom

We denote the Heisenberg operators by $\mathcal{O}^H(t)$. The atomic operators then read $\sigma_-^H(t)$, $\sigma_+^H(t)$ and $\sigma_z^H(t) \equiv (\sigma_+^H(t)\sigma_-^H(t) - \sigma_-^H(t)\sigma_+^H(t))/2$.

Then we define new operators $\sigma_-(t)$, $\sigma_+(t)$ and $\sigma_z(t)$ by evidencing the fast-rotating terms,

$$\sigma_-^H(t) \equiv \sigma_-(t) \exp\left(-i\nu_A t\right) \quad \text{and} \quad \sigma_+^H(t) \equiv \sigma_+(t) \exp\left(+i\nu_A t\right),$$

(1.5)

and $\sigma_z^H(t) = \sigma_z(t) \equiv (\sigma_+(t)\sigma_-(t) - \sigma_-(t)\sigma_+(t))/2$.

In the same way, the field operators in the Heisenberg picture are $a_\nu^H(t)$ and $b_\nu^H(t)$. The fast rotating terms are evidenced, so the new operators $a_\nu(t)$ and $b_\nu(t)$ are defined by

$$a_\nu^H(t) = a_\nu(t) \exp(-i\nu t) \quad \text{and} \quad b_\nu^H(t) = b_\nu(t) \exp\left(-i\nu t\right).$$

(1.6)

The atomic evolution equations are obtained for those new operators,

$$\frac{d}{dt}\sigma_-(t) = 2\sigma_z(t) \sum_\nu g_\nu [a_\nu(t) + b_\nu(t)] e^{-i(\nu-\nu_A)t}$$

(1.7)

and

$$\frac{d}{dt}\sigma_z(t) = -\sum_\nu g_\nu \left\{ \sigma_+(t)[a_\nu(t) + b_\nu(t)] e^{-i(\nu-\nu_A)t} + \text{H.c.} \right\}.$$

(1.8)

The field equations are formally integrated,

$$a_\nu(t) = a_\nu(0) + g_\nu \int_0^t dt' \sigma_-(t') e^{i(\nu-\nu_A)t'}.$$

(1.9)

Analogous expression holds for $b_\nu(t)$.

Eq.(1.9) is then applied to Eqs(1.7) and (1.8). The time integration is solved by noting that $\sum_\nu g_\nu^2 \, e^{-i(\nu-\nu_A)(t-t')}$ varies much faster than $\sigma_-(t')$ for optical frequencies [49], so that a *Markovian approximation* [19, 49] can be applied:

$$
\sigma_z(t) \sum_\nu g_\nu^2 \int_0^t dt' \; \sigma_-(t') \; e^{-i(\nu-\nu_A)(t-t')}
$$

$$
\approx \quad \sigma_z(t)\sigma_-(t) \int_0^t dt' \sum_\nu g_\nu^2 \; e^{-i(\nu-\nu_A)(t-t')}. \tag{1.10}
$$

We then use that [49]

$$
\int_0^t e^{i(\nu-\nu_A)(t'-t)} dt' \approx i\mathcal{P}\left(\frac{1}{\nu-\nu_A}\right) + \pi\delta(\nu-\nu_A), \tag{1.11}
$$

solving the time integration. The imaginary part gives the frequency shift that will be incorporated in the definition of ν_A. The real part provides the decay rate

$$
\frac{\gamma_1}{2} \equiv 2\pi \sum_\nu g_\nu^2 \; \delta(\nu-\nu_A). \tag{1.12}
$$

Note that γ_1 depends on the 1D density of modes ρ_{1D}, $\gamma_1 = 4\pi\rho_{1D}g_{\nu_A}^2$. The decay rate derived here is in accordance to Fermi's golden rule for the spontaneous decay of the atomic excitation. With the help ot the relation $\sigma_z\sigma_- = -\sigma_-/2$, the Heisenberg-Langevin equations for the atom are derived,

$$
\frac{d}{dt}\sigma_-(t) = -\frac{\gamma_1}{2}\sigma_-(t) + 2\sigma_z(t)\left(\frac{d}{i\hbar}E_{\text{a,free}}(z_A=0,t) + \frac{d}{i\hbar}E_{\text{b,free}}(z_A=0,t)\right)e^{i\nu_A t}, \tag{1.13}
$$

and

$$
\frac{d}{dt}\sigma_z(t) = -\gamma_1(\sigma_z(t) + 1/2)
$$

$$
- \left\{\sigma_+(t)\left[\frac{d}{i\hbar}E_{\text{a,free}}(z_A=0,t) + \frac{d}{i\hbar}E_{\text{b,free}}(z_A=0,t)\right]e^{i\nu_A t} + \text{H.c.}\right\}, \tag{1.14}
$$

where $E_{\text{a,free}}(z,t) \equiv i\sum_\nu \epsilon_\nu a_\nu(0)e^{-i\nu(t-z/c)}$ and $E_{\text{b,free}}(z,t) \equiv i\sum_\nu \epsilon_\nu b_\nu(0)e^{-i\nu(t+z/c)}$. The electric field per photon is ϵ_ν and the relation $\hbar g_\nu = d\epsilon_\nu$ has been applied.

1.1.3   Evolution of the field

The electromagnetic field operator in Heisenberg representation is

$$E^H(z,t) = E^{H(+)}(z,t) + E^{H(-)}(z,t), \tag{1.15}$$

being $E^{H(-)}(z,t) = \left(E^{H(+)}(z,t)\right)^\dagger$ and

$$E^{H(+)}(z,t) = i \sum_\nu \epsilon_\nu \left[a_\nu^H(t)e^{ik_\nu z} + b_\nu^H(t)e^{-ik_\nu z} \right], \tag{1.16}$$

where $k_\nu = |\vec{k}_\nu| = \nu/c$ gives the linear dispersion relation. The direction of propagation of the fields is indicated in the signs of the exponentials. The expression for the field per photon is $\epsilon_\nu = \sqrt{\hbar\nu/(2\varepsilon_0 V)}$ [14], being ε_0 the vacuum permittivity and V the volume of quantization[1].

Equations (1.6) and (1.9) are substituted in the definition of the electric field, Eq.(1.16), yielding a linear combination between free and emitted fields,

$$E^{H(+)}(z,t) = E_{a,\text{free}}(z,t) + E_{b,\text{free}}(z,t) + E_\sigma(z,t), \tag{1.17}$$

where

$$E_{a,\text{free}}(z,t) = i \sum_\nu \epsilon_\nu a_\nu(0) e^{-i\nu(t-z/c)} \tag{1.18}$$

and

$$E_{b,\text{free}}(z,t) = i \sum_\nu \epsilon_\nu b_\nu(0) e^{-i\nu(t+z/c)}, \tag{1.19}$$

consistently with the respective direction of propagation, $E_{a,\text{free}}(z,t) = E_{a,\text{free}}(z-ct,0)$ and $E_{b,\text{free}}(z,t) = E_{b,\text{free}}(z+ct,0)$.

The emitted field is given by $E_\sigma(z,t) = E_\sigma^a(z,t) + E_\sigma^b(z,t)$, where

$$
\begin{aligned}
E_\sigma^{a,b}(z,t) &= i \sum_\nu \epsilon_\nu \left(g_\nu \int_0^t dt' \sigma_-(t') e^{i(\nu-\nu_A)t'} \right) e^{-i\nu t} \, e^{\pm i k_\nu z} \\
&= i \sum_\nu \epsilon_\nu g_\nu \int_0^t dt' \sigma_-(t') e^{i(\nu-\nu_A)(t'-[t\mp z/c])} e^{-i\nu_A(t\mp z/c)}, \tag{1.20}
\end{aligned}
$$

---

[1]the volume of quantization is given by $V = \mathcal{A}L$, where L is the length of quantization of the 1D waveguide ($L \to \infty$) and $\mathcal{A}$ is the cross-section area as defined in Ref.[48].

where the sign depends on the mode under consideration. A Markovian approximation is applied here. The relation $\epsilon_\nu g_\nu = \hbar g_\nu^2/d$ allows us to immediatly identify Eq.(1.10),

$$\sum_\nu g_\nu^2 \int_0^t dt'\; \sigma_-(t')\; e^{-i(\nu-\nu_A)([t\mp z/c]-t')}\; e^{-i\nu_A(t\mp z/c)}$$

$$\approx\quad \sigma_-(t\mp z/c) \int_0^t dt' \sum_\nu g_\nu^2\; e^{-i(\nu-\nu_A)([t\mp z/c]-t')}\; e^{-i\nu_A(t\mp z/c)}, \tag{1.21}$$

where $\sigma_-(t') \approx \sigma_-(t\mp z/c)$ is valid for $0 < t' < t$, that is, for

$$0 < t \mp z/c < t. \tag{1.22}$$

Note that the inequality above states a crucial difference from the previous case. The fact that for $z > 0$, $t' = t - z/c < t$, and for $z < 0$, $t' = t + z/c < t$, allows us to approximate, for $\pm z > 0$,

$$\int_0^t e^{i(\nu-\nu_A)(t'-[t\mp z/c])}dt' \approx \int_{-\infty}^\infty e^{(i(\nu-\nu_A)(t'-[t\mp z/c]))}dt' = 2\pi\delta(\nu - \nu_A). \tag{1.23}$$

Eq.(1.23) applies to $\sigma_-(t') \approx \sigma_-(t\mp z/c)$ (i.e., $t' \approx t\mp z/c$ and $z \neq 0$), differently from Eq.(1.11), which is adequated to the case where $\sigma_-(t') \approx \sigma_-(t)$ (i.e., $t' \approx t$).

The lefthand side of inequality (1.22),

$$0 < t \mp z/c,$$

states that the argument of the atomic operator must be positive. That is, the time "t" at which we detect the electric field, at position "z", must be bigger than the time spent by the light, "$|z|/c$", to arrive at that position.

The righthand side of inequality (1.22),

$$\pm z > 0,$$

states that for propagation towards $+k$, only detection at $z > 0$ contains information about the atomic emitted field. Analogously, a detector at $z < 0$ can only be able to measure the signal coming from the emitted field propagating in the $-k$ direction.

By denoting $\Theta(z)$ the Heaviside step function, we include the above statements and obtain the emitted field

$$E_\sigma(z,t) = i\left(\sum_\nu \frac{\hbar}{d}\, g_\nu^2\, 2\pi\delta(\nu - \nu_A)\right)\ \left\{\sigma_-^H(t - z/c)\Theta(z)\Theta(t - z/c)\right.$$
$$\left. +\sigma_-^H(t + z/c)\Theta(-z)\Theta(t + z/c)\right\}. \quad (1.24)$$

Finally, the full electric field equation for the 1D atom is established,

$$
\begin{aligned}
E^{H(+)}(z,t) \ =\ & E_{a,\text{free}}(z,t) + E_{b,\text{free}}(z,t) \\
& +\eta\big\{\sigma_-^H(t - z/c)\ \Theta(z)\ \Theta(t - z/c) \\
& +\sigma_-^H(t + z/c)\ \Theta(-z)\ \Theta(t + z/c)\big\},
\end{aligned}
\qquad (1.25)
$$

where $\eta \equiv i\hbar\gamma_1/(2d)$ is the constant of proportionality. In the following we choose the initial state of the quantum evolution.

1.2   Incident field: a pure coherent state

In this chapter we will be interested in modeling the experimental condition in which a continuous-wave monochromatic laser is injected in the waveguide to probe the atom, as illustrated in Fig.1.2. This can be modeled by introducing a time-dependent c-number in the evolution equation of the atom. Equivalently, it can be modeled by a pure initial coherent state. This equivalence is presented below.

1.2.1   Canonical transformation

A single mode of frequency ν_L is in a coherent state denoted here by $|\alpha_L\rangle$. By definition, the coherent state is an eigenstate of the destruction operator [6],

$$a_{\nu_L}|\alpha_L\rangle = \alpha_L|\alpha_L\rangle, \qquad (1.26)$$

where $|\alpha_L|^2$ gives the average number of photons of that state. Using this definition, it can be shown that the coherent field is a displaced vacuum state [7],

$$|\alpha_L\rangle = \mathcal{D}[\alpha_L]|0_{\nu_L}\rangle, \qquad (1.27)$$
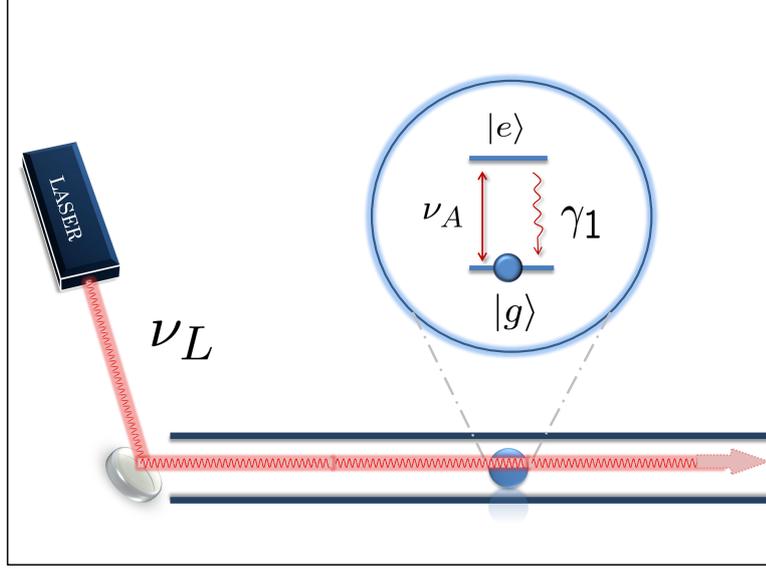
Figure 1.2: The incident field is a laser of frequency ν_L. This is modeled by a pure initial coherent state in the mode a_{ν_L}. The laser-atom detuning is denoted by $\delta_L = \nu_L - \nu_A$.

where the *displacement operator* reads $\mathcal{D}[\alpha_L] = \exp\left[\alpha_L a_{\nu_L}^\dagger - \alpha_L^* a_{\nu_L}\right]$. It can also be shown [7] from bosonic commutation relations that

$$\mathcal{D}^\dagger[\alpha_L]\, a_{\nu_L}\, \mathcal{D}[\alpha_L] = a_{\nu_L} + \alpha_L. \tag{1.28}$$

The coherent state properties shown above can now be applied to our particular case. Eqs.(1.14) and (1.13) are averaged by the initial state

$$
\begin{aligned}
\frac{d}{dt}\langle\alpha_L|\sigma_-(t)|\alpha_L\rangle &= -\frac{\gamma_1}{2}\,\langle\alpha_L|\sigma_-(t)|\alpha_L\rangle \\
&\quad + 2\frac{d}{i\hbar}e^{i\nu_A t}\,\langle\alpha_L|\sigma_z(t)E_{\text{a,free}}(0,t)|\alpha_L\rangle \\
&\quad + 2\frac{d}{i\hbar}e^{i\nu_A t}\,\langle\alpha_L|\sigma_z(t)E_{\text{b,free}}(0,t)|\alpha_L\rangle
\end{aligned}
\tag{1.29}
$$

and analogously for $\langle\sigma_z(t)\rangle$. We develop Eq.(1.29) using Eq.(1.27), the identity operator

$\mathbb{I} = \mathcal{D}^\dagger[\alpha_L]\mathcal{D}[\alpha_L]$, and defining $\tilde{\sigma}_{-,z}(t) \equiv \mathcal{D}^\dagger[\alpha_L]\sigma_{-,z}(t)\mathcal{D}[\alpha_L]$,

$$
\begin{aligned}
\frac{d}{dt}\langle 0_{\nu_L}|\tilde{\sigma}_-(t)|0_{\nu_L}\rangle &= -\frac{\gamma_1}{2}\,\langle 0_{\nu_L}|\tilde{\sigma}_-(t)|0_{\nu_L}\rangle \\
&\quad + 2\frac{d}{i\hbar}e^{i\nu_A t}\,\langle 0_{\nu_L}|\tilde{\sigma}_z(t)\mathcal{D}^\dagger[\alpha_L]E_{\mathrm{a,free}}(0,t)\mathcal{D}[\alpha_L]|0_{\nu_L}\rangle \\
&\quad + 2\frac{d}{i\hbar}e^{i\nu_A t}\,\langle 0_{\nu_L}|\tilde{\sigma}_z(t)\mathcal{D}^\dagger[\alpha_L]E_{\mathrm{b,free}}(0,t)\mathcal{D}[\alpha_L]|0_{\nu_L}\rangle \quad (1.30)
\end{aligned}
$$

Using the definition of $E_{\mathrm{a,free}}(z,t)$ and Eq.(1.28) we write

$$
\begin{aligned}
\mathcal{D}^\dagger[\alpha_L]E_{\mathrm{a,free}}(0,t)\mathcal{D}[\alpha_L] &= i\sum_\nu \epsilon_\nu\,\mathcal{D}^\dagger[\alpha_L]a_\nu(0)\mathcal{D}[\alpha_L]\,e^{-i\nu t} \\
&= i\sum_{\nu \neq \nu_L}\epsilon_\nu\,(a_\nu(0))\,e^{-i\nu t} + i\epsilon_{\nu_L}(a_{\nu_L}+\alpha_L)e^{-i\nu_L t} \\
&= i\sum_\nu \epsilon_\nu\,a_\nu(0)\,e^{-i\nu t} + i\epsilon_{\nu_L}\alpha_L e^{-i\nu_L t} \\
&= E_{\mathrm{a,free}}(0,t) + i\epsilon_{\nu_L}\alpha_L e^{-i\nu_L t}. \quad (1.31)
\end{aligned}
$$

We have supposed that the coherent state is within the a_ν modes, so it does not change modes b_ν, i.e., $\mathcal{D}^\dagger[\alpha_L]E_{\mathrm{b,free}}(z,t)\mathcal{D}[\alpha_L] = E_{\mathrm{b,free}}(z,t)$.

Now we apply Eq.(1.31) to Eq.(1.30). We also define the time-dependent c-number corresponding to the *classical* input field,

$$
\mathcal{E}^a_{\mathrm{in}}(z,t) \equiv i\epsilon_{\nu_L}\,\alpha_L\,e^{-i\nu_L(t-z/c)}, \quad (1.32)
$$

finding

$$
\begin{aligned}
\frac{d}{dt}\tilde{\sigma}_-(t) &= -\frac{\gamma_1}{2}\,\tilde{\sigma}_-(t) \\
&\quad + 2\frac{d}{i\hbar}e^{i\nu_A t}\tilde{\sigma}_z(t)\left[E_{\mathrm{a,free}}(0,t) + \mathcal{E}^a_{\mathrm{in}}(0,t)\right] \\
&\quad + 2\frac{d}{i\hbar}e^{i\nu_A t}\,\tilde{\sigma}_z(t)E_{\mathrm{b,free}}(0,t), \quad (1.33)
\end{aligned}
$$

for the transformed initial vacuum state $|0_{\nu_L}\rangle$. The same equation is obtained by introducing an external time-dependent potential of frequency ν_L and energy $\hbar\Omega_{\mathrm{classical}} = 2d\epsilon_{\nu_L}\alpha_L = 2\hbar g_{\nu_L}\,\alpha_L$. The parameter $\Omega_{\mathrm{classical}}$ is the *Rabi frequency*.

This shows that modeling a laser by a classical field, described by a time-dependent c-number, is equivalent to modeling the initial state of the quantum field as a pure coherent state. This analysis is found in Refs.[49] and [50].

1.2.2   Optical Bloch equations

The input field in a coherent state drives the atomic evolution via the so called *optical Bloch equations* [49]. In what follows, we show its expression firstly in the ideal case. Then we extend the result to include waveguide loss and pure dephasing of the two-level system. Finally, we discuss the solution of those equations in all regimes: transient/steady-state and linear/saturated.

We define the atomic operators in the frame rotating at the laser frequency ν_L,

$$\sigma_-^H(t) = S_-(t)\, e^{-i\nu_L t} \quad \text{and} \quad \sigma_z^H(t) = S_z(t), \tag{1.34}$$

which is equivalent to write $S_-(t) = \sigma_-(t)\, e^{i\delta_L t}$, where $\delta_L \equiv \nu_L - \nu_A$ is the laser-atom detuning. This eliminates the explicit time dependence in the coefficients.

Ideal case: no pure dephasing, no waveguide loss

Transformation (1.33) yields the following evolution for the atomic averages:

$$\frac{d}{dt}\langle S_-\rangle = -\left(\frac{\gamma_1}{2} - i\delta_L\right)\langle S_-\rangle + \Omega_1\,\langle S_z\rangle,$$

$$\frac{d}{dt}\langle S_z\rangle = -\gamma_1\left(\langle S_z\rangle + \frac{1}{2}\right) - \Omega_1\,\Re[\langle S_-\rangle], \tag{1.35}$$

where $\Re$ stands for the real part and the Rabi frequency here is given by $\Omega_1 = 2d\epsilon_{\nu_L}\alpha_L/\hbar = 2g_{\nu_L}\alpha_L = 2\alpha_L\sqrt{\gamma_1/(4\pi\rho_{1D})}$. We define a normalized (unitless) laser power p so that $\gamma_1 p$ is the average number of photons per atomic lifetime,

$$p \equiv \frac{|\alpha_L|^2}{2\pi\rho_{1D}\gamma_1}. \tag{1.36}$$

This definition is motivated by the fact that $\rho_{1D} = L/(2\pi c)$, that is, $2\pi\rho_{1D}$ is the time L/c the photon takes to propagate across the length of quantization L. So, $(2\pi\rho_{1D}\gamma_1)^{-1}$

gives a flux in units of lifetime γ_1^{-1}. Applying this definition to the Rabi frequency gives

$$\Omega_1 = \gamma_1 \sqrt{2p}. \tag{1.37}$$

Note that, in this particular 1D geometry, Rabi frequency is proportional to the atomic decay rate.

Nonideal case: pure dephasing and waveguide loss

Waveguide loss is described by an extra decay rate of the atom γ_0 (see Fig.2.2). Population decay rate now reads

$$\gamma \equiv \gamma_0 + \gamma_1,$$

so the ratio

$$\beta \equiv \frac{\gamma_1}{\gamma}$$

describes the relative coupling to the 1D environment, i.e., β is the waveguide efficiency. Coherences also decay with a modified rate, given by $\gamma/2$.

Figure 1.3: Realistic imperfections of 1D atoms: pure dephasing γ^* and decay to the waveguide leaky modes γ_0. The waveguide efficiency is $\beta = \gamma_1/\gamma$, where $\gamma = \gamma_0 + \gamma_1$.

Similarly, pure dephasing rate γ^*, typically present in solid-state artificial atoms [33, 56], can be included by adding a decay term in the coherence decay rates,

$$\frac{\gamma}{2} \rightarrow \frac{\gamma + \gamma^*}{2}, \tag{1.38}$$

while populations are left unchanged[2],

$$\frac{d}{dt}\langle S_- \rangle = -\left(\frac{\gamma + \gamma^*}{2} - i\delta_L\right)\langle S_- \rangle + \Omega\,\langle S_z \rangle,$$

$$\frac{d}{dt}\langle S_z \rangle = -\gamma\left(\langle S_z \rangle + \frac{1}{2}\right) - \Omega\,\Re[\langle S_- \rangle], \tag{1.39}$$

the symbol $\Re$ denoting the real part.

The Rabi frequency is modified to

$$\Omega = \gamma\sqrt{2p\beta}, \tag{1.40}$$

---

[2]Extra decay and pure dephasing can be modeled by coupling the system to extra environments. The former comes from a dipolar coupling to an extra continuum of modes (c_ν), while the latter comes from a coupling like $H_{\text{int}} = |e\rangle\langle e| \sum_{\nu,\nu'} c_\nu^\dagger c_{\nu'}$ [19]. Equivalently, Lindbladian operators [14, 19] can be used, yielding $\mathcal{L}_{\gamma_0}[\rho] = -\frac{\gamma_0}{2}(\sigma_+\sigma_-\rho + \rho\sigma_+\sigma_- - 2\sigma_-\rho\sigma_+)$ for spontaneous emission in 3D space and $\mathcal{L}_{\gamma^*}[\rho] = -\frac{\gamma^*}{4}(\rho - 4\sigma_z\rho\sigma_z)$ for pure dephasing [19].

where the normalized laser power is now given by

$$p = \frac{|\alpha_L|^2}{2\pi\rho_{1D}\gamma}. \tag{1.41}$$

The η factor in Eqs.(1.25) is rewritten as

$$\eta = i\epsilon_{\nu_L}\sqrt{\frac{\beta}{2}}\sqrt{2\pi\rho_{1D}\gamma}. \tag{1.42}$$

This expression for η evidences its dependency on the efficiency of the atom-waveguide coupling, given by the β factor. The term $\sqrt{2\pi\rho_{1D}\gamma}$ naturally cancels out with the same factor that also appears in the transformation $\alpha_L = \sqrt{p}\sqrt{2\pi\rho_{1D}\gamma}$, when the photodetection signals are computed.

Transient and steady-state regimes

At short times $t < \gamma^{-1}$, atomic populations $\langle S_z(t)\rangle$ and coherences $\langle S_-(t)\rangle$ are time-dependent quantities. This is called transient regime.

At long times $t_\infty \gg \gamma^{-1}$, atomic averages $\langle S_z(t_\infty)\rangle$ and $\langle S_-(t_\infty)\rangle$ acquire a stationary value, so $d\langle S_-\rangle/dt = d\langle S_z\rangle/dt = 0$. This defines the steady-state regime.

Linear and saturated regimes

In steady-state, the linear or saturated regimes are distinguished by a *saturation parameter s*. It is defined with respect to the steady-state excited-state population,

$$\left(\langle S_z\rangle + \frac{1}{2}\right) = \frac{1}{2}\left(\frac{s}{\frac{1}{\beta} + s}\right) \tag{1.43}$$

where the saturation parameter is [49]

$$s \equiv 4p\,\frac{1 + \gamma^*/\gamma}{(1 + \gamma^*/\gamma)^2 + (2\delta_L/\gamma)^2}.$$

So, if $s \ll \beta^{-1}$ the excited-state population is vanishingly small, $\langle S_z\rangle + \frac{1}{2} \ll 1$, and grows linearly with s. For $s \gg \beta^{-1}$, the excited state can no longer increase with s, becoming saturated at $\langle S_z\rangle + \frac{1}{2} = 1/2$.

Still in steady-state, we study how the linear/saturation transition affects the coherent atomic dipole $\langle S_- \rangle$. Given the incident field $\mathcal{E}_{\text{in}}^a(z, t)$ from Eq.(1.32), the atom dipole satisfies

$$\langle S_- \rangle = \chi \, \tilde{\mathcal{E}}_{\text{in}}^a(0, t), \tag{1.44}$$

where $\tilde{\mathcal{E}}_{\text{in}}^a(0, t) \equiv \mathcal{E}_{\text{in}}^a(0, t) \, e^{i\nu_L t} = i\epsilon_{\nu_L} \alpha_L$, and the complex atomic susceptibility, or the *atomic polarizability* is

$$\chi = -\frac{1}{\eta} \left(\frac{1}{1 + \frac{\gamma^*}{\gamma} - i2\delta_L/\gamma_1} \right) \frac{1}{\frac{1}{\beta} + s}, \tag{1.45}$$

In the linear regime, χ is a constant with respect to the incident field intensity. The phase of the atomic dipole becomes locked with respect to the phase of the field, behaving like a classical dipole. In the nonlinear, or saturated, regime the dipole coherence vanishes.

In the ideal 1D atom, $\beta = 1$, $\gamma^* = \delta_L = 0$, nonlinearity starts at the level of a single photon per atomic lifetime, $p \sim 1$, what is called a *giant optical nonlinearity*.

Linear or saturated regime is settled depending upon the pump power $p \propto (\Omega/\gamma)^2$. In the transient regime, low pump $p < 1$ leads to monotonic behaviour of the atomic populations and coherences, defining the linear regime. A very high pump $p \gg 1$ enforces the atom to realize many optical transitions between ground and excited states, performing the so called *Rabi oscillations* [14].

1.3   Interference between incoming and scattered fields

In this section we study interference effects between the classical pump and the field radiated by the atom. We first concentrate on average transmitted and reflected fields. Then we discuss second-order field correlations that evidence quantum properties of the fields.
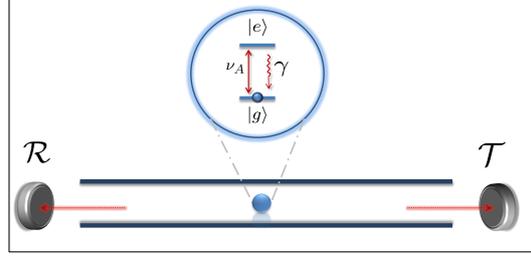
Figure 1.4: Detector placed in the transmission (reflection) channel measures transmission (reflection) light power $\mathcal{T}$ ($\mathcal{R}$).

The field detected in the transmission channel, $E_T(z, t)$, and the field detected in the reflection channel, $E_R(z, t)$, correspond to the quantum operators

$$E_T(z, t) \equiv E_{a,\text{free}}(z, t) + \eta \, \Theta(z) \, \Theta(t - z/c) \, \sigma_-^H(t - z/c) \tag{1.46}$$

and

$$E_R(z, t) \equiv E_{b,\text{free}}(z, t) + \eta \, \Theta(-z) \, \Theta(t + z/c) \, \sigma_-^H(t + z/c), \tag{1.47}$$

obtained from Eqs.(1.25), (1.18) and (1.19). With the above definitions we explore the photodetection relations in the following sections, illustrated in Fig.1.4.

1.3.1   Field expectation values

Transmitted and reflected powers

Photodetectors measure the rate of photon arrival. These rates are given by the transmitted power $\mathcal{T}$ and the reflected power $\mathcal{R}$,

$$\mathcal{T} = \gamma \, \frac{\langle E_T^\dagger(z_d, t) E_T(z_d, t) \rangle}{\epsilon_{\nu_L}^2} \quad \text{and} \quad \mathcal{R} = \gamma \, \frac{\langle E_R^\dagger(z_d, t) E_R(z_d, t) \rangle}{\epsilon_{\nu_L}^2}, \tag{1.48}$$

both in units of number of photons per atomic lifetime, measured at position z_d at time t. From the definitions above, the power of the incident field is

$$\mathcal{I} = \gamma \, \frac{\langle E_{a,\text{free}}^\dagger(z_d, t) E_{a,\text{free}}^\dagger(z_d, t) \rangle}{\epsilon_{\nu_L}^2} = \gamma \, \frac{\mathcal{E}_{\text{in}}^{a\,*}(z_d, t) \mathcal{E}_{\text{in}}^a(z_d, t)}{\epsilon_{\nu_L}^2} = \gamma \alpha_L^2 = \gamma p \, (2\pi \rho_{1D} \gamma). \tag{1.49}$$

Transmittance and reflectance

The ratio between the transmitted (reflected) and incident powers defines the transmittance T (reflectance R),

$$T = \frac{\mathcal{T}}{\mathcal{I}} \quad \text{and} \quad R = \frac{\mathcal{R}}{\mathcal{I}}, \tag{1.50}$$

where the definitions from Eqs.(1.48) and (1.49) have been applied.

In the steady-state regime, we obtain from Eq.(1.45) the solution

$$T = 1 + (2 - \beta)\,\Re[\eta\,\chi] \quad \text{and} \quad R = -\beta\,\Re[\eta\,\chi], \tag{1.51}$$

where the real part is denoted by $\Re$. Note that for a nondissipative waveguide, $\beta = 1$, total energy is conserved, $R + T = 1$ for all p, γ^* and δ_L. If $\beta < 1$, then $R + T < 1$. For a resonant laser $\delta_L = 0$ in the linear regime $p \ll 1$, and under ideal
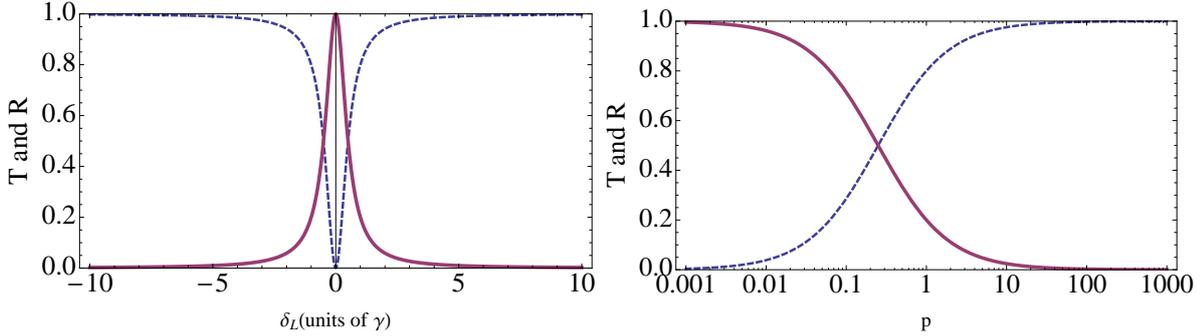
Figure 1.5: Left– transmittance (blue) and reflectance (red) as a function of the laser-atom detuning, showing total dipole-induced reflection at resonance in the linear regime, $p \ll 1$. Right – transmittance (blue) and reflectance (red) as a function of laser power, showing the giant optical nonlinearity at the single-photon level $p \sim 1$. In both cases the ideal condition is assumed, $\gamma^* = 0$ and $\beta = 1$.

conditions $\gamma^* = 0$ and $\beta = 1$, Eq.(1.51) yields $T = 0$ and $R = 1$. This *perfect reflection* occurs because the mean value of the field emitted by the atom has a π-phase shift[3]

---

[3]this π-phase shift has an instructive classical analog. First we shall remind that in the low-saturation limit, the average atomic dipole behaves classically, as a harmonic oscillator. The average incoming field is also a

with respect to the incoming field, i.e., $\eta \, \chi = -1$, causing a destructive interference between incoming and scattered fields. This is illustrated in Fig.1.5 (left), where we have plotted the transmittance and reflectance as a function of the detuning. It shows a sharp bump around the resonance, the width being given by γ. Fig.1.5 (right) shows the power dependence of the same functions at resonance. It demonstrates the giant optical nonlinearity arising at the single-photon level, $p \sim 1$. The nonideal case is studied in Ref.[45], modeling a semiconductor quantum-dot embedded in a micropillar.

Interference ceases when the atom is in the saturated regime, $p \gg 1$, so $T = 1$ and $R = 0$. Null reflection is a consequence of the laser power surpassing by far the saturated atomic contribution. It is worth noting that, even though transmission is maximal, the net transmission $T-1$ is still smaller then reflection, $(T-1)-R = -\left(\langle S_z \rangle + 1/2\right)/p < 0$. In particular, net transmission is negative, $(T-1)/R = 1 - 2/\beta < 0$, showing that the reflection channel is still favored with respect to the transmission channel.

Transmission and reflection

By performing homodyne detection [14], the mean fields $\langle E_{T(R)}(z_d, t) \rangle$ can be measured. This experiment provides, thus, access to the complex transmission t and the complex reflection r,

$$t \equiv \frac{\langle E_T(z,t) \rangle}{\mathcal{E}^a_{\mathrm{in}}(z,t)} \quad \text{and} \quad r \equiv \frac{\langle E_R(z,t) \rangle}{\mathcal{E}^a_{in}(z,t)}.$$

These are also the kind of signals measured in circuit QED experiments [44]. The mean fields oscillate at the frequency of the pump. Therefore, at moderate powers $p \sim 1$, $|t|^2 + |r|^2 \neq 1$, even for $\beta = 1$. That is, incoherent atomic contributions (fluctuations) prevent energy conservation at that particular frequency.

---

harmonic oscillator. Therefore, the problem reduces to two resonantly coupled classical harmonic oscillators, where one of them is imposed to oscillate sinusoidally with a well defined frequency. The solution of the other oscillator in steady-state is shown to be proportional to exactly the same sinusoidal function, apart from a $\pi/2$ phase shift. Evidently, the same effect happens between the dipole and its emitted field. Hence, another $\pi/2$ phase is added, creating a $\pi/2 + \pi/2 = \pi$ phase shift in the emitted field with respect to the incoming one.

In the steady-state regime, the explicit solution reads

$$t = 1 + \eta\chi \quad \text{and} \quad r = \eta\chi. \tag{1.52}$$

In both extreme low and high saturated regimes the transmission and transmittance coincide, $|t|^2 \to T$, as well as reflection and reflectance, $|r|^2 \to R$. The equality holds in the highly saturated regime because the signals are normalized by the incoming pump, so the contribution from the atom becomes negligible as compared to the huge incoming coherent power.

1.3.2 Field second-order correlation functions

Now we study the field second-order correlation functions [6]. They evidence quantum aspects of the field that are not captured by the average intensities [1] and are measured in Hanbury Brown and Twiss experiments [51].

The definitions for the transmission and reflection channels read

$$g_{T(R)}^{(2)}(t, t+\tau) = \frac{\langle E_{T(R)}^{\dagger}(t) E_{T(R)}^{\dagger}(t+\tau) E_{T(R)}(t+\tau) E_{T(R)}(t) \rangle}{\langle E_{T(R)}^{\dagger}(t) E_{T(R)}(t) \rangle \langle E_{T(R)}^{\dagger}(t+\tau) E_{T(R)}(t+\tau) \rangle}. \tag{1.53}$$

The numerator describes the probability density that a photon is detected at time t and another at time $t+\tau$. The position dependence is hidden.

We compute the correlations in the long-time (steady-state) limit, $g_{T(R)}^{(2)}(t_\infty, t_\infty + \tau)$, in the extreme linear regime, $p = 0.0001$, using quantum regression theorem [19, 49]. The result is equivalent to that from Ref.[42].

Fig.1.6 shows $g_R^{(2)}(t_\infty, t_\infty + \tau)$. No interference between input and emitted fields take place in the reflected channel. Therefore, the correlation is characteristic from a single two-level system in free space. That is, the reflected field shows antibunching [19], featuring the signature of a single-photon source.

The photon correlation in the transmitted field, Fig.1.7, is in clear contrast: instead of anti-bunching, it performs a huge bunching. Actually, the bunching diverges ($g_T^{(2)}(0) \to \infty$) in the perfect waveguide limit ($\beta \to 1$) [42, 52]. This is due to the interference
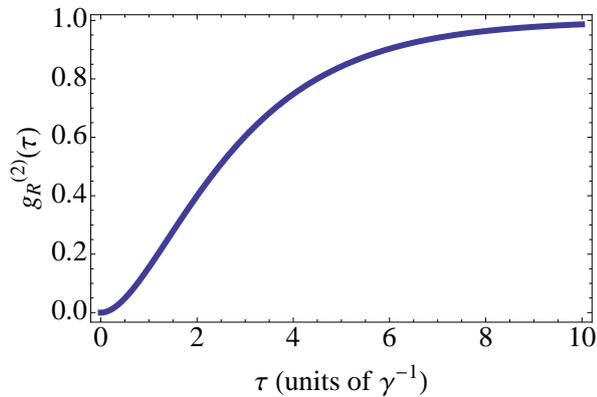
Figure 1.6: Antibunching arising from spontaneous emission as measured in the reflection channel.
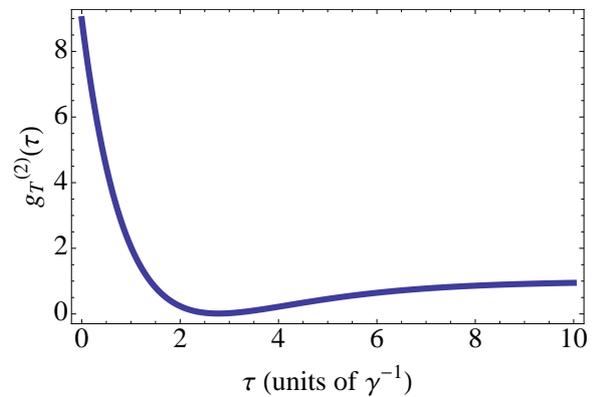
Figure 1.7: Huge bunching arising from destructive interference in the transmission channel.

between incoming and emitted fields, that reduces arbitrarily close to zero the chance of a single-photon to pass by the atom. But, whenever it does, it can only have been because of a two-photon fluctuation of the incoming coherent field, that instantaneously saturates the atom, making it transparent and thus letting the photon pair being transmitted. In both figures, $\beta = 2/3$.

1.4   Reversible stimulated emission at the single-photon level

The concept of stimulated emission has been introduced by Einstein in the problem of black-body radiation spectrum [4]. Its signatures appear both in matter and field. Stimulated emission affects the atomic dynamics, that can realize accelerated emission [14, 53] or negative absorption [54]. It also induces emission in the stimulating mode. In what follows, we study stimulated emission in 1D atoms by inverting its population [55], as illustrated in Fig.1.8. We explore both the transient and the steady-state regimes.
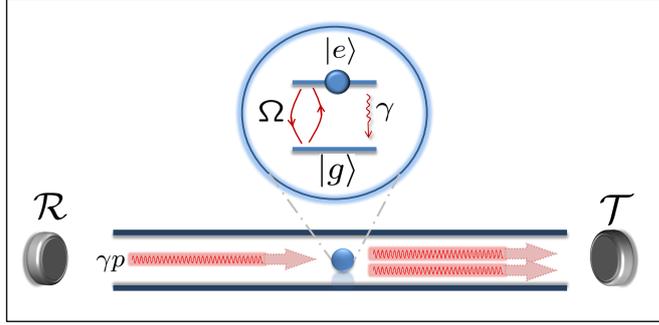
Figure 1.8: A monochromatic laser of power p stimulates the emission of an excited atom. Atomic emission is accelerated, performing negative absorption, while light is preferentially emitted in the stimulating mode a_{ν_L}.

1.4.1   Power gain and negative absorption in 1D atoms

From Eq.(1.48), we find for the 1D atom

$$\mathcal{T} = \gamma p + \Omega\Re[\langle S_-\rangle] + \frac{\gamma\beta}{2}\left(\langle S_z\rangle + \frac{1}{2}\right) \tag{1.54}$$

and

$$\mathcal{R} = \frac{\gamma\beta}{2}\left(\langle S_z\rangle + \frac{1}{2}\right), \tag{1.55}$$

valid for all atomic regimes. The reflected power is simply proportional to the excited state population. It can thus be interpreted as a spontaneous emission contribution, which feeds equally the transmission and reflection channels. It also feeds the side-emission channel if $\beta < 1$, defined by $\mathcal{S} = (1-\beta)(\langle S_z\rangle + 1/2)$. The transmission channel carries the incoming power γp plus an interference term, $\Omega\Re[\langle S_-\rangle]$. This interference term plays a key role in the 1D geometry under study, as it gives destructive interference in the perfect reflection scenario or constructive interference in the present scenario.

Following the notations of a seminal paper by Mollow [54], we point out that the atomic coherent absorption rate is described by

$$\mathcal{W} = -\Omega\Re[\langle S_-\rangle], \tag{1.56}$$

as it can be seen from the optical Bloch equations (1.58). Then, we identify from Eqs.(1.54) and (1.55) that the net transmitted power $\mathcal{T} - \gamma p$, when compared to the reflected one $\mathcal{R}$, yields precisely the negative of the atomic absorption rate $\mathcal{W}$, related to the interference term,

$$\mathcal{T} - \gamma p - \mathcal{R} = -\mathcal{W}. \tag{1.57}$$

This means that *gain in transmission power*, $\mathcal{T} - \gamma p > \mathcal{R}$, is followed by a *negative absorption* rate $\mathcal{W} < 0$ of the atom. So, light is emitted in the stimulating mode a_{ν_L}, breaking the spontaneous emission symmetry between net transmission and reflection.

These signatures of stimulated emission, peculiar to 1D atoms, are explored in the following subsections. Both transient and steady-state regimes are analyzed. In the former, inversion of population assumed as the initial condition. In the latter, inversion is obtained through incoherent pump.

1.4.2 Direct monitoring: transient regime

To analyse the transient regime, we prepare the atom in the excited state $|e\rangle$ at the initial time $t = 0$, and follow the temporal evolution of the field powers and the atomic excited-state population.

The case $p = 0$ corresponds to spontaneous decay, characterized by the exponential $\exp(-\gamma t)$ in Fig.(1.9). Increasing the pump power reduces the time the atom spends excited, stimulating its emission. However, stimulated emission does not happen to make the atomic decay faster, but reversible: this is the nonlinear regime of Bloch equations, characterized by the coherent exchange of photons between the atom and the field (Rabi oscillations) at the rate Ω. This regime is reached when Ω overcomes the typical dephasing and damping rates γ and γ^*. When $\gamma^* = 0$, this condition simplifies to $p \sim \beta^{-1}$ [see Eq. (1.58)], which corresponds to $p \sim 1$ in the ideal 1D case plotted in the figure. Therefore, a single photon per lifetime is enough to saturate a 1D atom, as previously evidenced.

If $\beta < 1$, a higher pump power will be necessary to reach the nonlinear regime. Single-
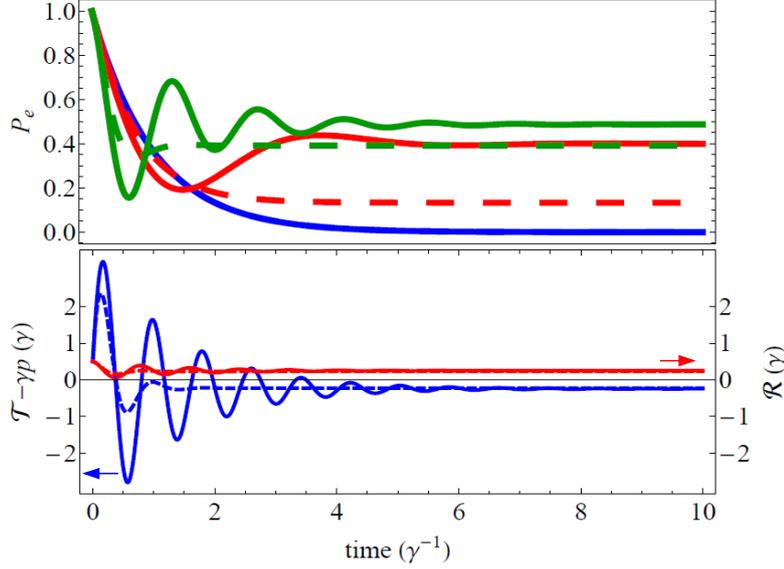
Figure 1.9: Top: Excited-state population $P_e(t)$ as a function of time (in units of γ^{-1}) for $p = 0$ (blue, monotonic decrease), $p = 1$ (red, lower-frequency oscillation), and $p = 10$ (green, higher-frequency oscillation). Bottom: $\mathcal{T} - \gamma p$ (blue, left arrow) and $\mathcal{R}$ (red, right arrow; both in units of γ) for $p = 30$, showing that net transmission overcomes reflection whenever stimulated emission takes place, in the transient regime. Remind that $\mathcal{R} \propto P_e$. Dashed curves correspond to $\gamma^* = 10\gamma$. For all cases, $\beta = 1$.

photon sensitivity is also altered by pure dephasing, as is shown in Fig. 1.9 where we have plotted the population with $\gamma^* = 10\gamma$, a typical value for quantum dots [56] (note that this is an upper bound, pure dephasing rates as low as $\gamma^* = 0.15\gamma$ being currently reached in circuit QED [44]). Still, with realistic parameters, the power needed to reach stimulation remains of the order of a few photons per lifetime, so that the great sensitivity of the device is preserved.

Fig.(1.9) shows the evolution of the radiated fields in the regime of stimulated emission, $p = 30$. Rabi oscillations are also visible in the reflected and transmitted fields. In particular, one observes that each decrease in $\mathcal{R}$ corresponds to the stimulated emission of a photon, which feeds the transmission channel. These processes have $\mathcal{T} - \gamma p > \mathcal{R}$,

confirming that the "stimulated channel" $\mathcal{T}$ is favored. Note that, on the other hand, if the atom is initially prepared in the ground state $|g\rangle$, emission is favored in the reflection channel at the initial time, as we have already discussed.

1.4.3 Direct monitoring: steady-state regime
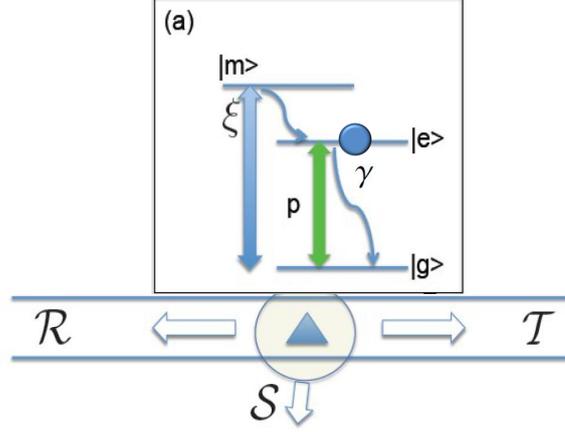
Figure 1.10: Level scheme of the 1D-atom, inverted under incoherent pumping. Incoherent pump can be obtained by weakly and resonantly pumping an ancilla level $|m\rangle$ and adiabatically eliminating it afterwards.

Steady-state population inversion is obtained by an incoherent pumping, in our modeling. It can be introduced in Bloch equations by a rate ξ obeying two conditions: it destroys coherence and inverts population, so that $P_e(\xi \to \infty) = 1$,[4]

$$\frac{d}{dt}\langle S_-\rangle = -\left(\frac{\gamma + \gamma^* + \xi}{2} - i\delta_L\right)\langle S_-\rangle + \Omega\,\langle S_z\rangle,$$

$$\frac{d}{dt}\langle S_z\rangle = -(\gamma + \xi)\left(\langle S_z\rangle + \frac{1}{2}\right) + \xi - \Omega\,\Re[\langle S_-\rangle]. \tag{1.58}$$

It is worth mentioning that this pump mechanism can be effectively described by a third ancilla level (denoted by $|m\rangle$ in Fig.1.11) coherently pumped at rate γ_p that decays towards $|e\rangle$ at rate γ_e. When $\gamma_p \ll \gamma_e$ the ancilla can be adiabatically eliminated, and we are left with an effective incoherent pump rate $\xi \approx 4\gamma_p^2/\gamma_e$ for the two-level system.

Now we study the influence of the resonant light on the steady-state $(d\langle S_-\rangle/dt = d\langle S_z\rangle/dt = 0)$ atomic population P_e and radiated fields $\mathcal{R}$ and $\mathcal{T} - \gamma p$ [55]. The population is pictured in Fig. 1.11 as a function of p. We have plotted the results for two

---

[4]The corresponding Lindbladian is $\mathcal{L}_\xi[\rho] = -\frac{\xi}{2}(\sigma_-\sigma_+\rho + \rho\sigma_-\sigma_+ - 2\sigma_+\rho\sigma_-)$.

different values of the incoherent pump $\xi = 3\gamma$ and 15γ, yielding two different population inversions when $p = 0$. We also show the net total rate of photons emitted by the atom,

$$N \equiv \mathcal{T} - \gamma p + \mathcal{R} + \mathcal{S}. \tag{1.59}$$

Moreover, we have defined and plotted the ratios $\beta_R(\beta_T)$ of photons emitted in the reflection (transmission) channel in the following way:

$$\beta_R \equiv \frac{\mathcal{R}}{N} \quad \text{and} \quad \beta_T \equiv \frac{\mathcal{T} - \gamma p}{N}. \tag{1.60}$$

These quantities measure the propensity of the atom to emit in the reflection (transmission) channels and appear as natural figures of merit for stimulated emission in steady-state. Two regimes can be observed in the figure. A vanishing pump $p \to 0$ gives rise to an incoherent regime characterized by the spontaneous emission of photons. The excited-state population reads $P_e = \frac{\xi}{\gamma + \xi}$ and the net total rate of emitted photons is $N = \gamma P_e$. In this regime, no channel is favored, and the net transmitted and reflected fields are equal.

Increasing the pump p to arbitrarily high values sets up the coherent regime of Rabi oscillations. The excited-state population P_e decreases, eventually becoming equal to the ground-state population P_g, which is the usual limit of Bloch equations when the atom is saturated [49]. This means that the more coherent power is injected in the input channel, the less intensely light is reflected, given that the reflected power and excited state population are proportional. Simultaneously, the net total rate of photons increases to $N = \xi/2$. This is an unusual situation where the emitted light power does not follow the same evolution as the atomic population. As a matter of fact, the rate N represents the rate of photons exchanged between the atom and the field, which scales as the Rabi frequency Ω and increases with the pump power p. Simultaneously, the transmission channel is markedly favored with respect to the reflection channel ($\beta_T > \beta_R$ [5]). The transition between these two regimes happens when

$$p > p_{\text{th}} = \frac{(\gamma + \gamma^* + \xi)(\gamma + \xi)}{4\beta\gamma^2},$$

---

[5] note that $\beta_T \to 1$ if ξ is sufficiently large, but still smaller than p (only for $\beta = 1$, of course).

which simplifies to $p_{\text{th}} = \frac{1}{4}(1 + \frac{\xi}{\gamma})^2$ for $\beta = 1$ and $\gamma^* \ll \gamma$. This confirms that Rabi oscillations appear when coherent processes, quantified by p, overcome incoherent ones, quantified by ξ. As in the transient case, pure dephasing and lower β increase the threshold needed to reach the coherent regime, up to values that remain of the order of a few photons per lifetime in the physical systems modeled.
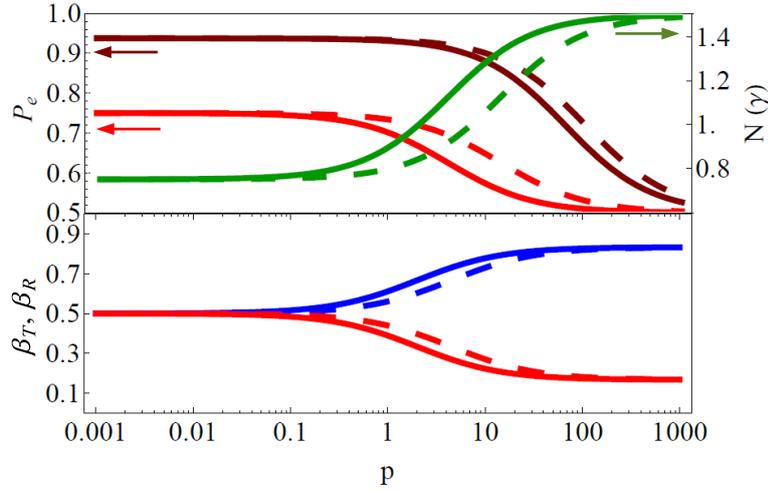
Figure 1.11: Top: Steady-state population (red, left arrows) of the excited level (proportional to reflected power) as a function of the resonant pump for $\xi = 3\gamma$ (light red, lower) and 15γ (dark red, upper). Increasing net rate of emitted photons N (green, right arrow; in units of γ) ranging from γP_e to $\xi/2$ (plotted with $\xi = 3\gamma$). Bottom: Ratios β_T (blue, upper) and β_R (red, lower) showing predominance of emission in the transmission channel for $p > 1$. Dashed curves: $\gamma^* = 10\gamma$. We took $\beta = 1$.

The analytic solutions for the atomic averages are shown below:

$$\langle S_- \rangle = -\left(\frac{\gamma - \xi}{\gamma + \xi}\right) \frac{\gamma\sqrt{2p\beta}(\gamma + \gamma^* + \xi + 2i\delta_L)}{(\gamma + \gamma^* + \xi)^2 + (2\delta_L)^2 + 4\gamma^2 p\beta\left(\frac{\gamma + \gamma^* + \xi}{\gamma + \xi}\right)}, \tag{1.61}$$

and

$$P_e = \frac{\xi}{\gamma + \xi} + \left(\frac{\gamma - \xi}{\gamma + \xi}\right) \frac{2\gamma^2 p\beta\left(\frac{\gamma + \gamma^* + \xi}{\gamma + \xi}\right)}{(\gamma + \gamma^* + \xi)^2 + (2\delta_L)^2 + 4\gamma^2 p\beta\left(\frac{\gamma + \gamma^* + \xi}{\gamma + \xi}\right)}. \tag{1.62}$$

Note, from Eq.(1.61), that the destructive interference which causes perfect reflection is turned into a constructive interference, causing stimulated emission, when ξ becomes larger than γ. This can be seen by the change of sign in $\langle S_- \rangle$, implying a change of sign in the interference term $\Omega \Re[\langle S_- \rangle]$. At the same time, Eq.(1.62) shows population getting inverted when ξ crosses γ.

1.4.4   Indirect monitoring
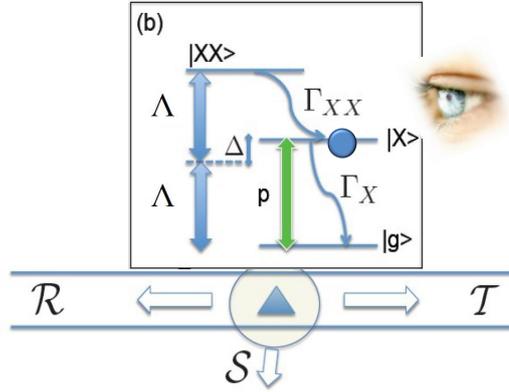
Figure 1.12: Level scheme of the 1D-atom, in the quantum-dot case (exciton $|X\rangle$ and biexciton $|XX\rangle$), under coherent two-photon excitation at rate Λ^2/Δ. By directly observing transition $|XX\rangle \to |X\rangle$, one obtains information on the net transmitted power, indirectly.

Measurement of the ratios β_R and β_T is experimentally quite demanding. As a matter of fact, it requires the ability to quantify the total power radiated by the atom, in particular the net transmitted power $\mathcal{T} - \gamma p$, and hence to filter the pump to extract a tiny atomic emission. Therefore, we propose [55] an experimentally feasible way to measure this quantity, by exploiting a third atomic level $|XX\rangle$ as pictured in Fig. 1.13. This three-level structure can model the biexcitonic and the excitonic transitions of a quantum dot [33, 57], a terminology that we shall use from now on without losing the generality of the scheme. Population inversion on the excitonic transition ($P_X > P_g$) is reached by resonantly pumping a biexciton in the dot using the two-photon-

absorption technique. This mechanism can be described by an effective Hamiltonian $H_{2\mathrm{ph}} = \hbar\Lambda^2/\Delta(|XX\rangle\langle g|e^{-i\nu t} + \mathrm{H.c.})$, where $\Delta = (E_{XX} - E_X)/2$ and Λ is the Rabi frequency of the pump [58]. As usual, Lindbladians describe the decays $|XX\rangle \to |X\rangle$, with rate Γ_{XX}, and $|X\rangle \to |g\rangle$, with rate Γ_X.

The populations of the excitonic P_X and biexcitonic states P_{XX} are computed in the steady-state regime, as a function of the resonant probe p. The results are plotted in Fig. 1.13. When $p = 0$, the presence of a large pump power $\Lambda^2/\Delta > \Gamma_{XX}$ leads to equalization of the populations of the ground and biexcitonic states, whereas detailed balance conditions require $P_X/P_{XX} = \Gamma_{XX}/\Gamma_X$. The usual quantum dot parameters satisfy $\Gamma_{XX} \approx 2\Gamma_X$ [33], leading to $P_{XX} = P_g = 1/4$ and $P_X = 1/2$. Increasing the probe power p leads to the depletion of the excitonic level because of stimulated emission, and thus to the increase of the steady-state biexcitonic population, as is shown in Fig. 1.13. This increase can be monitored by measuring the rate of photon emission $\Gamma_{XX}P_{XX}$ at the biexcitonic frequency, which provides an easily observable signature of stimulated emission at the single-photon level.

Moreover, we have verified from the equations for the three levels that

$$\Gamma_{XX}P_{XX} = \Gamma_X P_X - \mathcal{W}[p] = N, \tag{1.63}$$

where $\mathcal{W}[p]$ is the interference term between the probe and the light emitted at the excitonic frequency, as defined in Eq.(4.27), and N is the net total rate of photons, from Eq.(1.59). Namely, the rate of photon emission in the biexcitonic line exactly equals the rate N emitted in the excitonic one, taking into account stimulated processes. Stimulated emission of the excitonic transition can thus be simply monitored by measuring the rate of photon emission at the biexcitonic frequency. This rate can be used to build the ratio β_R defined above, without having to measure the net transmitted power. This is also represented in Fig. 1.13, where we have plotted

$$\beta_R^{3\mathrm{L}} = \frac{\frac{\Gamma_X}{2}P_X}{\Gamma_{XX}P_{XX}}, \tag{1.64}$$

the index $3L$ standing for three levels. This definition simply comes from the fact that

$\mathcal{R} = \frac{\gamma}{2} P_e = \frac{\Gamma_X}{2} P_X$, in addition to Eq.(1.63) and the definition for $\beta_R = \mathcal{R}/N$. For the sake of comparison, we have plotted on the same figure the quantity β_R defined in the case of a two-level atom. The equivalence between the models is clearly shown in the coincidence of the two curves for low power p ($\Omega = \gamma\sqrt{2\beta p} < \Lambda^2/\Delta$). A divergence becomes unavoidable when p is strong enough to generate Autler-Townes splitting [59] of the ground level. The biexcitonic transition thus becomes out of resonance with the driving field. So the population of the biexciton state drastically decreases, making the ratio $\beta_R^{3\mathrm{L}}$ arbitrarily large and equalizing exciton and ground-state populations.

A possible drawback of experiments performed with quantum dots can be imperfect two-photon absorption, leading to incoherent feeding of the excitonic level via phonons, even for large Δ [60]. However, a recent experimental work [61] shows that the two-photon transition can be made very clean, so that the incoherent exciton pumping is negligible in this case. Finally, note that a scheme to fully protect entanglement has been proposed using the same mechanism of biexcitonic pumping and readouts of the light emitted in each possible transition [62].
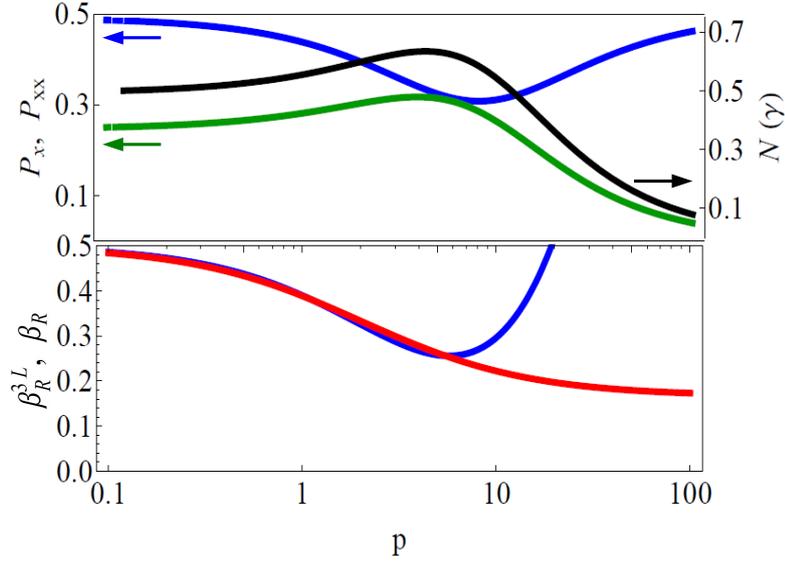
Figure 1.13: Top: Populations (left arrows) P_X (blue, upper) and P_{XX} (green, lower) of the three-level system *vs* p. Net rate of photon emission N (black, right arrow; in units of γ) in the exciton transition. Bottom: Comparison between the ratios of emission given by the two (β_R, red, lower) and three (β_R^{3L}, blue, upper) levels, assuming $\xi \sim 3\gamma$ and $\Lambda^2/\Delta \sim 4\Gamma_X$. In both cases, $\gamma^* = 0$ and $\beta = 1$.

1.4.5 Field second-order correlation functions

We finish the chapter with a brief discussion that naturally arises in this context, namely, whether photon bunching occurs in the transmitted field as a consequence of stimulated emission.

Fig.1.4.5 (left) shows $g_T^{(2)}(\tau)$ at $p = 1$ and $\xi = 4\gamma$. Indeed, it shows a tiny bunching at initial times of $g^{(2)}(0) = 1.2$.

Fig.1.4.5 (right) shows that this value decreases for increasing p, though. That is because the coherent field contributions dominate over the atomic signature for $p \gg 1$, leading to $g^{(2)}(0) \to 1$. In Fig.1.4.5 (right) we plot $g^{(2)}(0)$ as a function of the coherent pump power p, for fixed $\xi = 4\gamma$. We see that for vanishing pump, $p \to 0$, the atom is inverted and spontaneously emitting single photons, thus realizing antibunching. We

then increase the pump and see that bunching happens around the standard value for stimulation, $p \sim 1$. Then, for $p \gg 1$, the coherent pump overcomes the stimulated emission, making a mostly classical field in the transmission channel, $g^{(2)}(0) = 1$. Note that in the correlation function one cannot simply subtract the incoming power to have access to the net transmitted field, as done in the previous analysis with the field intensities. A possible strategy to effectively filter the pump could be to compute cross-correlations between transmitted and reflected fields ($\propto \langle E_T^\dagger(t) E_R^\dagger(t+\tau) E_R(t+\tau) E_T(t) \rangle$). Intuitively, one can expect that stimulation appears as vanishing cross-correlation at $\tau = 0$. The reason would be that once a photon is detected at the transmitted channel the other photon, emitted by stimulation, should also be found in the transmitted channel and not in the reflected one.
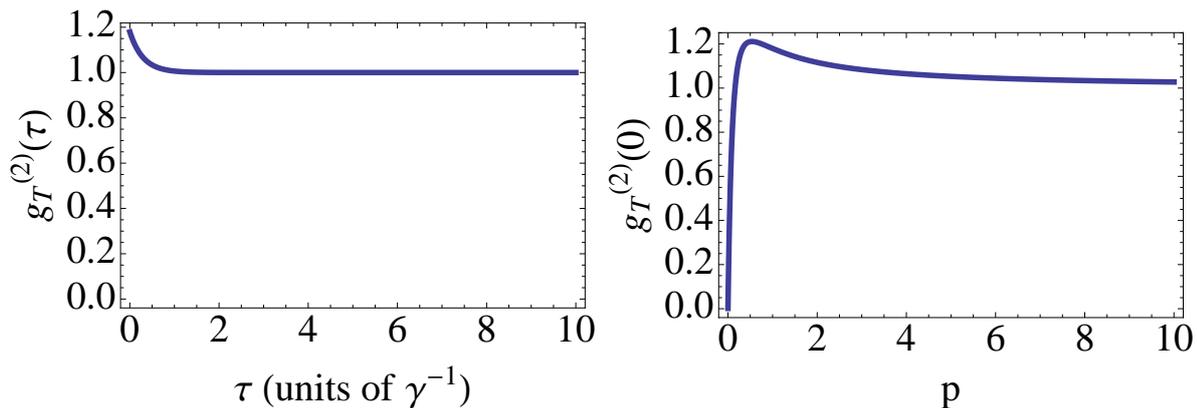
Figure 1.14: Left– Second-order correlation function $g^{(2)}(\tau)$ as a function of the time delay τ (in units of γ^{-1}), for $\xi = 4\gamma$ and $p = 1$. A tiny bunching occurs in the transmitted channel. Right – Second-order correlation function $g^{(2)}(0)$ as a function of power p, for $\xi = 4\gamma$. For low powers, there is antibunching coming from the atomic inversion of population. For moderate powers $p \sim 1$, there is a tiny bump coming from stimulated emission, which generates a two-photon correlated state. For huge powers $p \gg 1$, the coherent pump contribution surpasses the atomic emission, so the field becomes mostly classical again, i.e., with poissonian distribution $g^{(2)}(0) = 1$.

1.5 Conclusions

In the first part of this chapter we presented the one-dimensional atom. It has been characterized by means of the electric fields in the output channels and the atomic evolution, given by the optical Bloch equations. In that context, we have shown the dipole induced reflection that arises through destructive interference between incoming and emitted fields. We have also demonstrated the giant optical nonlinearity of 1D atoms, at the single-photon level.

In the second part, we have evidenced signatures of stimulated emission at the single-photon level, giving rise to potentially observable effects with state-of-the-art solid-state atomic devices interacting with 1D light fields. In particular, we propose an experiment to probe the stimulated (optical) transition, based on the monitoring of an ancillary transition.

Chapter 2

Optimal irreversible stimulated emission

Things should be made as simple as possible, but not any simpler.

Albert Einstein

In Chapter 1 we have investigated optical properties of 1D atoms when probed by a monochromatic classical field. In particular, we have shown that it can behave either as a perfect mirror for beams of very low intensity, based on dipole-induced reflection, or as an amplifier, based on stimulated emission. The single-photon sensitivity of those effects are due to the fact that the coupling with 1D modes are much stronger than the coupling with 3D free-space modes. In principle, this can be achieved in a strongly dissipative directional cavity [37, 38, 47, 45, 63]. However, the perspectives offered by a genuinely broadband waveguide go way beyond cavity-based schemes, as it allows for free propagation of wavepackets with finite bandwidth. In Chapters 2 and 3, we explore regimes where this broadband aspect is of utmost importance, allowing for effects that could not be obtained otherwise.

In Chapter 2, we describe a fully quantized dynamics in a semi-infinite waveguide, where the input field is a single photon, and investigate emission stimulated by a single-

photon wavepacket. This situation is drastically different from stimulated emission obtained by a classical pump, as it is by essence irreversible. The effective lifetime of the atom is reduced by a factor of 2, which is optimal. Contrary to what could be expected, this optimization occurs when the spectral linewidth of the incoming photon packet is three times as large as the atomic linewidth.

2.1 The semi-infinite 1D waveguide
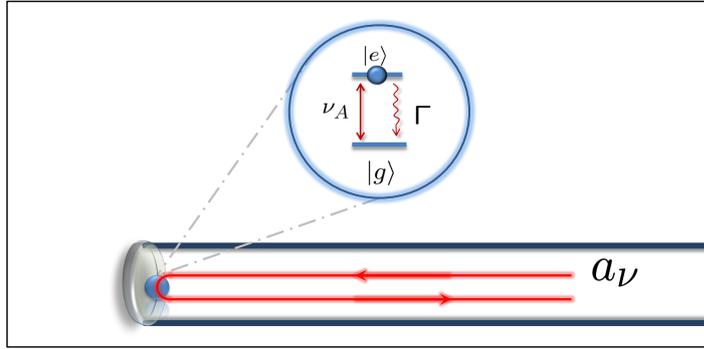
Figure 2.1: Illustrative representation of the semi-infinite 1D waveguide model, involving a single input channel and a single output channel.

We focus on the case in which a semi-infinite waveguide is coupled to a two-level system. This is modeled by the new Hamiltonian $H = H_{\text{field}} + H_{\text{atom}} + H_{\text{int}}$, where propagation occurs in the a modes [64],

$$H_{\text{int}} = -i \sum_{\nu=0}^{\infty} \hbar g_\nu \left[a_\nu \sigma_+ - \text{H.c.} \right]. \tag{2.1}$$

The semi-infinite waveguide model corresponds, in principle, to a physical situation where a mirror [65], or a metallic nanotip [66], is placed close to the atom, as illustrated in Fig.2.1. It has been chosen because it maximizes stimulation, as discussed below. The atom and field Hamiltonians are unchanged, $H_{\text{field}} = \sum_{\nu=0}^{\infty} \hbar \nu \, a_\nu^\dagger a_\nu$ and $H_{\text{atom}} = \hbar \nu_A \, \sigma_+ \sigma_-$.

2.1.1   Single-excitation subspace

Describing the complete light-matter system with a pure quantum state $|\psi(t)\rangle$ is suitable for the problem under consideration, where the number of excitations is conserved. In the case of a two-level system in the single-excitation subspace,

$$|\psi(t)\rangle = \psi_A(t) \, |e, 0\rangle + \sum_{\nu=0}^{\infty} \phi_\nu(t) \, a_\nu^\dagger |g, 0\rangle. \tag{2.2}$$

The temporal evolution follows from Schrödinger equation,

$$\frac{\partial}{\partial t} \psi_A = -i\nu_A \psi_A - \sum_\nu g_\nu \phi_\nu$$

and

$$\frac{\partial}{\partial t} \phi_\nu = -i\nu \phi_\nu + g_\nu \psi_A. \tag{2.3}$$

In the following we solve the equations above for two different initial conditions.

Spontaneous emission: the Wigner-Weisskopf theory revisited

The spontaneous emission scenario ideally corresponds to the initial condition of an inverted atom $\psi_A(0) = 1$ and the field in vacuum state $\phi_\nu(0) = 0$. We formally integrate Eq.(2.3),

$$\phi_\nu(t) = \int_0^t dt' \, g_\nu \, e^{-i\nu(t-t')} \psi_A(t') \tag{2.4}$$

and substitute it back into the equation for ψ_A,

$$\frac{\partial}{\partial t} \tilde{\psi}_A(t) = -\sum_{\nu=0}^{\infty} 2g_\nu^2 \int_0^t dt' \, e^{-i(\nu-\nu_A)(t-t')} \tilde{\psi}_A(t') \tag{2.5}$$

in the frame rotating at the atomic frequency $\psi_A(t) = \tilde{\psi}_A(t)e^{-i\nu_A t}$. Within Markovian approximation, the time integration gives $\pi\delta(\nu - \nu_A)$ as real part and the imaginary part
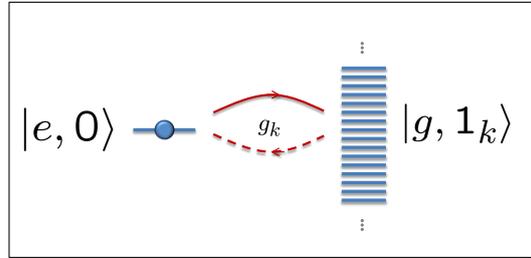
Figure 2.2: Level scheme for spontaneous emission. The atom-field starts at state $|e, 0\rangle$ and irreversibly decays towards the continuum $|g, 1_k\rangle$. The dashed arrow represents the virtual reabsorption that leads to g_k^2 in the coupled equations.

gives the usual frequency shift, so that

$$\frac{\partial}{\partial t}\tilde{\psi}_A(t) = -\frac{\Gamma}{2}\tilde{\psi}_A(t), \tag{2.6}$$

where $\Gamma = \sum_{\nu=0}^{\infty} 2\pi g_\nu^2 \delta(\nu - \nu_A) = 2\pi g_A^2 \rho_{1D}$, as derived by Fermi golden rule. Thus, $\psi_A(t) = \psi_A(0)e^{-(\Gamma/2+i\nu_A)t}$ so the excited-state population is

$$|\psi_A(t)|^2 = \exp\left(-\Gamma t\right). \tag{2.7}$$

We finally define the real-space representation for the spontaneously emitted photon,

$$\phi(r,t) = \sum_{\nu=0}^{\infty} \phi_\nu(t)\ e^{ik_\nu r}, \tag{2.8}$$

in which we substitute Eq.(2.4), giving

$$\phi(r,t) = \int_0^t dt' \psi_A(t') \sum_{\nu=0}^{\infty} g_\nu\ e^{i\nu\left(\frac{r}{c}-(t-t')\right)}.$$

By assuming the continuum limit $\sum_\nu \to \int d\nu\ \rho_{1D}$ and $g_\nu \approx g_A$, we find that

$$\phi(r,t) = 2\pi g_A \rho_{1D}\ \Theta(r)\Theta\left(t - \frac{r}{c}\right)\ \psi_A\left(t - \frac{r}{c}\right), \tag{2.9}$$

where $\Theta(r)$ is the Heaviside step function. Combining the above result with the solution of Eq.(2.6), we find

$$\phi(r,t) = \sqrt{2\Gamma\pi\rho_{1D}}\ \Theta(r)\Theta\left(t - \frac{r}{c}\right)e^{-\left(\frac{\Gamma}{2}+i\nu_A\right)\left(t-\frac{r}{c}\right)}. \tag{2.10}$$

The resulting wavepacket will be used as the initial condition in the dynamics of stimulated emission. Eqs.(2.7) and (2.10) are Wigner-Weisskopf theory [67] applied to the 1D geometry.

Single-photon scattering: the π-phase shift revisited

In Chapter 1 we have shown that a monochromatic coherent field of very low power is reflected by the 1D atom with a π-phase shift. Here we revisit this effect in the case where the atom scatters a single-photon wavepacket. The atom initially in ground state

$|g\rangle$, $\psi_A(0) = 0$. The initial photon packet has been spontaneously emitted by another ficticious atom,

$$\phi(r,0) = \mathcal{N}\Theta(-r)e^{\left(\frac{\Delta}{2}+i\nu_L\right)\frac{r}{c}}, \tag{2.11}$$

where $\mathcal{N}^2 = 2\pi\rho_{1D}\Delta$ is the normalization factor and Δ is the packet linewidth, i.e., its inverse gives the typical time duration of the pulse. The monochromatic condition is obtained in the $\Delta \ll \Gamma$ limit. The central frequency of the photon is ν_L, so that the detuning is $\delta_L = \nu_L - \nu_A$.

Given the new initial conditions, the evolution equations become

$$\frac{\partial}{\partial t}\psi_A = -\left(\frac{\Gamma}{2} + i\nu_A\right)\psi_A - \sqrt{\frac{\Gamma}{2\pi\rho_{1D}}}\phi(-ct,0) \tag{2.12}$$

and

$$\phi(r,t) = \phi(r - ct, 0) + \sqrt{2\pi\rho_{1D}\Gamma}\,\Theta(r)\Theta\left(t - \frac{r}{c}\right)\psi_A\left(t - \frac{r}{c}\right). \tag{2.13}$$

We integrate the excited-state amplitude, finding

$$\psi_A(t) = -\sqrt{\Gamma\Delta}\,e^{-\left(\frac{\Gamma}{2}+i\nu_A\right)t}\left[\frac{e^{\left(\frac{\Gamma-\Delta}{2}-i\delta_L\right)t} - 1}{\frac{\Gamma-\Delta}{2} - i\delta_L}\right].$$

Note that in the monochromatic limit $\Delta \ll \Gamma$ the atom acquires almost no excitation $|\psi_A(t)|^2 < 4\Delta/\Gamma \ll 1$. Still in the $\Delta \ll \Gamma$ regime, and at resonance ($\delta_L = 0$), we find the outgoing wavepacket

$$\phi(r,t) \approx \phi(r - ct, 0) - 2\,\mathcal{N}\Theta(t - r/c)e^{-\left(\frac{\Delta}{2}+i\nu_A\right)(t-r/c)} = -\phi(r - ct, 0), \tag{2.14}$$

where we have neglected the relatively fast decaying spontaneous contribution $\exp(-\Gamma t)$. The outgoing field is π-phase shifted with respect to the highly monochromatic input field [68].

2.2 Single-photon packet interacting with excited 1D atom

The calculations in the previous section were a prelude to the study of stimulated emission by a single propagating photon [69]. From now on the two-excitation subspace
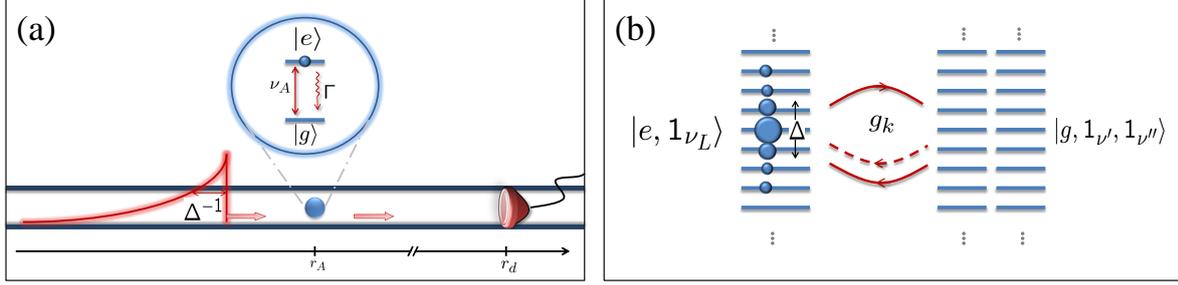
Figure 2.3: (a) Real-space scheme of the two-level atom at position r_A stimulated by a single photon pulse of size Δ^{-1}. The spontaneous decay rate is Γ and the transition frequency is ν_A. The direction indicated by the arrows is the only allowed one. The light field is detected by a photodetector positioned at r_d, put sufficiently far from the atom. (b) The same scheme, in frequency domain. The photon is prepared centered at ν_L with linewidth Δ. The dashed arrow represents spontaneous emission (virtual reabsorption) while the solid arrow represents real reabsorption of the atom.

is considered, where the incoming packet is scattered by an initially excited atom. The new Ansatz is constructed as

$$|\psi(t)\rangle = \sum_{\nu=0}^{\infty} \psi_\nu(t)\, a_\nu^\dagger |e,0\rangle + \sum_{\nu_1,\nu_2=0}^{\infty} \phi_{\nu_1,\nu_2}(t)\, a_{\nu_1}^\dagger a_{\nu_2}^\dagger |g,0\rangle, \qquad (2.15)$$

that evolves according to the Schrödinger equation,

$$\frac{\partial}{\partial t}\psi_\nu = -i(\nu_A + \nu)\psi_\nu - 2\sum_{\nu'=0}^{\infty} g_{\nu'}\phi_{\nu,\nu'}, \qquad (2.16)$$

and

$$\frac{\partial}{\partial t}\phi_{\nu,\nu'} = -i(\nu + \nu')\phi_{\nu,\nu'} + \frac{1}{2}(g_{\nu'}\psi_\nu + g_\nu\psi_{\nu'}). \qquad (2.17)$$

Our initial state of interest is an excited atom with an incoming photon wavepacket centered at frequency ν_L and having linewidth Δ, $|\psi(0)\rangle = \sum_{\nu=0}^{\infty} \psi_\nu(0)\, a_\nu^\dagger |e,0\rangle$, as illustrated in Fig.2.3. The two-photon components satisfy $\phi_{\nu_1,\nu_2}(0) = 0$.

2.2.1   Excited state amplitude in real-space representation

Here again we adopt a real space representation of the quantum state,

$$\psi(r,t) \equiv \sum_{\nu=0}^{\infty} \psi_\nu(t) \, e^{ik_\nu r},$$

where $k_\nu = |\vec{k}_\nu| = \nu/c$. With the help of the transformation

$$\sum_\nu \nu \, \psi_\nu e^{ik_\nu r} = -ic\partial_r \sum_\nu \psi_\nu e^{ik_\nu r}, \tag{2.18}$$

we rewrite Eq. (2.16) in the form

$$\left[\frac{\partial}{\partial t} + c\frac{\partial}{\partial r}\right] \psi(r,t) = -i\nu_A \, \psi(r,t) - 2\sum_{\nu,\nu'} g_{\nu'} \, \phi_{\nu,\nu'} e^{ik_\nu r}. \tag{2.19}$$

Note that in the trivial uncoupled case $g_\nu = 0$ the solution to the equation above is simply a product of a free time-dependent atomic evolution $f(t) = \exp(-i\nu_A t)$ and a propagating pulse $p(r - ct)$, where $p(r)$ is the initial pulse wavefunction.

We integrate Eq.(2.17),

$$\phi_{\nu,\nu'}(t) = \frac{1}{2} \int_0^t [g_{\nu'}\psi_\nu(t') + g_\nu\psi_{\nu'}(t')]e^{-i(\nu+\nu')(t'-t)}, \tag{2.20}$$

choosing the initial condition $\phi_{\nu,\nu'}(0) = 0$, and reinsert it into Eq.(2.19). We assume the fast rotating reference frame, $\psi(r,t) = \tilde{\psi}(r,t)\exp(-i\nu_A t)\exp(-i\nu_L(t - r/c))$, where ν_L is the central frequency of the incident wavepacket. The first term arising from the substitution is

$$\int_0^t dt'\tilde{\psi}(r - c(t - t'),t')\sum_{\nu'} g_{\nu'}^2 e^{-i(\nu'-\nu_A)(t-t')} = \frac{\Gamma}{2} \, \tilde{\psi}(r,t),$$

under Markovian approximation. The decay constant is $\Gamma \equiv \sum_{\nu'} 2\pi g_{\nu'}^2 \delta(\nu' - \nu_A)$, just as before. The other term plays the role of a source and can be shown to satisfy

$$\sum_{\nu,\nu'} g_{\nu'} \int_0^t g_\nu\psi_{\nu'}(t')e^{-i(\nu+\nu')(t'-t)}e^{ik_\nu r} = \Gamma\Theta(r)\Theta(t - r/c)e^{-i\delta_L r/c}\tilde{\psi}(-r,t - r/c),$$

under the usual approximations $g_\nu \approx g_{\nu_A}$ and the continuum limit $\sum_\nu \to \int d\nu \rho_{1D}$. Finally, we have been able to eliminate self-consistently the dependence on the two-photon amplitude, finding

$$\left[\frac{\partial}{\partial t} + c\frac{\partial}{\partial r}\right] \tilde{\psi}(r,t) = -\frac{\Gamma}{2} \, \tilde{\psi}(r,t) - \Gamma \, \Theta(r)\Theta(t - r/c)e^{-i\delta_L r/c}\tilde{\psi}(-r, t - r/c). \quad (2.21)$$

As expected, in the high detuning limit, $\delta_L \gg \Gamma$, the solution is simply $\tilde{\psi}(r,t) = e^{-\frac{\Gamma}{2}t}\tilde{\psi}(r - ct, 0)$, i.e., the product of a decaying atom and a freely propagating photon. The general solution for Eq.(2.21) reads

$$\tilde{\psi}(r,t) = \quad \tilde{\psi}(r - ct, 0) \, e^{-\frac{\Gamma}{2}t} - \Gamma \, \Theta(r) \, \Theta(t - r/c) \, e^{-\frac{\Gamma}{2}t} \, e^{-\left(\frac{\Gamma}{2} - i\delta_L\right)(t - r/c)}$$

$$\times \int_{t - r/c}^{t} e^{\left(\frac{\Gamma}{2} - i\delta_L\right)t'} \, \tilde{\psi}(-ct', 0) \, dt', \quad (2.22)$$

where the initial condition of the wavepacket is written in $\tilde{\psi}(r, 0)$. Here we study the case of an incident photon of exponential shape, as if it had been spontaneously emitted by a neighboring atom of natural linewidth Δ and central frequency ν_L, i.e.,

$$\psi(r, 0) = \mathcal{N}e^{\left(\frac{\Delta}{2} + i\nu_L\right)\frac{r}{c}}\Theta(-r),$$

where $\mathcal{N}^2 = 2\pi\rho_{1D}\Delta$ stands for normalization, just as in Eq.(2.11) and illustrated in Fig.2.3.

2.2.2   Two-photon amplitude in real-space representation

The two-photon component are also defined in real space as

$$\phi(r_1, r_2, t) \equiv \sum_{\nu, \nu'} \phi_{\nu, \nu'}(t)e^{ik_\nu r_1 + ik_{\nu'} r_2}.$$

Within the same approximations done before, we find

$$\phi(r_1, r_2, t) = \quad \sqrt{\frac{\pi\rho_{1D}\Gamma}{2}}[\Theta(t - r_2/c)\Theta(r_2)\psi(r_1 - r_2, t - r_2/c)$$

$$+\Theta(t - r_1/c)\Theta(r_1)\psi(r_2 - r_1, t - r_1/c)] \quad (2.23)$$

written in the original reference frame. In the limit of vanishing interaction between the incoming photon and the atom (e.g., $\delta_L \gg \Gamma$), the two-photon wavefunction consist in a symmetrized product of two independent single-photon wavefunctions, one describing spontaneous emission ($\psi_{\text{sp.em.}}(r,t) = \exp[-(\Gamma/2 + i\nu_A)(t - r/c)]$) and another describing the free propagation of the field ($\psi_{\text{free prop.}}(r - ct, 0)$).

In the limit of $t_\infty \gg 1/\Gamma$, the excitations are entirely in the field and the dynamics also reduces to free propagation, so that one can define the function ϕ_∞ satisfying

$$\phi(r_1, r_2, t_\infty) = \phi_\infty(ct_\infty - r_1, ct_\infty - r_2). \tag{2.24}$$

2.3 Time-resolved signatures of stimulated emission

We address now the signatures of stimulated emission. We first compute the excited-state population of the atom $\rho_{ee}(t)$ as a function of time. We define an effective lifetime τ_{eff} of the atom and show that such quantity is minimized when stimulation takes place. The light field is characterized by the two-time correlation function $G^{(2)}(t, t + \tau)$, which shows optimal photon bunching.

2.3.1 Excited-state population dynamics

The reduced density matrix for the atom is obtained by tracing out the field. Its excited-state population is given by the matrix element corresponding to the $|e\rangle$ state,

$$\rho_{ee}(t) = \langle e | \text{Tr}_{\text{field}}[|\psi(t)\rangle\langle\psi(t)|] |e\rangle = \frac{1}{2\pi\rho_{1D}c} \int_{-\infty}^{\infty} |\psi(r,t)|^2 \, dr.$$

Given our choice for the initial state, it reads

$$
\begin{aligned}
\rho_{\text{ee}}(t) &= e^{-(\Gamma+\Delta)t} \left\{ 1 + |1 + Q|^2 (e^{\Delta t} - 1) + |Q|^2 \frac{\Delta}{\Gamma}(e^{\Gamma t} - 1) \right. \\
&\quad \left. - 2\Re \left[(Q^* + |Q|^2) \frac{2\Delta}{\Gamma + \Delta + 2i\delta} (e^{\frac{\Gamma + \Delta + 2i\delta}{2}t} - 1) \right] \right\},
\end{aligned}
\tag{2.25}
$$

where we have defined the factor $Q \equiv 2\Gamma/(\Gamma - \Delta - 2i\delta_L)$ and $\Re$ stands for the real part. First, we note that in the strongly detuned case $\delta_L \gg \Gamma$ ($Q \to 0$), the atom is

transparent to the incident photon,

$$\rho_{ee}(t)|_{\delta_L \to \infty} = \exp(-\Gamma t),$$

and spontaneous emission is recovered.

Optimal stimulation

By definition, stimulation is optimal when it minimizes the effective atomic lifetime. The adimensional effective lifetime is defined here as

$$\tau_{\text{eff}} \equiv \Gamma \int_0^\infty \rho_{\text{ee}}(t) \ dt.$$

Using Eq.(3.9) at resonance, $\delta_L = 0$, we find

$$\tau_{\text{eff}} = 1 - \frac{4\Gamma}{\Gamma + \Delta} + \frac{8\Gamma^2}{(\Gamma + \Delta)^2}, \tag{2.26}$$

which is minimized at

$$\Delta = 3\Gamma \quad \Rightarrow \quad \tau_{\text{eff}} = \frac{1}{2}. \tag{2.27}$$

Note that the wavepacket presenting mode matching with spontaneous emission, $\Delta = \Gamma$, does not stimulate atomic decay, $\tau_{\text{eff}} = 1$, in contrast to intuition.

Eq.(2.27) shows that effective atomic lifetime is reduced by a factor of 2 in the optimal case. In what follows, we present the limitations of simple analogies or explanations to the effect we present in this chapter.

Can $\tau_{\text{eff}} = 1/2$ be explained simply from rate equations?

An intuitive derivation of the optimal effective lifetime can be obtained by modelling the 1D atom as an ultimate gain medium, e.g. a single emitter initially inverted, irreversibly decaying into a collection of modes $\{n_j\}$. Einstein rate equations for the excited-state population can be written [4, 53]

$$\frac{d}{dt}\rho_{\text{ee}} \stackrel{?}{=} -\Gamma(1 - \beta)(1 + n_l) \ \rho_{\text{ee}} - \Gamma(1 + n_k)\beta \ \rho_{\text{ee}}, {}^1$$

---

[1] The symbol " $\stackrel{?}{=}$ " expresses hypothesis. The equations where it appears are a naïve explanation for the reduction of the effective lifetime of the emitter, as if it could be explained using standard laser theory. We show

where n_k is the number of photons in the stimulating mode, n_l the number of photons in the other modes. β is the fraction of coupling with the one-dimensional (1D) channel with respect to the 3D continuum of modes, as defined in the previous chapter [55]. Let us assume that $n_l = 0$. In the conventional 3D scenario, $\beta \ll 1$, the emitter's decay is not modified unless $n_k > \beta^{-1}$. In the 1D case under consideration, $\beta = 1$, a single photon, $n_k = 1$, is enough to stimulate the transition and shorten the lifetime by a factor of 2,

$$\dot{\rho}_{ee} \stackrel{?}{=} -2\Gamma \rho_{ee}.$$

Even though it is intuitive, this simplified picture does not capture all the physics of the problem. The atomic evolution presented here does not obey a rate equation, justifying the Hamiltonian resolution adopted here. To give an example, let us consider the best stimulation condition, $\Delta = 3\Gamma$. In that case,

$$\rho_{ee} = -2e^{-4\Gamma t} + 3e^{-3\Gamma t}, \tag{2.28}$$

so

$$\frac{d\rho_{ee}}{dt} = 8\Gamma e^{-4\Gamma t} - 9\Gamma e^{-3\Gamma t} \neq -2\Gamma \, \rho_{ee}, \tag{2.29}$$

clearly evidencing a difference between standard laser systems and the present scenario.

Can optimal irreversible stimulation be reached with a cavity?

In non-dissipative monomode cavities, the dynamics of the two-excitation subspace is accelerated by a $\sqrt{2}$ factor when compared to the single-excitation subspace, $g_{\nu_A} \to \sqrt{2}g_{\nu_A}$ [67]. This $\sqrt{2}$ factor yields optimal stimulation, but reversible. To understand roughly the link between the $\sqrt{2}$ factor and $\tau_{\text{eff}}^{-1} = 2$, a naïve (but incomplete, as shown by Eq.(2.29)) analysis can be applied, describing stimulation by a modified decay rate, in a Fermi golden rule framework: $\Gamma \propto g_{\nu_A}^2 \to (\sqrt{2}g_{\nu_A})^2 \propto 2\Gamma$.

In a dissipative cavity, atomic emission cannot be optimally stimulated by an additional photon injected in the mode of the cavity. As a matter of fact, this photon would

---

in Eq.(2.29) that the novel effect we find cannot be explained by that naïve explanation.

escape the cavity in a typical time $1/\kappa$, way too fast to stimulate any atomic emission that would take place on κ/g^2, where the atom-cavity coupling strength g checks in the weak coupling regime $g \ll \kappa$. Hence, stimulated emission by a single photon can only be simultaneously optimal and irreversible with pulse-shaped photons propagating in broadband waveguides.

Another important remark is that no stimulation occurs when one substitutes the two-level system inside the waveguide by a single-mode cavity of good quality ($\kappa \sim \Gamma$). As it is shown by Rephaeli and Fan [70], the reduction of the effective lifetime is absent in that case, i.e., $\tau_{\text{eff}}^{\text{cav}} > 1$ for all finite Δ. This reinforces the fundamental need for nonlinearity to generate stimulated emission.

Stimulation is irreversible

The dynamics described by Eq.(2.25) is completely different from the one obtained through a classical pump, as studied in the previous chapter, where stimulated emission was reversible (classical Rabi oscillations). Reversible dynamics is also found in monomode cavities in the strong coupling regime, where a single photon in the cavity stimulates the emission of an excited atom, which reabsorbs back the excitation (quantum Rabi oscillations).

Here, although emission is stimulated by a single photon, no strong coupling takes place. That is, optimal stimulation is irreversible in 1D atoms. This fact can be seen from Eq.(2.29), which shows that excited-state population never increases under ideal stimulation $\Delta = 3\Gamma$, $\frac{d\rho_{\text{ee}}}{dt} = \Gamma e^{-4\Gamma t}(8 - 9e^{\Gamma t}) \leq 0$.

Other regimes shown by $\rho_{\text{ee}}(t)$ and $\tau_{\text{eff}}(\Delta)$

Fig. 2.4 shows the plots of Eqs.(2.25) and (2.26). The case $\Delta \gg \Gamma$ corresponds to a very short pulse in time and also gives rise to free propagation of the pulse followed by spontaneous atomic decay ($\tau_{\text{eff}} = 1$) as the spectral overlap with the atom is negligible.

On the opposite case, a highly monochromatic photon ($\Delta \ll \Gamma$) increases the effective
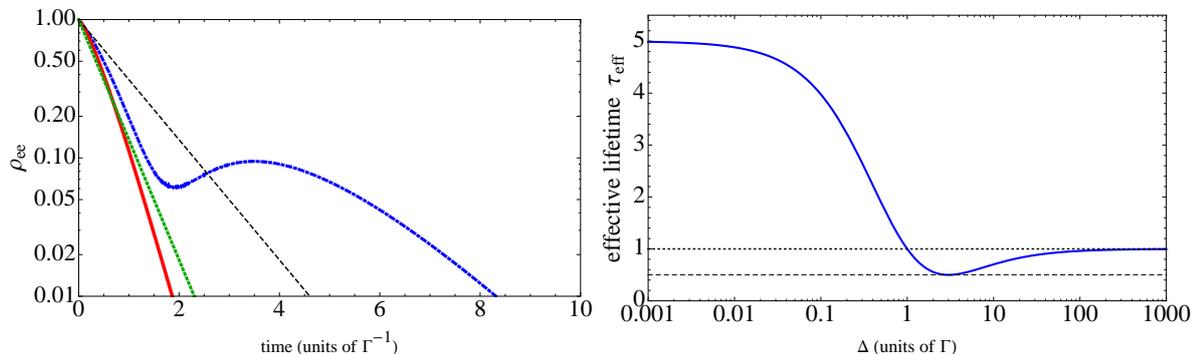
Figure 2.4: Left – Excited-state population $\rho_{ee}(t)$. The blue dot-dashed curve, for $\Delta = \Gamma$, shows stimulation for very short times and reabsorption after $2\Gamma^{-1}$. The red solid curve represents the maximally stimulated relaxation, for $\Delta = 3\Gamma$, which for times smaller (bigger) than Γ^{-1} goes above (below) the reference $\exp{(-2\Gamma t)}$ (green dotted). The black dashed curve represents the spontaneous emission evolution $\exp{(-\Gamma t)}$. Right – Effective population lifetime τ_{eff} as a function of Δ. The dashed line indicates the optimal value $\tau_{\text{opt}} = 1/2$.

lifetime due to the efficient absorption of the incident wavepacket, after the atom has spontaneously relaxed.

If $\Delta = \Gamma$, the integrated effect of the stimulation exactly compensates for the total absorption and $\tau_{\text{eff}} = 1$. The atom can absorb a tail from the incoming photon after having emitted, causing a small re-excitation bump. This effect reduces the efficiency of the stimulating process. To lower such chance for the atom to absorb the incoming photon, a shorter packet in time domain must be prepared, or equivalently, a pulse larger then the atom in frequency domain. Shortening of the atomic lifetime induced by stimulation can be observed for $\Gamma < \Delta \lesssim 100\Gamma$. The case where $\Delta = 3\Gamma$ minimizes the reabsorption effect.

2.3.2 Temporal correlations in the output field

A consequence of the atomic relaxation enhancement is the emergence of bunching in the output field. Photodetection signals are registered with a detector positioned

at $r_d \gg c/\Gamma$ as pictured in Fig.2.5, so that all the excitations are in the light field. This regime corresponds to free propagation, so that the characteristics of the field only depend on the variable $r - ct$ and eq.(2.24) is valid. We shall use the reference frame of the photodetector, of origin r_d and $t_d = r_d/c$. The density of probability to detect one click at time t and one click at time $t + \tau$ is obtained from the second-order correlation function [7] that in our case checks

$$G^{(2)}(t, t+\tau) = |\phi_\infty(ct, c(t+\tau))|^2.$$

From Eqs.(2.22) and (2.23), we find for $\tau > 0$

$$G^{(2)}(t, t+\tau) = \Delta\Gamma e^{-(\Gamma+\Delta)t} \left|(1+Q)e^{-\frac{\Gamma}{2}\tau} + (1-Q)e^{-\left(\frac{\Delta}{2}+i\delta_L\right)\tau}\right|^2, \qquad (2.30)$$

where $Q = 2\Gamma/(\Gamma - \Delta - 2i\delta_L)$ is the effective coupling factor as defined in the atomic population dynamics. A clear interpretation can be given to the expression above. Between time t and time $t + \tau$, the system is projected on the single excitation subspace, giving rise to two interfering quantum paths. In one case, the first click comes from the incident field. The remaining excitation is in the atom, that will finally spontaneously relax: this corresponds to the dynamics $\exp[-\Gamma\tau/2]$ of weight $1 + Q$. In the other case, the photon emitted by the atom clicks before the incident one. This second situation, related to stimulated emission, gives rise to the component $\exp[-(\Delta/2 + i\delta_L)\tau]$ weighted by $1 - Q$. The condition $1 + Q = 0$ allows to cancel spontaneous emission and to maximize stimulated emission. This is obtained exactly for $\Delta = 3\Gamma$ and $\delta_L = 0$, i.e., the very same condition that minimizes the atomic lifetime.

This optimal regime for stimulated emission leads to the emission of both photons in a typical time $1/3\Gamma$, giving rise to bunching in the output field. The effect can be observed on Fig.2.5, where we have plotted the probability $P(\tau_{\text{final}})$ of detecting the two photons within a time τ_{final},

$$P(\tau_{\text{final}}) = \int_0^{\tau_{\text{final}}} d\tau \int_0^\infty dt \, G^{(2)}(t, t+\tau) \qquad (2.31)$$

at resonance, for different values of the parameter Δ. The fastest convergence is obtained for $\Delta = 3\Gamma$. Keeping this optimal value of Δ we have plotted the same function, on Fig.

2.5, for different detunings, clearly showing as well the importance of the resonance on the stimulation efficiency.
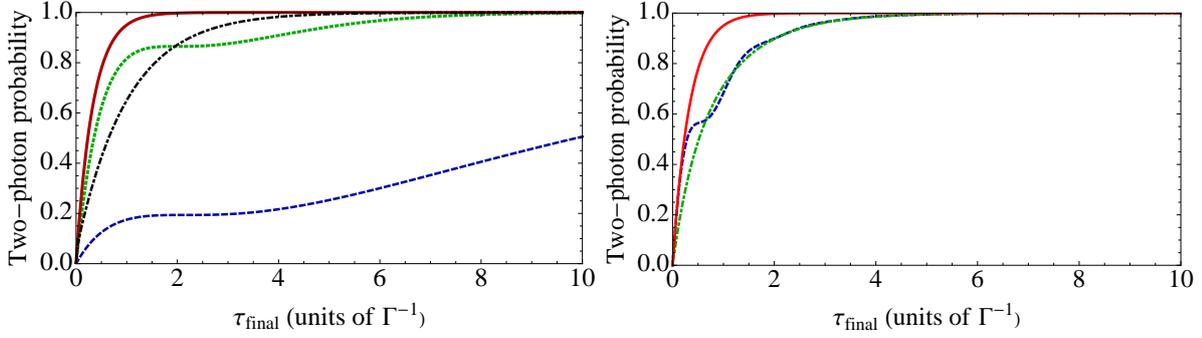
Figure 2.5: Left – Probability $P(\tau_{\text{final}})$ of detecting 2 photons within a time interval τ_{final} for $\Delta = 0.1\Gamma$ (blue), 1Γ (green), 3Γ (red), and 100Γ (black). Right – Same function at $\Delta = 3\Gamma$ for different detunings: $\delta_L = 0$ (red), $\delta_L = 5\Gamma$ (blue), and $\delta_L \to \infty$ (green).

2.4 Applications to amplification

Stimulated emission can be exploited to obtain preferential emission of light in the stimulated mode rather than in other empty modes. With this aim, we explore in this section the case of an atom interacting with two one-dimensional electromagnetic fields a and b, the former containing a single propagating photon and the latter being in the vacuum state. Two paradigmatic systems are considered in the light of the time-resolved study performed above (see Fig.2.6). The first is a two-level atom in a transmitting/reflecting infinite waveguide [70], where the fields a and b correspond respectively to photons propagating to the right and to the left. In this case, an amplification of the classical information encoded in the direction of propagation of the photon is obtained. The other system is a lambda-shaped three level atom in a semi-infinite waveguide [71], the fields a and b corresponding to photons of two orthogonal polarizations in the half waveguide. This corresponds to amplification of the quantum information encoded in the polarization of the incoming photon.
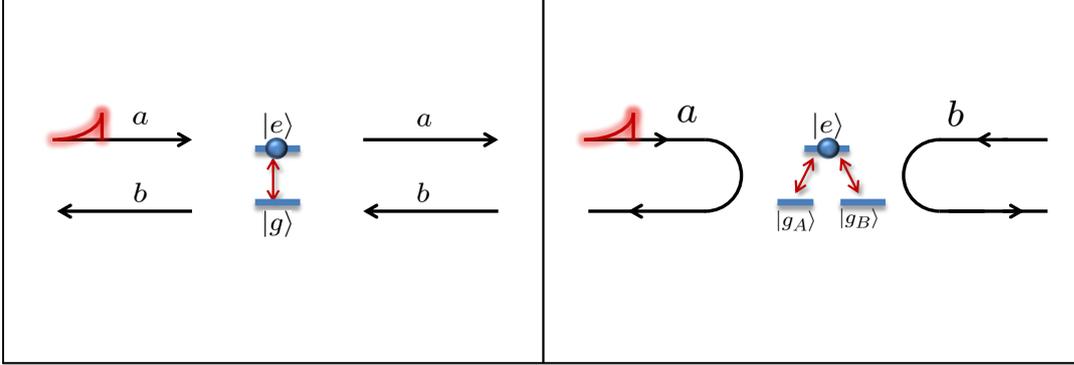
Figure 2.6: Comparison between different types of two-continua of modes in 1D atoms. On the left, the reflection b/transmission a are the two degrees of freedom. On the right, the degrees of freedom are represented by the a/b polarizations. The decay of the excited-state population is the same in both cases. In contrast, the probabilities of emission in each channel, p_{ab} and p_{bb}, crucially differ.

2.4.1 Two-level atom in a transmitting/reflecting waveguide

Atomic population dynamics

The Hamiltonian for such system reads $H = H_{1D} + H_{atom} + H_{int}$ and the new interaction is given by

$$H_{int} = -i \sum_{\nu=0}^{\infty} \hbar g_\nu \left[(a_\nu + b_\nu)\sigma_+ - \text{H.c.} \right], \qquad (2.32)$$

where a_ν is the forward and b_ν is the backward propagating modes [48]. Following the approach from Ref.[70], one can decompose the problem in two parts by using the even $\hat{e}_\nu = (a_\nu + b_\nu)/\sqrt{2}$ and odd $\hat{o}_\nu = (a_\nu - b_\nu)/\sqrt{2}$ field modes. The new interaction Hamiltonian (2.32) depends only on the even modes,

$$H_{int}^e = -i \sum_{\nu=0}^{\infty} \hbar \sqrt{2} g_\nu \left[\hat{e}_\nu \sigma_+ - \text{H.c.} \right], \qquad (2.33)$$

while the odd modes contribute only to the free evolution. The spontaneous emission rate Γ' of the transmitting 1D atom is doubled with respect to the case of an atom in a closed waveguide, i.e. $\Gamma' = 2\Gamma$, which is due to the doubling of the resonant modes available for atomic relaxation[2].

In the case of stimulated emission under study, the initial state of the field writes $|1_a, 0_b\rangle$, which checks $|1_a, 0_b\rangle = (|1_o, 0_e\rangle + |0_o, 1_e\rangle)/\sqrt{2}$, where $|1_o\rangle$ (resp. $|1_e\rangle$) is the corresponding propagating photon in the odd (resp. even) mode. Hence, the system can have two equiprobable dynamics, stimulated and spontaneous emission, so that the excited state population of the full transmitting/reflecting 1D atom checks

$$\rho_{\text{ee}}^{\text{full}}(t) = \frac{1}{2} \ \rho_{\text{ee}}^{\text{semi}}(t) + \frac{1}{2} \ e^{-\Gamma't}, \tag{2.34}$$

in terms of the population $\rho_{\text{ee}}^{\text{semi}}(t)$ of the semi-infinite two-level 1D atom.

As previously, the minimal value of the effective atomic lifetime for this system is obtained at $\Delta = 3\Gamma'$. Because of intrinsic spontaneous emission in odd modes, the effective lifetime is averaged and increases to $\tau_{opt} = 3/4$ as demonstrated in [70].

Potential for single-photon amplification

The emission in the stimulated mode is conveniently quantified by the density of probability $G_{aa}^{(2)}(t, t+\tau)$ of detecting a click at time t and $t+\tau$ in that mode. In both the transmitting/reflecting waveguide and the lambda systems this is given by

$$G_{\text{aa}}^{(2)}(t, t+\tau) = \Delta\Gamma' e^{-(\Gamma'+\Delta)t} \left|(1+Q_f) \ e^{-\frac{\Gamma'}{2}\tau} + (1-Q_f) \ e^{-\left(\frac{\Delta}{2}+i\delta_L\right)\tau}\right|^2, \tag{2.35}$$

where $Q_f = \Gamma'/(\Gamma' - \Delta - 2i\delta_L) = Q/2$ is the new effective coupling factor. Again, the term evolving like $e^{-\Gamma'\tau/2}$ corresponds to spontaneous emission of the atom in mode a while the second term, $e^{-\left(\frac{\Delta}{2}+i\delta_L\right)\tau}$, is linked to stimulated emission of the atom in the same mode. Extinction of spontaneous emission is realized when $1+Q_f = 0$. This yields $\Delta_{opt} = 2\Gamma'$, a condition which does not minimize the effective lifetime, as it was the

---

[2]Note that this result is consistent with the definition from the previous chapter, $\gamma_1 = \Gamma'$, obtained from a Heisenberg picture formalism.

case in the half waveguide case. Nevertheless, it maximizes the probability p_{aa} that two photons are emitted in the stimulated mode a. This signature of stimulated emission is analogous to the net transmitted power in the semiclassical problem. We have calculated that[3]

$$p_{\mathrm{aa}} = \frac{\Delta}{2\Gamma'} \frac{4 + \Delta/\Gamma'}{(1 + \Delta/\Gamma')^2}, \qquad (2.36)$$

that visibly reaches its maximum, $p_{aa} = 2/3$, at $\Delta = 2\Gamma'$ [70]. The signature of optimal stimulation we have used for atomic population is now found in the field:

$$p_{\mathrm{aa}} = 2\,(p_{\mathrm{ab}} + p_{\mathrm{bb}}), \qquad (2.37)$$

that is, emission in the stimulated mode is twice more probable than emission in the empty modes. p_{ij} is the probability of one photon emitted in mode i and another in j.

A convenient figure of merit for this device is the fidelity of copying the incident photon $(a \rightarrow aa)$,

$$\mathcal{F} = p_{\mathrm{aa}} + \frac{p_{\mathrm{ab}}}{2}, \qquad (2.38)$$

which provides access to the amplification ratio $\mathcal{A}$, defined below, and to the average number of transmitted photons $N_T \equiv 2\mathcal{F}$, in the transmitting waveguide case. It gives the transmission fidelity $\mathcal{F}^T$ in the present case and also the cloning fidelity in the lambda case.

For the transmitting/reflecting waveguide case,

$$p_{\mathrm{ab}} = \frac{1 + (\Delta/\Gamma')^2}{2(1 + \Delta/\Gamma')^2} \qquad (2.39)$$

and, evidently, $p_{\mathrm{bb}} = 1 - (p_{\mathrm{aa}} + p_{\mathrm{ab}})$. With results (2.36) and (2.39) we can plot the function $\mathcal{F}^T$ (see Fig.2.7), where the superscript simply specifies the transmitting waveguide case.

The transmitting atom can be used as an ultimate gain medium to efficiently amplify the classical state of the photon, encoded in the direction of propagation. The convenient

---

[3]a detailed explanation of this result is reserved for Chapter 3.

criterium in that case is the amplification ratio (called *visibility* in [72] and *gain* in [44])

$$\mathcal{A} \equiv \frac{\mathcal{F}_{opt}^T(\delta_L = 0) - \mathcal{F}^T(\delta_L \to \infty)}{\mathcal{F}^T(\delta_L \to \infty)}. \tag{2.40}$$

The upper bound for the amplification ration is $\mathcal{A}_{max} = 1/9$. This can realized by noting that $\mathcal{F}_{\max} = 5/6$, obtained when $p_{aa} = 2/3$ and $p_{ab} = 1/3$. Besides, $\mathcal{F}^T(\delta_L \to \infty) = 3/4$, given that $p_{aa} = p_{ab} = 1/2$, as expected from a completely spontaneous emission scenario. This upper bound is not reached in the transmitting waveguide case. This is due to the nonvanishing chance of double reflection, $p_{bb} \neq 0$, as previously discussed. The transmission fidelity is plotted in fig.2.7 as a function of the packet linewidth, its maximal value being $\mathcal{F}_{opt}^T = (39/40) \times (5/6)$, that is,

$$\mathcal{F}_{opt}^T = 97,5\% \times \frac{5}{6},$$

reached at $\Delta = 3\Gamma'$. We find then $\mathcal{A} = 1/12 \approx 8,3\%$, that means almost one order of magnitude higher than previously reported gains, around $\sim 1\%$ [72, 44], working in the regime where the probe is continuous as studied in the previous chapter and in Ref. [55].

The short wavepacket limit ($\Delta \gg \Gamma'$) corresponds to the spontaneous emission regime, where the incoming packet passes by without interacting and the atom has a chance of one half to emit to each side. Then, $p_{aa} = p_{ab} = 1/2$ and, of course, $\mathcal{F}^T(\Delta \to \infty) = \mathcal{F}^T(\delta_L \to \infty) = 3/4$. The opposite limit is much more interesting, though. In that case, the photon is highly diluted in time. It then keeps scattering through the atom much after it has spontaneously emitted. The incident photon is also highly monochromatic ($\Delta \ll \Gamma'$). These are the precise conditions for dipole induced reflection, studied in Chapter 1. Indeed, the spontaneous emission feeds equally both channels and the incident photon is totally reflected, so that $p_{aa} = 0$ and $p_{bb} = p_{ab} = 1/2$.
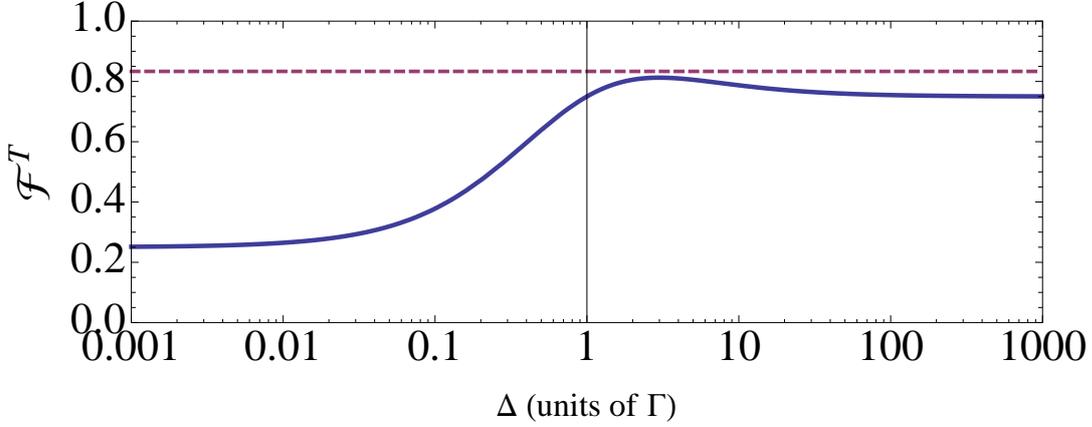
Figure 2.7: Transmission fidelity $\mathcal{F}^T$ as a function of the packet width Δ. The optimal value is $\mathcal{F}^T_{opt} = 97,5\% \times (5/6)$, found for $\Delta = 3\Gamma'$. The dashed line indicates the maximal value $\mathcal{F}^T_{max} = 5/6$.

2.4.2 Lambda-shaped atom in reflecting waveguide

Atomic population dynamics

In the case of a three level atom in the lambda configuration coupled to a half waveguide, the initially excited atom $|e\rangle$ can decay by emitting an a or a b polarized photon, ending up in state $|g_a\rangle$ or $|g_b\rangle$ respectively. The interaction Hamiltonian writes now

$$H_{\text{int}} = -i \sum_{\nu=0}^{\infty} \hbar g_\nu \left[(a_\nu \sigma_a^\dagger + b_\nu \sigma_b^\dagger) - \text{H.c.} \right],\tag{2.41}$$

where $\sigma_a = |g_a\rangle\langle e|$ and $\sigma_b = |g_b\rangle\langle e|$ are the lowering atomic operators. As above, the spontaneous emission rate is doubled, and the system evolution in the presence of a single propagating photon in mode a also splits into two paths, namely spontaneous emission in mode b, or stimulated emission in mode a. This formal analogy leads to the same excited-state population decay as in Eq.(2.34), and thus to the same conditions of minimization of the effective atomic lifetime.

Potential for quantum cloning

The crucial difference between these two systems is embodied in the probability for each photon being emitted in a different channel p_{ab} and, consequently, also in p_{bb}. This difference comes from the fact that after having spontaneously emitted a photon in mode b, the atom in state $|g\rangle$ can still interact with the incoming field in mode a. Thus, it is possible to finally get two photons in mode b, so that $p_{bb} \neq 0$, lowering the fidelity. This situation is forbidden for a lambda atom that relaxes in state $|g_b\rangle$ and becomes transparent to the incoming field, making $p_{\mathrm{bb}} = 0$, for all Δ.

By preventing emission of two photons in the unwanted mode b, $p_{\mathrm{bb}} = 0$ and p_{aa} is given by Eq.(2.36). Thus, $p_{\mathrm{ab}} = 1 - p_{\mathrm{aa}}$. This implies that $p_{\mathrm{ab}} = 1/3$ when $p_{\mathrm{aa}} = 2/3$, at $\Delta = 2\Gamma'$, which means that, contrary to the transmitting waveguide case, the lambda atom saturates the upper bound for the fidelity, $\mathcal{F}_{\mathrm{max}} = 5/6$. In Chapter 3 we show the connection between this fidelity and optimal universal quantum cloning.

2.5   Conclusions

We have shown the influence of the incoming photon on the atom decay as a function of the packet shape. An irreversible and maximally accelerated stimulated emission occurs for the broadband mode-matching condition where the incoming photon is three times shorter than the spontaneously emitted one. We have also studied the influence of stimulation on the output field two-photon correlation function, which shows optimal photon bunching.

Finally, we added a second one-dimensional field to explore quantum and classical amplification. In the classical case, amplification has been shown in the average transmitted field, which reaches 97.5% of the ideal case. This effect has led to a transistor-like amplification that can overcome the continuous-wave approach by a factor 8. In the quantum case, the possibility to achieve universal optimal cloning of polarization has been announced and will be explored in the next chapter.

Chapter 3

Cloning and entanglement in 1D atoms

> *Physics is like sex: sure, it may give some practical results,*
>
> *but that's not why we do it.*
>
> *Richard Feynman*

The present chapter is devoted to an application of irreversible stimulated emission in 1D atoms to quantum cloning, as announced in the previous chapter. We show that a three-level atom in a semi-infinite waveguide achieves both optimal and universal quantum cloning [71].

Quantum cloning is a key concept in quantum mechanics as well as in quantum information science. If it could be implemented in a perfect manner, that would allow the ascertainment of the exact state of a single quantum system by replicating it as far as needed. However, perfect quantum cloning of an arbitrary state is not at all possible, as establishes the so called no-cloning theorem [74]. This fact guarantees the impossibility of faster-than-light communication through quantum nonlocality [75, 76]. It can also be applied in quantum cryptography, since any eavesdropper who tries to copy the shared quantum information will be detected, in principle. Interestingly, a finite optimal bound

exists for quantum cloning. Understanding the limits and implementations of optimal quantum cloning is still an open problem.

Another key concept in quantum information theory is quantum entanglement, that provides correlations that are genuinely quantum [77]. We demonstrate that the same three-level 1D atom creates quantum entanglement in the polarization of two photons [71]. The selection between the two processes is solely due to the linewidth of the input wavepacket. The broadband character of 1D waveguides is a key ingredient to guarantee the versatility of the device.

3.1   Quantum cloning

Quantum cloning is the copy of information encoded in an arbitrary quantum state $|\psi\rangle$. The ideal process could be represented as $|0\rangle|\psi\rangle \to |\psi\rangle|\psi\rangle$, where $|0\rangle$ is the initial state of the clone. Some basic concepts are discussed in the following subsection.

Basic concepts

The no-cloning theorem is a consequence of the linearity of quantum mechanics. A sketch of the proof is given, based on Ref.[75].

No-cloning theorem.– The most general evolution for a quantum state can be implemented by adding an ancilla state $|M\rangle$, representing here the cloning machine state, then performing an unitary evolution U in the whole system and finally tracing out the ancilla[1]. We assume that we know how to clone a well-defined state $|\uparrow\rangle$ by the process $U|0\rangle|\uparrow\rangle|M(0)\rangle = |\uparrow\rangle|\uparrow\rangle|M(\uparrow)\rangle$, where $|\uparrow\rangle$ is the input state and $|0\rangle$ is the empty state in which the copy is written. Since the transformation is unitary, it equally applies to the othogonal state $|\downarrow\rangle$, $U|0\rangle|\downarrow\rangle|M(0)\rangle = |\downarrow\rangle|\downarrow\rangle|M(\downarrow)\rangle$. Because of the linearity of quantum mechanics, this applies to an arbitrary superposition $|\psi\rangle = \alpha|\uparrow\rangle + \beta|\downarrow\rangle$ as $U|0\rangle(\alpha|\uparrow\rangle + \beta|\downarrow\rangle)|M(0)\rangle = \alpha|\uparrow\uparrow\rangle|M(\uparrow)\rangle + \beta|\downarrow\downarrow\rangle|M(\downarrow)\rangle$. But this state does not obey the definition of the clone, i.e., $(\alpha|\uparrow\rangle + \beta|\downarrow\rangle) \otimes (\alpha|\uparrow\rangle + \beta|\downarrow\rangle) \otimes |M(\uparrow + \downarrow)\rangle$. This shows

---

[1]this is an operational realization of the so called trace-preserving completely-positive (CP) maps

that no quantum operation exists that can duplicate perfectly an arbitrary quantum state.

While perfect copies of unknown quantum states are prohibited, unperfect quantum clones are allowed. In particular for two-level systems (qubits), an optimal fidelity has been derived for a universal quantum cloning machine,

$$\mathcal{F}_{n \to m} = \frac{mn + m + n}{mn + 2m},$$

where n and m are respectivelly the initial and final number of copies [78, 79]. In the $1 \to 2$ case, $\mathcal{F}_{1 \to 2} = 5/6$. The most compact proof for that result is based on a link between quantum cloning and state estimation [73]. This emphasizes the fact that cloning provides ascertainment of the state of a single quantum system, although not with complete certainty. We sketch the calculations contained in Ref. [73].

Optimal fidelity. – The input qubit is assumed in pure state $|\psi_{in}\rangle$, that can be written as $\varrho^{in} \equiv |\psi_{in}\rangle\langle\psi_{in}| = \frac{1}{2}(1 + \vec{\mu} \cdot \vec{\sigma})$, where $\vec{\mu}$ is the original Bloch vector and $\vec{\sigma} = (\sigma_x, \sigma_y, \sigma_z)$ is the vector of Pauli operators. This notation allows for a simple representation of the output reduced state, $\varrho^{out} = \frac{1}{2}(1 + \eta_{n,m}\vec{\mu} \cdot \vec{\sigma})$ where $\eta_{n,m}$ is the shrinking factor of the mixed state. This factor satisfies the simple property that, for two concatenated cloning steps, $n \to m \to \infty$, they multiply; in the optimal case, $\eta_{n,m}^{opt}\eta_{m,\infty}^{opt} = \eta_{n,\infty}^{opt}$, i.e., $\eta_{n,m}^{opt} = \eta_{n,\infty}^{opt}/\eta_{m,\infty}^{opt}$. It can be shown using quantum state estimation that $\eta_{n,\infty}^{opt} = \eta_n^{opt} = n/(n+2)$, where η_n^{opt} is the optimally estimated shrinking factor for n identical replicas of an unknown pure state ϱ^{in}. Therefore, $\eta_{n,m}^{opt} = \frac{n(m+2)}{m(n+2)}$. Moreover, the fidelity is given only in terms of the shrinking factor, $\mathcal{F} \equiv \langle\psi_{in}|\rho^{out}|\psi_{in}\rangle = \text{Tr}[\varrho^{in}\varrho^{out}] = (1 + \eta_{n,m}^{opt})/2 = (mn + m + n)/(mn + 2m)$, which completes the sketch. Note that the fidelity does not depend on $\vec{\mu}$, i.e., it is the same for all input states. This is the definition of universality.

Universality allows, thus, the preparation of optimal clones. To obtain optimality one pays the price of losing the possibility of cloning perfectly the state of the basis. For instance, the optimal cloning machine assumed in the proof of the no-cloning theorem is able to duplicate the orthogonal states $|\uparrow\rangle$ and $|\downarrow\rangle$ with 100% fidelity. This gives a hint on the reason why cloning is somehow possible in spite of the linearity of quantum

mechanics.

A two-level system in a transmitting/reflecting waveguide is not enough

A first attempt to implement quantum cloning in 1D atoms is to copy direction of propagation in a transmitting/reflecting waveguide. The two degrees of freedom would be represented by the photons propagating to left, $|\text{left}\rangle = |b\rangle$, or to right, $|\text{right}\rangle = |a\rangle$.

The interaction Hamiltonian in that case is not invariant under basis rotation. On the contrary, it naturally establishes a preferential coupling basis, namely, the even modes, $(a + b)/\sqrt{2}$, while the odd modes, $(a - b)/\sqrt{2}$, evolve freely, as we have shown in the previous chapter. This introduces the first limitation: cloning is not universal for two-level atoms in transmitting/reflecting waveguides.

We have also analyzed in Sec. 2.4.1 the (transmission) fidelity for that cloning process, which yields $\mathcal{F}^T = 97.5\% \times \frac{5}{6}$, in the best case $\Delta = 3\Gamma'$. So, cloning is not optimal for two-level atoms, even under ideal conditions, where we neglect dissipation to 3D modes and pure dephasing.

The Hamiltonian of a three-level atom in lambda configuration is invariant under basis rotation, keeping its form $\sigma_u^\dagger \, u + \sigma_v^\dagger \, v = \sigma_a^\dagger \, a + \sigma_b^\dagger \, b$ for any $u = \alpha \, a + \beta \, b$, $v = \beta^* \, a - \alpha^* \, b$ so that $|\alpha|^2 + |\beta|^2 = 1$. Here, modes a and b represent polarization degrees of freedom rather than direction of propagation. Hence, lambda atoms provide universality. In the following, we study the fidelity of the cloning protocol.

3.2 Lambda-atom in semi-infinite waveguide

Model

A three-level atom in lambda configuration is composed of two ground states, $|g_A\rangle$ and $|g_B\rangle$, and one excited state $|e\rangle$. Here, the two ground states will be assumed to be degenerated so the free Hamiltonian of the atom is $H_{\text{atom}} = \hbar\nu_A|e\rangle\langle e|$. The two optical transitions are coupled to two continua of mutually orthogonal polarization modes, a_ν

and b_ν, through the Hamiltonian

$$H_\mathrm{I} = \sum_\nu -i\hbar \left[g_\nu^a \, a_\nu \sigma_+^a + g_\nu^b \, b_\nu \sigma_+^b - \mathrm{H.c.} \right],$$ (3.1)

where $\sigma_+^a = |e\rangle\langle g_A|$, $\sigma_+^b = |e\rangle\langle g_B|$ and the coupling constants are denoted by g_ν^a and g_ν^b. This system is illustrated in Fig. 3.1. The initial condition is chosen similarly to the previous chapter, namely, the product of an excited atom and a single-photon packet with exponential temporal profile.
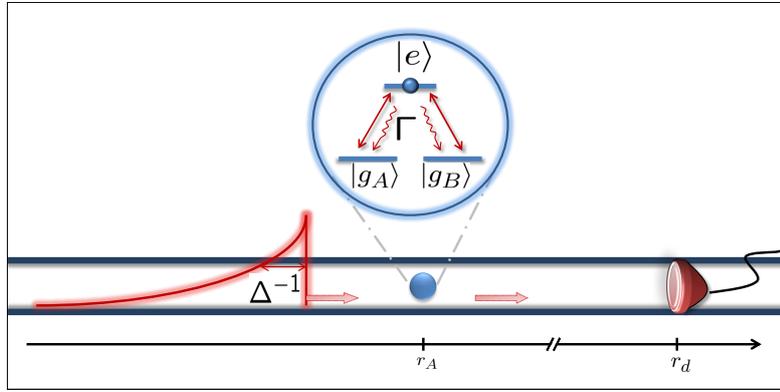
Figure 3.1: Scheme of the 1D atom in lambda configuration with incoming photon of arbitrary polarization and exponential wavepacket shape. In the model, the atom at position r_A is embedded in a semi-infinite 1D electromagnetic channel, so that the emitted light propagates only in the forward direction and is detected at r_d arbitrarily far from the emitter.

Ansatz of the state vector

The Ansatz for this new configuration in the two-excitation subspace is composed of six types of amplitudes. Two of them describe the atomic excited state, one for each polarization mode, ψ_ν^a and ψ_ν^b. Other two kinds of amplitudes describe the possible photonic configurations when the atom is in ground state A: either both photons are in the same polarization mode, ϕ_{ν_1,ν_2}^{aa}, or in different ones, $\phi_{A\ \nu_1,\nu_2}^{ab}$. Finally, it follows

analogously to ground state B, where we have either $\phi^{bb}_{\nu_1,\nu_2}$ or $\phi^{ab}_{B\ \nu_1,\nu_2}$, so

$$
\begin{aligned}
|\psi(t)\rangle \;=\; & \sum_\nu [\psi^a_\nu(t)\ a^\dagger_\nu + \psi^b_\nu(t)\ b^\dagger_\nu]|e,0\rangle + \\
& \sum_{\nu_1,\nu_2} [\phi^{aa}_{\nu_1,\nu_2}\ a^\dagger_{\nu_1} a^\dagger_{\nu_2} + 2\phi^{ab}_{A\ \nu_1,\nu_2}\ a^\dagger_{\nu_1} b^\dagger_{\nu_2}]|g_A,0\rangle + \\
& [\phi^{bb}_{\nu_1,\nu_2}\ b^\dagger_{\nu_1} b^\dagger_{\nu_2} + 2\phi^{ab}_{B\ \nu_1,\nu_2}\ a^\dagger_{\nu_1} b^\dagger_{\nu_2}]|g_B,0\rangle.
\end{aligned}
\tag{3.2}
$$

Note that amplitudes involving two photons in polarization a and the atom in B, or vice versa, evolve freely. Therefore they are not of interest in the problem under consideration given our choice for the initial state.

Evolution equations

The evolution is obtained from Schrödinger equation, yielding

$$
\begin{aligned}
\frac{\partial}{\partial t}\psi^a_\nu &= -i(\nu_A + \nu)\ \psi^a_\nu - 2\sum_{\nu'}[g^a_{\nu'}\ \phi^{aa}_{\nu,\nu'} + g^b_{\nu'}\ \phi^{ab}_{B\ \nu,\nu'}] \\
\frac{\partial}{\partial t}\psi^b_\nu &= -i(\nu_A + \nu)\ \psi^b_\nu - 2\sum_{\nu'}[g^b_{\nu'}\ \phi^{bb}_{\nu,\nu'} + g^a_{\nu'}\ \phi^{ab}_{A\ \nu',\nu}]
\end{aligned}
\tag{3.3}
$$

for the excited-state amplitudes and

$$
\begin{aligned}
\frac{\partial}{\partial t}\phi^{aa(bb)}_{\nu,\nu'} &= -i(\nu+\nu')\phi^{aa(bb)}_{\nu,\nu'} + \frac{1}{2}(g^{a(b)}_\nu\ \psi^{a(b)}_{\nu'} + g^{a(b)}_{\nu'}\ \psi^{a(b)}_\nu) \\
\frac{\partial}{\partial t}\phi^{ab}_{A\ \nu,\nu'} &= -i(\nu+\nu')\phi^{ab}_{A\ \nu,\nu'} + \frac{1}{2}g^a_\nu\ \psi^b_{\nu'} \\
\frac{\partial}{\partial t}\phi^{ab}_{B\ \nu,\nu'} &= -i(\nu+\nu')\phi^{ab}_{B\ \nu,\nu'} + \frac{1}{2}g^b_{\nu'}\ \psi^a_\nu.
\end{aligned}
\tag{3.4}
$$

Real-space solutions

We use real-space representation, $\psi(r,t) = \sum_\nu \psi_\nu(t)e^{ik_\nu r}$. Assuming identical couplings for both transition, $g^a_\nu = g^b_\nu$, the excited-state amplitudes satisfy

$$
\begin{aligned}
\left[\frac{\partial}{\partial t} + c\frac{\partial}{\partial r}\right]\psi^{a(b)}(r,t) \;=\; & -\left(\frac{\Gamma'}{2} + i\nu_A\right)\psi^{a(b)}(r,t) \\
& -\frac{\Gamma'}{2}\Theta(r)\Theta\left(t - \frac{r}{c}\right)\psi^{a(b)}(-r,t-r/c),
\end{aligned}
\tag{3.5}
$$

where the decay rate is $\Gamma' = \sum_\nu 4\pi g_\nu^2 \delta(\nu - \nu_A)$, as defined in Chapter 2. The solution for the above equation reads

$$
\begin{aligned}
\psi^{a(b)}(r,t) \;=\; & \psi^{a(b)}(r - ct, 0)e^{-\left(\frac{\Gamma'}{2} + i\nu_A\right)t} \;-\; \frac{\Gamma'}{2}\Theta(r)\Theta(t - r/c)e^{-\left(\frac{\Gamma'}{2} + i\nu_A\right)t}e^{-\left(\frac{\Gamma'}{2} + i\nu_A\right)(t - r/c)} \\
& \times \int_{t - r/c}^{t} e^{\left(\frac{\Gamma'}{2} + i\nu_A\right)t'}\, \psi^{a(b)}(-ct', 0)\, dt'.
\end{aligned}
\tag{3.6}
$$

The two-photon amplitudes are also written in real-space representation,

$$
\phi^{aa(bb)}(r_1, r_2, t) \;=\; \frac{\sqrt{\pi\rho_{1D}\Gamma'}}{2}\;[\Theta(t - r_2/c)\Theta(r_2)\psi^{a(b)}(r_1 - r_2, t - r_2/c) + \\
\Theta(t - r_1/c)\Theta(r_1)\psi^{a(b)}(r_2 - r_1, t - r_1/c)],
$$

$$
\phi_A^{ab}(r_1, r_2, t) = \frac{\sqrt{\pi\rho_{1D}\Gamma'}}{2}\left[\Theta(t - r_1/c)\Theta(r_1)\psi^{b}(r_2 - r_1, t - r_1/c)\right],
$$

$$
\phi_B^{ab}(r_1, r_2, t) = \frac{\sqrt{\pi\rho_{1D}\Gamma'}}{2}\left[\Theta(t - r_2/c)\Theta(r_2)\psi^{a}(r_1 - r_2, t - r_2/c)\right],
\tag{3.7}
$$

that can be promptly computed using the result from eq.(3.6).

The initial state is $\psi^a(r, 0) = \mathcal{N}\Theta(-r)\exp\left(\frac{\Delta}{2} + i\nu_L\right)\frac{r}{c}$ for polarization mode a and vacuum state for mode b, $\psi^b(r, 0) = 0$. We denote Δ the spectral width of the wave packet, $\delta_L = \nu_L - \nu_A$ its detuning with respect to the atomic frequency ν_A and $\mathcal{N} = \sqrt{2\pi\rho_{1D}\Delta}$ the normalization. Note that the problem is totally symmetrical with respect to any change of polarization basis, so that we can choose an arbitrary polarization a for the incident photon, without restricting the generality of the problem.

Excited-state population

Similarly to what has been shown in the previous chapter, the excited-state population of the lambda atom is a sum of the population of the two-level atom, where stimulated emission can take place, and an exponential decay, describing spontaneous emission, i.e.,

$$
\rho_{ee}^{3L}(t) = \frac{1}{2}\,\rho_{ee}^{2L}(t) + \frac{1}{2}\,e^{-\Gamma't},
\tag{3.8}
$$

where $\rho_{\text{ee}}^{2\text{L}}(t)$ is shown in Chapter 2,

$$
\begin{aligned}
\rho_{\text{ee}}^{2\text{L}}(t) &= e^{-(\Gamma'+\Delta)t}\left\{1+|1+Q|^2(e^{\Delta t}-1)+|Q|^2\frac{\Delta}{\Gamma'}(e^{\Gamma't}-1)\right. \\
&\left.-2\Re\left[(Q^*+|Q|^2)\frac{2\Delta}{\Gamma'+\Delta+2i\delta_L}\left(e^{\frac{\Gamma'+\Delta+2i\delta_L}{2}t}-1\right)\right]\right\},
\end{aligned}
\tag{3.9}
$$

being $Q=2\Gamma'/(\Gamma'-\Delta-2i\delta_L)$ the same factor as previously defined.

Average number of photons

We are interested in the average number of photons N^a emitted in mode a, and N^b for mode b,

$$
N^a = \langle\psi(t_\infty)|\sum_\nu a_\nu^\dagger a_\nu|\psi(t_\infty)\rangle \quad\text{and}\quad N^b = \langle\psi(t_\infty)|\sum_\nu b_\nu^\dagger b_\nu|\psi(t_\infty)\rangle.
$$

We assume the long time limit $t_\infty \gg \max[\Gamma',\Delta]$, where all excitations are in the field, so that $N^a + N^b = 2$. These averages are written in terms of the probabilities p_{ij} of the atom to emit one photon in mode i and another in j,

$$
N^a = 2p_{\text{aa}} + p_{\text{ab}} \quad\text{and}\quad N^b = 2p_{\text{bb}} + p_{\text{ab}}.
\tag{3.10}
$$

The explicit expressions for those probabilities are

$$
p_{\text{aa}} = \sum_{\nu,\nu'} 2|\phi_{\nu,\nu'}^{aa}(t_\infty)|^2 = \frac{2}{(2\pi\rho_{\text{1D}}c)^2}\int_{-\infty}^{\infty}|\phi^{aa}(r,r',t_\infty)|^2\,drdr'
$$

and

$$
\begin{aligned}
p_{\text{ab}} &= \sum_{\nu,\nu'} 4(|\phi_{A\ \nu,\nu'}^{ab}(t_\infty)|^2 + |\phi_{B\ \nu,\nu'}^{ab}(t_\infty)|^2) \\
&= \frac{4}{(2\pi\rho_{\text{1D}}c)^2}\int_{-\infty}^{\infty}|\phi_A^{ab}(r,r',t_\infty)|^2 + |\phi_B^{ab}(r,r',t_\infty)|^2\,drdr',
\end{aligned}
$$

and $p_{\text{bb}} = \sum_{\nu,\nu'} 2|\phi_{\nu,\nu'}^{bb}(t_\infty)|^2 = 1 - (p_{\text{aa}} + p_{\text{ab}})$.

Signatures of optimal stimulation in the field

It is straightfoward to see from Eqs.(3.6) and (3.7) that once the initial state for mode b is vacuum, then $\psi^b(r, r', t) \equiv 0$ for all t and, similarly, $\phi^{bb}(r, r', t) \equiv 0$. This implies that $p_{bb} = 0$ whenever the initial packet has polarization a. After performing the integrations, one finds that

$$p_{\text{aa}} = \frac{\Delta(4\Gamma' + \Delta)}{2(\Gamma' + \Delta)^2} \quad \text{and} \quad p_{\text{ab}} = \frac{1}{2}\left(1 + \frac{\Gamma'^2 - 2\Delta\Gamma'}{(\Gamma' + \Delta)^2}\right), \tag{3.11}$$

at resonance, which are plotted in Fig.3.2. In the very short packet limit, $\Delta \gg \Gamma'$, spontaneous emission takes place, so the two probabilities equalize. In the case of optimal stimulation, $\Delta = 2\Gamma'$, we have

$$p_{aa} = \frac{2}{3} \quad \text{and} \quad p_{ab} = \frac{1}{3}. \tag{3.12}$$

Optimal stimulated emission reduces the effective atomic lifetime by a factor of 2. As far as the field is concerned, the probability of emission in the stimulating mode is 2 times the probability of spontaneous emission in the vacuum modes. That is verified in Eq.(3.12), where optimal stimulation yields $p_{aa} = 2\,p_{ab}$. The implications of that are discussed in the next section.

Although the long packet limit $\Delta \ll \Gamma'$ also corresponds to spontaneous emission of the atom, the properties of the field are surprisingly different from the opposite limit. In particular, the probability of two photons being in polarization a vanishes. This point is tackled in section 3.4.

3.3 Cloning of a single-photon polarization state

We have pointed out that optimal stimulation saturates the bound of probability that the emitted photon is identical to the stimulating one, $p_{\text{aa}} = 2/3$ at $\Delta = 2\Gamma'$. We have also noticed that such copying process is independent of the input polarization. That is, it works equally well for all $|a\rangle = \vartheta|H\rangle + \varphi|V\rangle$, where $|H\rangle$ and $|V\rangle$ are respectivelly horizontal and vertical polarization states with arbitrary complex normalized coefficients
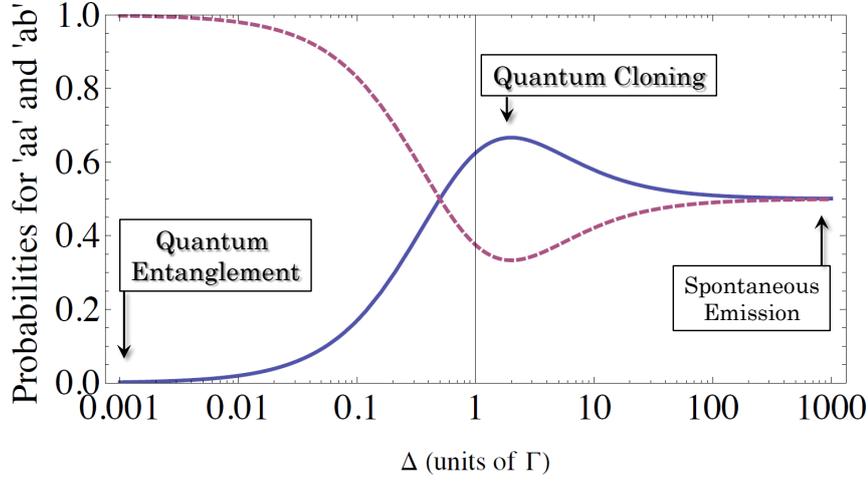
Figure 3.2: Probabilities p_{aa} (solid blue curve) and p_{ab} (dashed red curve) for two photons created with the same polarizations and orthogonal polarizations, respectively.

ϑ and φ. These facts strongly indicate that optimal stimulated emission provides optimal universal quantum cloning in 1D lambda atoms.

Actually, stimulated emission was the first process thought of as a concrete example for copying quantum states [74]. However, along with stimulation, there is always spontaneous emission. It was soon realized the intrinsic connection between the unavoidable presence of spontaneous emission and the impossibility of perfectly cloning arbitrary states via stimulated emission [80].

More recently, this connection has been studied quantitatively: it has been shown that stimulated emission can provide optimal cloning [81], saturating the bound imposed by spontaneous emission. We outline an intuitive picture of that result. The probabilities of two photons in the same mode, p_{equal}, and in different modes, p_{diff}, have to be determined. Once those probabilities are known, the cloning fidelity via stimulated emission $\mathcal{F}_{\text{stim}}$ can be found,

$$\mathcal{F}_{\text{stim}} = p_{\text{equal}} \, \mathcal{F}_{\text{equal}} + p_{\text{diff}} \, \mathcal{F}_{\text{diff}},$$

where $\mathcal{F}_{\text{equal}}$ is the fidelity of a perfectly correct cloning, $\mathcal{F}_{\text{equal}} = 1$, and $\mathcal{F}_{\text{diff}}$ is the

fidelity for two different photons, the initial one in the correct mode and the other one in the wrong mode, $\mathcal{F}_{\text{diff}} = 1/2$. Stimulated emission can give rise to $p_{\text{equal}} = 2/3$ and $p_{\text{diff}} = 1/3$, at best, so

$$\mathcal{F}_{\text{stim}} = \frac{2}{3} \times 1 + \frac{1}{3} \times \frac{1}{2} = \frac{5}{6}, \tag{3.13}$$

which coincides with the value previously shown, $\mathcal{F}_{\text{stim}} = \mathcal{F}_{1 \rightarrow 2}$.

In Ref.[81], the probabilities p_{equal} and p_{diff} are calculated for two scenarios: (i) a non-dissipative monochromatic cavity coupled to three-level atoms and (ii) a nonlinear crystal.

In case (i), V-shape atoms are chosen, where transitions correspond to orthogonal polarization states of the photon, equally coupled to the cavity. The atoms are prepared in a symmetric mixture, where both excited states are populated with a half probability, which guarantees universality under polarization basis. A photon is initially prepared in the cavity mode corresponding to polarization a, orthogonal to b. The time-dependent probabilities $p(k, l)$ are obtained, for k photons having polarization a and l photons having polarization b. The presence of N photons in a given polarization stimulates by a $\sqrt{N+1}$ factor the quantum Rabi oscillations with respect to the other polarization mode, initially in the vacuum state. Thus, for very initial times, the fidelity is indeed optimal. The temporal region where optimality occurs is thoroughly short. It is so short that the average number of photons in the cavity, hence of clones, is as small as $N \sim 1.1$. Hence, the clones are optimal though their presence is quite unlikely. Another drawback of that scheme for any practical reason is that the cavity does not dissipate, keeping the clones trapped inside.

In case (ii), two nonlinear crystals are pumped by two intense classical pulses. The first one produces the photon that eventually stimulates emission of another photon from the second crystal. In turn, the second crystal produces two more photons, either by stimulation or spontaneously, depending on the mode-matching. The obtained clones are once again optimal and universal. In this case, the clones do not get trapped. On the other hand, the whole process is probabilistic, with quite low efficiency. Under reported

experimental conditions [82], the probability for each input pulse to contain a photon is 5×10^{-2}, the probability of producing a downconverted pair is 10^{-3}, and the overall detection efficiency is 0.10 per photon. That gives 5×10^{-6} of efficiency for the whole process.

We can now make a comparison with 1D atoms. The fact that Eq.(3.11) gives $p_{\mathrm{aa}} = 2/3$ at $\Delta = 2\Gamma'$ turn 1D atoms into a novel platform to realize optimal universal quantum cloning. Indeed, it checks $\mathcal{F} = p_{\mathrm{aa}} \times 1 + p_{\mathrm{ab}} \times 1/2 = 5/6$. One practical advantage of 1D atoms is that the cloned photon packet propagates freely. Another one is that it is deterministic, as a consequence of the irreversible nature of the stimulation process. Theoretically, the main difference with respect to the previous proposals is the broadband character of the packet. In both cases previously shown, light is effectively monochromatic: the cavity is non-dissipative and the nonlinear crystal Hamiltonian does not depend on frequency [81]. It is not evident a priori whether a pulse, which has a finite bandwidth, can realize optimal cloning. Here we have presented an affirmative answer to that theoretical question.

3.4 Quantum entanglement

Basic properties

A pure state $|\psi_{AB}\rangle$, composed by two subsystems A and B, is entangled if and only if it satisfies $|\psi_{AB}\rangle \neq |\psi_A\rangle \otimes |\psi_B\rangle$ [77]. In other words, knowlegde about the complete system is fully available, described by $|\psi\rangle$. In contrast, knowledge about each subsystem is only partial. The subsystem cannot be described by an independent pure state, but rather by the reduced mixed state $\rho_{\mathrm{A}} \equiv \mathrm{Tr}_B[|\psi_{AB}\rangle\langle\psi_{AB}|]$ (or, $\rho_{\mathrm{B}} \equiv \mathrm{Tr}_A[|\psi_{AB}\rangle\langle\psi_{AB}|]$). The degree of uncertainty, or mixedness, of a quantum state is given by the von Neumann entropy, $S(\rho) = -\mathrm{Tr}[\rho \ln\rho]$. Note that $S(\rho_A) = S(\rho_B)$ for a pure state $|\psi_{AB}\rangle$. The von Neumann entropy of the reduced state can be used as a quantitative measure of entanglement of pure bipartite quantum states. Actually, it is the unique entanglement

measure E satisfying the following criteria: (*1*) invariant under local unitary operations, (*2*) continuous, and (*3*) additive over several copies of the system, $E(|\psi_{AB}\rangle \otimes |\phi_{AB}\rangle) = E(|\psi_{AB}\rangle) + E(|\phi_{AB}\rangle)$.

Once we know how to quantify entanglement, we can identify four maximally entangled two-qubit states, also known as Bell states, that form a complete orthonormal basis for the two-qubit Hilbert space,

$$|\phi^{\pm}\rangle = \frac{1}{\sqrt{2}}(|0\rangle_A|0\rangle_B \pm |1\rangle_A|1\rangle_B),$$
$$|\psi^{\pm}\rangle = \frac{1}{\sqrt{2}}(|0\rangle_A|1\rangle_B \pm |1\rangle_A|0\rangle_B). \tag{3.14}$$

Entanglement in three-level 1D atoms

We now focus on the photonic state created in the long photon limit ($\Delta \ll \Gamma'$) and show how it is related to Bell states [71]. In that limit, the analysis can be made in two steps: (*i*) spontaneous creation of one photon, followed by (*ii*) scattering of the incoming one.

(*i*) At short times, $t \lesssim 1/\Gamma'$, the atomic excited-state population decays exponentially, as a result of spontaneous emission. Formally, one can write the Ansatz in the single excitation subspace for process (*i*),

$$|\psi(t)\rangle = \psi_x(t)|e,0\rangle + \sum_{\nu} \phi_{\nu}^a(t)\, a_{\nu}^{\dagger}|g_A,0\rangle + \phi_{\nu}^b(t)\, b_{\nu}^{\dagger}|g_B,0\rangle, \tag{3.15}$$

and compute the time evolution with Schrödinger equation. One promptly finds the decay of population, $|\psi_x(t)|^2 = \exp[-\Gamma't]$. After the excitation has left the atom, the system reaches an entangled final state between the two ground states of the atom and the two photon polarization states,

$$|\psi(T)\rangle = |g_A\rangle \otimes \left(\sum_{\nu} \phi_{\nu}^a\, a_{\nu}^{\dagger}|0\rangle\right) + |g_B\rangle \otimes \left(\sum_{\nu} \phi_{\nu}^b\, b_{\nu}^{\dagger}|0\rangle\right), \tag{3.16}$$

where $\Delta^{-1} \gg T \gg \Gamma'^{-1}$. Given that $\phi_{\nu}^a(t) = \phi_{\nu}^b(t)$, this state is nothing but a Bell state $|\phi^+\rangle$. The temporal size of the spontaneously created wavepacket is of the order of Γ'^{-1}. We shall call it a short packet, as compared to the size of the long input photon of the order of $\Delta^{-1} \gg \Gamma'^{-1}$.

(*ii*) The long photon scatters through the atom left in the state from Eq.(3.16). From the linearity of quantum mechanics, the two state components follow independent time evolutions. The component $|g_B\rangle$, corresponding to ground state B, is transparent to the incoming photon of polarization a. The resulting component is thus $|g_B\rangle \otimes |b_S\rangle|a_L\rangle$, where the subscript $_S$ corresponds to the short (spontaneously emitted) wavepacket and $_L$ to the long (incoming) one. On the opposite, component $|g_A\rangle$ follows a remarkable path. If Eq.(3.15) is solved now for the initial condition $|\psi(0)\rangle = |g_A\rangle|a\rangle$, it is found that

$$\phi^{a,b}(r,t) = \phi^{a,b}(r-ct,0) + \sqrt{\Gamma'\pi\rho_{1D}}\ \Theta(r)\Theta(t-r/c)\ \psi_x(t-r/c), \tag{3.17}$$

while

$$\psi_x(t) = -\sqrt{\frac{\Gamma'}{\pi\rho_{1D}}}\mathcal{N}e^{-\left(\frac{\Gamma'}{2}+i\nu_A\right)t}\left(\frac{e^{\left(\frac{\Gamma'-\Delta}{2}-i\delta_L\right)t}-1}{\Gamma'-\Delta-2i\delta_L}\right). \tag{3.18}$$

In the regime under analysis, $\delta_L = 0$ and $\Delta \ll \Gamma'$, that implies

$$\Theta(t-r/c)\ \psi_x(t-r/c) \approx -\frac{1}{\sqrt{\Gamma'\pi\rho_{1D}}}\phi^a(r-ct,0),$$

where we have neglected the fast decaying term $\exp[-\Gamma't]$. This is the three-level analogous to the π-phase shift studied at section 2.1.2 of Chapter 2. For $r > 0$, this results in

$$\phi^a(r,t) = \phi^a(r-ct,0) - \phi^a(r-ct,0) = 0,$$
$$\phi^b(r,t) = \phi^b(r-ct,0) - \phi^a(r-ct,0) = 0 - \phi^a(r-ct,0). \tag{3.19}$$

Eqs.(3.19) tell us that the long photon packet of polarization a is totally scattered into polarization b, while keeping the same packet profile apart from a π-phase shift, $|a_L\rangle \to -|b_L\rangle$. Meanwhile, atomic population is adiabatically transfered into ground state B as well, $|g_A\rangle \to |g_B\rangle$. The full map for that component is then $|g_A\rangle|a_S\rangle|a_L\rangle \to -|g_B\rangle|a_S\rangle|b_L\rangle$. Combining the two components, we recognize that the atom disentangles from the field, while transfering its entanglement to the two photons,

$$|\psi(t_\infty)\rangle = |g_B\rangle \otimes \frac{1}{\sqrt{2}}(|b_S\rangle|a_L\rangle - |a_S\rangle|b_L\rangle), \tag{3.20}$$

forming a Bell state $|\psi^-\rangle$ of polarizations. Note that the separation in two steps we did is valid only if the overlap between the two photons is negligible, as it occurs for $\Delta \ll \Gamma'$. In that case, a short packet is completely distinguishable from a long packet, $\langle a_L|a_S\rangle = \langle b_L|b_S\rangle = 2\sqrt{\Delta/\Gamma'}/(1 + \Delta/\Gamma') \to 0$.

The final state shown in Eq.(3.20) has no component with both photons in the same polarization a. It gives, thus, a clear explanation to the values of the probabilities, $p_{\mathrm{ab}} = 1$ and $p_{\mathrm{aa}} = 0$, calculated from Eqs.(3.11) at $\Delta/\Gamma' \to 0$.

3.5   Possible experimental error sources

The model developed in the last two chapters is suitable for the case where both waveguide losses and pure dephasing of the emitter are absent. The model can be artificially adapted to include waveguide loss, by adding an imaginary term to the atomic Hamiltonian, $-i(\Gamma_{3D}/2)|e\rangle\langle e|$, where Γ_{3D} is the decay to modes outside the waveguide, still describing the whole system with a wavefunction $|\psi\rangle$. Nevertheless, this approach cannot be extended to treat pure dephasing. No effective Hamiltonian can mimic phase fluctuations of a quantum state, just as no state vector $|\psi\rangle$ can represent a mixed state. Density operators are the only formalism that encompass both pure dephasing and waveguide loss.

It is possible to rough estimate small imperfections, using the results from Chapter 1 to find how coherences are affected. Coherence, hence interference, is related to $\mathcal{W} = -\Omega\Re[\langle S_-\rangle] \propto \beta(1+\gamma^*/\gamma+\beta)^{-1} \approx \beta(1-\gamma^*/\gamma) + \mathcal{O}(\beta^2)$ in stationary regime for $\gamma^* \ll \gamma$, where γ^* is the pure dephasing rate, and the β-factor gives the ratio between 1D and total decay rates, $\beta = \Gamma'/\gamma < 1$, being $\gamma = \Gamma' + \Gamma_{3D}$.

Experimental values for β achieve 0.98 in 1D nanophotonic systems made of photonic wires [33] or 1D waveguides in photonic crytals [83], and almost 1 in circuit QED [84]. Pure dephasing rates of $\gamma^* \approx 0.1\gamma$ have been measured in quantum dots [85] and superconducting qubits [44]. Such imperfections would affect the cloning fidelity and the entanglement by a factor of the order $\sim \beta(1 - \gamma^*/\gamma)$, for $\beta \approx 1$ and $\gamma^* \ll \gamma$, given that

both cloning and entanglement are coherence-dependent effects. This would lower the real cloning fidelity and entanglement to about 90% of their optimal values for circuit QED systems and 88% for nanophotonic systems.

3.6 Conclusions

We have presented a unique versatile device that can realize either universal optimal cloning or maximal entanglement in photon polarization, depending only on the spectral shape of the incoming photon. Optimal irreversible stimulated emission, reached for a pulse spectrally twice as large as the atomic linewidth, is a resource for optimal cloning of a broadband propagating packet.

For a highly monochromatic photon, a π-phase shift has been responsible for adiabatic transfer of population, redirecting the spontaneous atom-photon entanglement to photon-photon entanglement. A realistic single-photon pulse shape has been considered, yielding maximal efficiencies on both processes.

Chapter 4

Phonon-assisted cavity feeding

Attraction is beyond our will or ideas sometimes.

Juliette Binoche

The field of cavity quantum electrodynamics has seen great advances during the past decades. While pioneering experiments used real atoms coupled to cavities in free space, recent developments have achieved single emitter-single photon interaction in solid-state systems [14]. A quantum dot is a nanodimensional semiconducting drop (e.g., InAs) with a bandgap smaller than the semiconducting matrix in which it is embedded (e.g., GaAs), strongly confining single electron-hole pairs (called excitons) [86]. This confinement creates discrete states, so the recombination of excitons provide sharp optical transitions. Therefore, quantum dots are considered as artificial atoms, as illustrated in Fig.4.1.

Remarkable experimental advances have allowed for deterministic coupling between a single quantum dot and a single-mode microcavity, reaching Purcell factors of the order of ten or more. Deterministic coupling has been achieved, for instance, in photonic planar cavities [87] and in semiconducting micropillar cavities [88], as illustrated in Fig.4.1. This guarantees that the simple model of a single emitter coupled to a single cavity mode is appropriate.

Understanding the deviations of artificial atom-cavity system from the standard atom-cavity behaviour became a promising research topic. A representative example of such deviation is the anomalous cavity emission at frequencies way above the quantum dot optical transition [89], as illustrated in Fig.4.2. This effect, now commonly called *cavity feeding*, consists in the main motivation for our study.

An intuitive picture of this effect is provided by noting that, in general, a solid-state environment broadens the optical transition of the emitter, as it creates off-resonance mechanisms (due to charge fluctuations, or phonons, for instance). This allows for eventual emission at the frequency of the cavity, even if cavity and emitter are quite off-resonance. Finally, the rate of emission at the cavity frequency is enhanced due to Purcell effect, so an efficient off-resonance emission occurs. This intuitive picture has been quantitatively analyzed in Ref.[90], where the broadening mechanism is modeled by a pure dephasing rate in a two-level system.

In this chapter we will be interested in how the coupling with phonons affects the spontaneous emission of a quantum dot. Two types of electromagnetic environment are considered: free space and an optical microcavity.
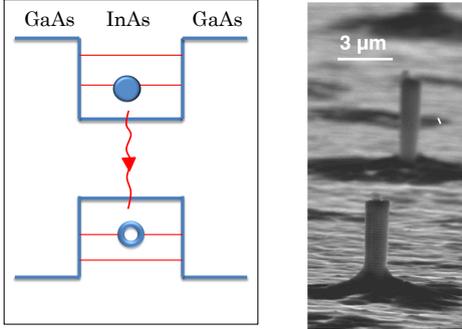
Figure 4.1: Level scheme of a InAs quantum dot embedded in a GaAs matrix. Exciton recombines emitting a sharp linewidth photon. Micropillars deterministically coupled to quantum dots (Dr. Pascale Senellart – LPN/CNRS)
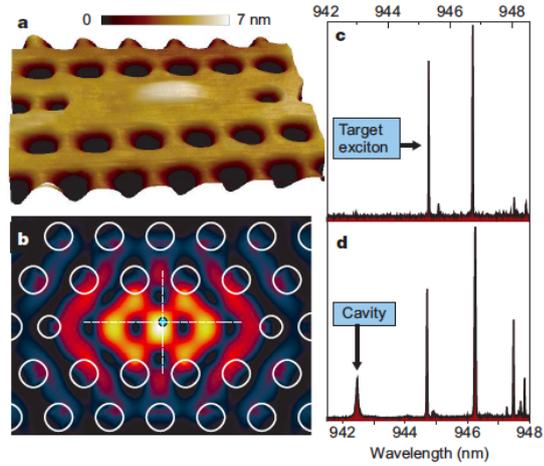
Figure 4.2: Photonic crystal cavity built around the quantum dot. The cavity peak is identified off-resonance, fed by the excitonic transition (K. Hennessy *et. al.*, Ref.[89]).

4.1 Spontaneous emission of a quantum dot in the presence of phonons

This section is devoted to spontaneous emission in free space, where the emitter is not subjected to any cavity but only to the unstructured vacuum state of the electromagnetic field. We first present the model of the system under analysis. Then we develop a formalism to compute the spectrum of light spontaneously emitted.

4.1.1 Model

In a quantum dot, the excited state $|e\rangle$ corresponds to a confined exciton, at the size of a few nanometers . The ground state $|g\rangle$ is the empty quantum dot. The lattice vibrations of the bulk cause compression and strain of the quantum dot. An exciton in the quantum dot responds to single quanta of vibration excitations, called phonons. In the ground state there are no bound excitons, so phonons are exclusively coupled to the

excited state. This interaction can be modeled by the Hamiltonians $H_{\text{phonon}} + H_{\text{qd}-\text{phonon}}$ [86, 91],

$$H_{\text{qd}} = \hbar\omega_0 \, |e\rangle\langle e| \tag{4.1}$$

$$H_{\text{phonon}} = \sum_{\vec{q}} \hbar\omega_{\vec{q}} \, a_{\vec{q}}^\dagger a_{\vec{q}} \tag{4.2}$$

$$H_{\text{qd}-\text{phonon}} = \sum_{\vec{q}} \hbar\lambda_{\vec{q}} \, |e\rangle\langle e| \left(a_{\vec{q}}^\dagger + a_{\vec{q}} \right). \tag{4.3}$$

The expressions for the electron-phonon coupling $\lambda_{\vec{q}}$ and phonon dispersion $\omega_{\vec{q}}$ depend on the type of phonons, that can be acoustic or optical. We specify this in the following subsection. In any case, the Hamiltonian defined by $H_{\text{ibm}} = H_{\text{qd}} + H_{\text{qd}-\text{phonon}} + H_{\text{phonon}}$ defines the so called *independent boson model* [92] and can be exactly diagonalized.

We analyse the problem in the $|e\rangle$ subspace by applying the projection $|e\rangle\langle e|H_{\text{ibm}}|e\rangle\langle e| = |e\rangle H_{\text{ibm}}^{\text{eff}}\langle e|$. The diagonalization of

$$H_{\text{ibm}}^{\text{eff}} = \hbar\omega_0 + \sum_{\vec{q}} \hbar\lambda_{\vec{q}} \left(a_{\vec{q}}^\dagger + a_{\vec{q}} \right) + \sum_{\vec{q}} \hbar\omega_{\vec{q}} \, a_{\vec{q}}^\dagger a_{\vec{q}} \tag{4.4}$$

is obtained by means of the transformation

$$a_{\vec{q}} = \tilde{a}_{\vec{q}} + \Lambda_{\vec{q}}, \tag{4.5}$$

where $\Lambda_{\vec{q}}$ is a *c*-number to be determined. By choosing $\Lambda_{\vec{q}} = -\frac{\lambda_{\vec{q}}}{\omega_{\vec{q}}}$, the Hamiltonian can be rewritten as

$$H_{\text{ibm}}^{\text{eff}} = \left(\hbar\omega_0 - \sum_{\vec{q}} \hbar\frac{\lambda_{\vec{q}}^2}{\omega_{\vec{q}}} \right) + \sum_{\vec{q}} \hbar\omega_{\vec{q}} \, \tilde{a}_{\vec{q}}^\dagger \tilde{a}_{\vec{q}}. \tag{4.6}$$

The excited state thus creates new eigenstates of dressed phonons $\prod_{\vec{q}} |\tilde{n}_{\vec{q}}\rangle$ from the non-dressed phonon states $\prod_{\vec{q}} |n_{\vec{q}}\rangle$, defined by

$$\tilde{a}_{\vec{q}}|\tilde{0}_{\vec{q}}\rangle = 0 \tag{4.7}$$

and $\left(\tilde{a}_{\vec{q}}^\dagger \right)^n |\tilde{0}_{\vec{q}}\rangle = \sqrt{n_{\vec{q}}} \, |\tilde{n}_{\vec{q}}\rangle$. Inserting Eq.(4.5) into (4.7), we notice that the dressed state $|\tilde{0}_{\vec{q}}\rangle$ is an eigenstate of the original destruction operator,

$$a_{\vec{q}} \, |\tilde{0}_{\vec{q}}\rangle = \Lambda_{\vec{q}} \, |\tilde{0}_{\vec{q}}\rangle. \tag{4.8}$$

It means that the dressed zero-phonon state is a coherent state of the phonon field, displaced from vacuum by the amount $\Lambda_{\vec{q}}$, proportional to the coupling $\lambda_{\vec{q}}$. That is, $|\tilde{0}_{\vec{q}}\rangle = \mathcal{D}[\Lambda_{\vec{q}}]|0_{\vec{q}}\rangle$, where the displacement operator is given by $\mathcal{D}[\Lambda_{\vec{q}}] \equiv \exp\left[\Lambda_{\vec{q}}\, a^{\dagger}_{\vec{q}} - \Lambda^{*}_{\vec{q}}\, a_{\vec{q}}\right]$. Besides, it can be shown that this relation holds for all $n_{\vec{q}}$, i.e.,

$$|\tilde{n}_{\vec{q}}\rangle = \mathcal{D}[\Lambda_{\vec{q}}]|n_{\vec{q}}\rangle. \tag{4.9}$$

This means that the exciton shifts the equilibrium lattice position, as illustrated in Fig 4.3. In addition to the coordinate shift, the coupling to phonons lowers the exciton energy to $\tilde{\omega}_0 = \omega_0 - \sum_{\vec{q}} \hbar\lambda_{\vec{q}}^2/\omega_{\vec{q}}$.

Figure 4.3: For each wavevector $\vec{q}$, the lattice harmonic vibration of frequency $\omega_{\vec{q}}$ is displaced by $\Lambda_{\vec{q}}$ when an exciton of energy $E_0 = \hbar\tilde{\omega}_0$ is present. The transitions a, b and c respectively correspond to zero-phonon, one-phonon emission and one-phonon absorption.

The optical transition between $|e\rangle$ and $|g\rangle$ is sharp and can have a homogeneous linewidth about six orders of magnitude below the transition frequency. This subsystem is described by $H_{\text{qd}} + H_{\text{light}} + H_{qd-light}$, where

$$H_{\text{light}} = \sum_{\vec{k}} \hbar\omega_{\vec{k}}\, b^{\dagger}_{\vec{k}} b_{\vec{k}} \tag{4.10}$$

$$H_{\text{qd}-\text{light}} = \sum_{\vec{k}} \hbar g_{\vec{k}} \left(|e\rangle\langle g|\, b_{\vec{k}} + |g\rangle\langle e|\, b^{\dagger}_{\vec{k}}\right). \tag{4.11}$$

The dipole coupling is $\hbar g_{\vec{k}} = d\, [\hbar\omega_{\vec{k}}/(2\epsilon_0 V)]^{1/2}$, where d is the dipole constant, ϵ_0 is the vacuum permitivity and V is the free-space volume of quantization. The volume V is taken to infinity by introducing the free-space density of states $\rho_{\text{free}}(\omega_{\vec{k}}) = 4V\omega_{\vec{k}}^2/[(2\pi)^2 c^3]$, so that $\rho_{\text{free}}(\omega_{\vec{k}})g_{\vec{k}}^2$ remains finite.

In Fig.4.3, three optical transitions from excited state $|e\rangle$ to ground state $|g\rangle$ have been shown: a is a zero-phonon transition of frequency $\tilde{\omega}_0$, b contains one-phonon emission resulting in a lower frequency $\tilde{\omega}_0 - \omega_{\vec{q}}$ and c contains one-photon absorption resulting in a higher frequency $\tilde{\omega}_0 + \omega_{\vec{q}}$. Variation in the number of phonons in mode $\vec{q}$ simply comes

from the finite overlap $\langle \tilde{n}_{\vec{q}} | n_{\vec{q}} \rangle$ between different equilibrium positions of the atoms in the crystal lattice according to the presence ($\tilde{n}_{\vec{q}}$) or the absence ($n_{\vec{q}}$) of an exciton trapped in the quantum dot. This qualitative discussion will be analysed quantitatively in the following subsection.

4.1.2 Spectrum

Experiments with single quantum dots (QD) have clearly shown that spontaneous emission (photoluminescence) spectra do not fit a single Lorentzian function [93]. Fig.4.4, taken from Ref.[93], shows a typical low temperature spectrum for QD emission. The solid line is a Lorentzian fit, which does not match the "wings" around the central peak. The wings are a consequence of the coupling with acoustic phonons [93], as we show in the following.

Figure 4.4: Typical emission spectrum of a single quantum dot at low temperature, $T = 30K$. Lorentzian fit does not match experimental data.

The emission spectrum $S(\omega)$ is defined as the rate of emission in a given frequency ω [50]. In the case of spontaneous emission (denoted here by $|\text{initial}\rangle \rightarrow |\text{final}\rangle$), Fermi's golden rule can be used to access the spontaneous emission spectrum. It gives the decay rate at each final frequency $\Gamma(\omega_f)$, so the total decay rate Γ is a sum over all frequencies,

$$\Gamma = \int d\omega_f \; \rho(\omega_f) \; \Gamma(\omega_f), \tag{4.12}$$

where $\rho(\omega)$ is the density of final states. Denoting the perturbation potential by $\mathcal{V}$,

$$\Gamma(\omega_f) = \frac{2\pi}{\hbar^2} |\langle \text{final}|\mathcal{V}|\text{initial}\rangle|^2 \; \delta(\omega_f - \omega_i). \tag{4.13}$$

The normalized spectrum is then obtained,

$$S(\omega) = \rho(\omega) \times \Gamma(\omega)/\Gamma. \tag{4.14}$$

Note that this method does not take quantum fluctuations of the vacuum into account. In the case where $\langle \text{final}|\mathcal{V}|\text{initial}\rangle = \hbar g_k$, for instance, $S(\omega) = 2\pi g_k^2 \rho(\omega_0)\, \delta(\omega - \omega_0)$. The natural linewidth is included phenomenologically.
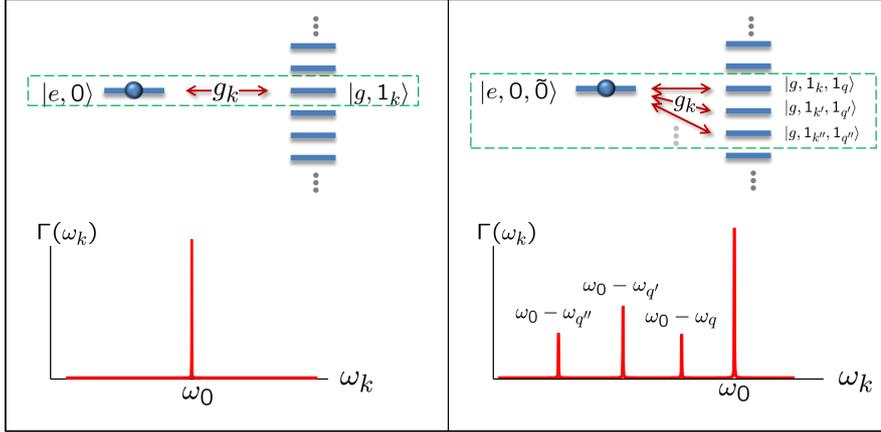
Figure 4.5: Frequency-dependent decay rate $\Gamma(\omega_k)$ given by Fermi golden rule. Left– Two-level system emitting a photon at frequency $\omega_k = \omega_0$ (sharp transition). Right– quantum dot emitting a phonon of frequency ω_q and a photon of frequency $\omega_k = \omega_0 - \omega_q$ (broad transition). The coupled phonon bath is illustrated at zero temperature, $|\tilde{0}\rangle$. Our model is valid for arbitrary temperatures and exciton-phonon couplings.

We now concentrate on our particular case, where the continuum of phonons is taken into account. Our initial state is an excited emitter, a thermal distribution of dressed phonons with probability $P\{n\}$ and vacuum state in the electromagnetic field,

$$|\text{initial}\rangle = |e\rangle \otimes \prod_{\vec{q}} |\tilde{n}_{\vec{q}}\rangle \otimes \prod_{\vec{k}} |0_{\vec{k}}\rangle. \tag{4.15}$$

The final states are all possibilities for emission of one-photon of frequency $\omega_{\vec{k}}$ and emission of $m_{\vec{q}} - n_{\vec{q}}$ phonons (i.e. absorption, if $m_{\vec{q}} < n_{\vec{q}}$) in mode $\vec{q}$,

$$|\text{final}\rangle = |g\rangle \otimes \prod_{\vec{q}} |m_{\vec{q}}\rangle \otimes |1_{\omega_{\vec{k}}}\rangle \prod_{\vec{k}'} |0_{\vec{k}' \neq \vec{k}}\rangle. \tag{4.16}$$

The electromagnetic potential is $\mathcal{V} = H_{\text{qd-light}}$ (Eq.4.11), that couples $|e\rangle$ and $|g\rangle$ with

constant g_k independent of the phonon states, so we finally have

$$\Gamma(\omega_k) = 2\pi g_k^2 \sum_{\{n\}} P\{n\} \sum_{\{m\}} \prod_{\vec{q}} |\langle m_{\vec{q}}|\tilde{n}_{\vec{q}}\rangle|^2 \, \delta\left(\tilde{\omega}_0 - \omega_k - \sum_{\vec{q}}(m_{\vec{q}} - n_{\vec{q}})\,\omega_{\vec{q}}\right). \quad (4.17)$$

We used the compact notation $\{n\} = \{n_{\vec{q}_1}, ..., n_{\vec{q}_\infty}\}$, so that $\sum_{\{n\}} = \sum_{n_{\vec{q}_1}} \cdots \sum_{\vec{q}_\infty} = \prod_{\vec{q}} \sum_{n_{\vec{q}}}$. The thermal probability distribution is $P\{n\} = \prod_{\vec{q}} e^{-\beta n_{\vec{q}} \hbar \omega_{\vec{q}}}/\mathcal{Z}_{\text{phonon}}$, being $\beta = (k_B T)^{-1}$, k_B the Boltzmann constant and T, the phonon bath temperature. Eq.(4.17) is a sum of multiphononic transitions, namely, zero-phonon line, one-phonon line and so on.

For spontaneous emission in free space, the density of modes does not vary appreciably in the region of optical frequencies, $\rho(\omega) \approx \text{const}$. So the spectrum of the quantum dot is $S_{\text{QD}}(\omega) = \Gamma(\omega)$. On the other hand, for spontaneous emission in a cavity, the density of modes is a Lorentzian $\rho(\omega) = S_{\text{cav}}(\omega)$, so the total normalized spectrum of the composite system is $S(\omega) = S_{\text{cav}}(\omega) \times S_{\text{QD}}(\omega)/\Gamma$. $S(\omega)$ is experimentally obtained by collecting the emission through the cavity channel.

Note that the term $\langle m_{\vec{q}}|\tilde{n}_{\vec{q}}\rangle$ gives the overlap between the dressed and non-dressed phonon states. At zero dot-phonon coupling ($\lambda_{\vec{q}} = 0$), for instance, one has $\langle m_{\vec{q}}|\tilde{n}_{\vec{q}}\rangle = \langle m_{\vec{q}}|n_{\vec{q}}\rangle = \delta_{m,n}$. The result for spontaneous emission of a sharp two-level system is thus reobtained, given that $\sum_{\{n\}} P\{n\} = 1$.

The influence of phonons on the spontaneous emission of a quantum dot is totally embodied in the overlap term $\langle m_{\vec{q}}|\tilde{n}_{\vec{q}}\rangle$. This is what we have to calculate in order to obtain an explicit expression for $\Gamma(\omega)$. This task will be accomplished using two different approaches. The first one gives an exact mathematical treatment, following some algebraic identities as used in Ref.[92]. The second one gives a more physical picture, following the ideas of a seminal paper by Huang and Rhys [94].

Exact approach

We rewrite Eq.(4.17) as the Fourier transform of a time-dependent function with the help of Eq.(4.9),

$$\Gamma(\omega_k) = g_k^2 \sum_{\{n\}} P\{n\} \sum_{\{m\}} \prod_{\vec{q}} \langle n_{\vec{q}} | \mathcal{D}^\dagger(\Lambda_{\vec{q}}) | m_{\vec{q}} \rangle \langle m_{\vec{q}} | \mathcal{D}(\Lambda_{\vec{q}}) | n_{\vec{q}} \rangle$$
$$\times \int_{-\infty}^{\infty} dt \; e^{i(\tilde{\omega}_0 - \omega_k - \sum_{\vec{q}} m_{\vec{q}}\omega_{\vec{q}} + \sum_{\vec{q}} n_{\vec{q}}\omega_{\vec{q}})t}. \tag{4.18}$$

This allows us to transfer the time evolution into the matrix element,

$$\Gamma(\omega_k) = g_k^2 \int_{-\infty}^{\infty} dt \; e^{-i\omega_k t} e^{i\tilde{\omega}_0 t} \sum_{\{n\}} P\{n\} \sum_{\{m\}} \prod_{\vec{q}} \langle n_{\vec{q}} | e^{\frac{i}{\hbar}H_{\text{ph}}t} \mathcal{D}^\dagger(\Lambda_{\vec{q}}) e^{-\frac{i}{\hbar}H_{\text{ph}}t} | m_{\vec{q}} \rangle \langle m_{\vec{q}} | \mathcal{D}(\Lambda_{\vec{q}}) | n_{\vec{q}} \rangle. \tag{4.19}$$

The closure relation can be applied at this point, $\sum_{\{m\}} \prod_{\vec{q}} |m_{\vec{q}}\rangle\langle m_{\vec{q}}| = \mathbb{I}$. We also denote $\mathcal{D}^\dagger[\Lambda_{\vec{q}}, t] \equiv e^{\frac{i}{\hbar}H_{\text{ph}}t} \mathcal{D}^\dagger(\Lambda_{\vec{q}}) e^{-\frac{i}{\hbar}H_{\text{ph}}t}$ and get

$$\Gamma(\omega_k) = g_k^2 \int_{-\infty}^{\infty} dt \; e^{-i\omega_k t} e^{i\tilde{\omega}_0 t} \sum_{\{n\}} P\{n\} \prod_{\vec{q}} \langle n_{\vec{q}} | \mathcal{D}^\dagger[\Lambda_{\vec{q}}, t] \mathcal{D}[\Lambda_{\vec{q}}, 0] | n_{\vec{q}} \rangle. \tag{4.20}$$

We rearrange the product of displacement operators into a product of two simple exponentials. This is done with the help of the Baker-Campbell-Hausdorff formula. In our specific case, $[A, [A, B]] = [B, [A, B]] = 0$, so $\exp(A + B) = \exp(A) \exp(B) \exp{-\frac{1}{2}[A, B]}$, where $A = \Lambda_{\vec{q}} \, a_{\vec{q}}^\dagger$ and $B = -A^\dagger$. It gives

$$\sum_{\{n\}} P\{n\} \prod_{\vec{q}} \langle n_{\vec{q}} | \mathcal{D}^\dagger[\Lambda_{\vec{q}}, t] \mathcal{D}[\Lambda_{\vec{q}}, 0] | n_{\vec{q}} \rangle = \prod_{\vec{q}} \sum_{n_{\vec{q}}} \frac{e^{-\beta n_{\vec{q}}\hbar\omega_{\vec{q}}}}{\mathcal{Z}_{\text{ph}}} = \langle n_{\vec{q}} | \mathcal{D}^\dagger[\Lambda_{\vec{q}}, t] \mathcal{D}[\Lambda_{\vec{q}}, 0] | n_{\vec{q}} \rangle$$
$$= \prod_{\vec{q}} \left(1 - e^{-\beta\hbar\omega_{\vec{q}}}\right) e^{-\Lambda_{\vec{q}}^2 \left(1 - e^{-i\omega_{\vec{q}}t}\right)} \times$$
$$\sum_{n_{\vec{q}}=0}^{\infty} e^{-\beta n_{\vec{q}}\hbar\omega_{\vec{q}}} \langle n_{\vec{q}} | e^{\Lambda_{\vec{q}} \, a_{\vec{q}}^\dagger \left(1 - e^{i\omega_{\vec{q}}t}\right)} e^{-\Lambda_{\vec{q}} \, a_{\vec{q}} \left(1 - e^{-i\omega_{\vec{q}}t}\right)} | n_{\vec{q}} \rangle. \tag{4.21}$$

We use the following relation, proven in Ref.[92],

$$\left(1 - e^{-\beta\hbar\omega_{\vec{q}}}\right) \sum_{n_{\vec{q}}=0}^{\infty} e^{-\beta n_{\vec{q}}\omega_{\vec{q}}} \langle n_{\vec{q}} | e^{u_{\vec{q}}^* a_{\vec{q}}^\dagger} e^{-u_{\vec{q}} \, a_{\vec{q}}} | n_{\vec{q}} \rangle = e^{-|u_{\vec{q}}|^2 N_{\vec{q}}}, \tag{4.22}$$

where $N_{\vec{q}} = [\exp(\beta\hbar\omega_{\vec{q}}) - 1]^{-1}$ is the Bose-Einstein distribution and, in our case, $u_{\vec{q}} = \Lambda_{\vec{q}}(1 - e^{-i\omega_{\vec{q}}t})$. This yields

$$\sum_{\{n\}} P\{n\} \prod_{\vec{q}} \langle n_{\vec{q}} | \mathcal{D}^\dagger[\Lambda_{\vec{q}}, t]\mathcal{D}[\Lambda_{\vec{q}}, 0] | n_{\vec{q}}\rangle = \prod_{\vec{q}} e^{-\phi_{\vec{q}}(t)}, \qquad (4.23)$$

where

$$
\begin{aligned}
\phi_{\vec{q}}(t) &= \Lambda_{\vec{q}}^2[(N_{\vec{q}} + 1)(1 - e^{-i\omega_{\vec{q}}t}) + N_{\vec{q}}(1 - e^{i\omega_{\vec{q}}t})] = \\
&\quad \Lambda_{\vec{q}}^2 \left\{ 2N_{\vec{q}} + 1 - [N_{\vec{q}}(N_{\vec{q}} + 1)]^{1/2} \left(e^{-i\omega_{\vec{q}}(t+i\hbar\beta/2)} + e^{i\omega_{\vec{q}}(t+i\hbar\beta/2)} \right) \right\} = \\
&\quad \Lambda_{\vec{q}}^2 \left\{ 2N_{\vec{q}} + 1 - [N_{\vec{q}}(N_{\vec{q}} + 1)]^{1/2} 2\cos[\omega_{\vec{q}}(t + i\hbar\beta/2)] \right\}. \qquad (4.24)
\end{aligned}
$$

We get rid of the cosine in the exponential by expanding it in a series of Bessel functions of complex argument $I_p(z)$,

$$e^{z\cos\theta} = \sum_{p=-\infty}^{\infty} I_p(z)e^{ip\theta}, \qquad (4.25)$$

so we identify $z = 2\Lambda_{\vec{q}}^2[N_{\vec{q}}(N_{\vec{q}} + 1)]^{1/2}$ and $\theta = \omega_{\vec{q}}(t + i\hbar\beta/2)$. Finally, we obtain from Eq.(4.20)

$$\Gamma(\omega_k) = 2\pi g_k^2 \sum_{\{p\}=-\infty}^{\infty} \prod_{\vec{q}} W_{p_{\vec{q}}}[\omega_{\vec{q}}] \, \delta\left(\tilde{\omega}_0 - \omega_k - \sum_{\vec{q}} p_{\vec{q}}\omega_{\vec{q}}\right), \qquad (4.26)$$

where

$$W_{p_{\vec{q}}}[\omega_{\vec{q}}] = \left(\frac{N_{\vec{q}} + 1}{N_{\vec{q}}}\right)^{\frac{p_{\vec{q}}}{2}} e^{-\Lambda_{\vec{q}}^2(2N_{\vec{q}}+1)} \, I_{p_{\vec{q}}}\left(2\Lambda_{\vec{q}}^2\sqrt{N_{\vec{q}}(N_{\vec{q}} + 1)}\right). \qquad (4.27)$$

In the delta function of Eq.(4.26), $p_{\vec{q}}$ indicates that p phonons are emitted in mode $\vec{q}$, with frequency $\omega_{\vec{q}}$. The weight with which such phonon emission occurs is given by $W_{p_{\vec{q}}}[\omega_{\vec{q}}]$, as described by Eq.(4.27). The above calculations provide the same spectrum previously used to describe spontaneous emission of a single quantum dot interacting with acoustic phonons [93]. In section 4.41 we particularize the general expressions above to the case of zero temperature.

Huang-Rhys approach

We now compare the exact approach developed above with the method used by Huang and Rhys [94]. They calculated the absorption spectrum by bound charges in F-centres,

coupled to phonons. Their result became a paradigm for this kind of system, what makes this comparison worth.

Huang and Rhys have shown that each electronic state displaces differently the equilibrium position of the atoms in the lattice, in perfect agreement with our calculations, where we have introduced the displacement operator $\mathcal{D}(\Lambda_{\vec{q}})$. In our formalism, their notation is translated as the Taylor expansion of the displacement operator,

$$\langle m_{\vec{q}}|\tilde{n}_{\vec{q}}\rangle = \langle m_{\vec{q}}| \sum_{j=0}^{\infty} \frac{(-\tau_{\vec{q}})^j}{j!} \hat{p}_{\vec{q}}^j |n_{\vec{q}}\rangle, \tag{4.28}$$

where $\tau_{\vec{q}} \equiv i\Lambda_{\vec{q}}$ and $\hat{p}_{\vec{q}} \equiv i(a_{\vec{q}}^{\dagger} - a_{\vec{q}})$ is the momentum operator. In real-space basis, the momentum operator generates the coordinate derivatives of the positions of the atoms in the lattice, as originally described by the authors.

The major difference between our exact approach, Eqs.(4.18)-(4.27), and Huang-Rhys analysis comes now. The distinguishing step is to take advantage of the degeneracy of the phonons, i.e., $\omega_{\vec{q}} = \omega_{|\vec{q}|}$. This property implies the following: for each phonon mode within a given frequency, transitions involving 2 or more phonons in that particular mode are negligible. It means that if p phonons are created at a frequency ω_q, the only finite contributions are those in which $s + p$ modes gain one quantum, s modes loose one quantum, while all the others remain unchanged, under the condition that all such modes $\vec{q}$ satisfy $\omega_{\vec{q}} = \omega_{|\vec{q}|} = \omega_q$. This statement is justified *a posteriori*, below Eq.(4.30). From now on we deal with transitions satisfying $m_{\vec{q}} - n_{\vec{q}} = \pm 1, 0, \forall \vec{q}$ checking $\omega_q = $ constant. This allows us to compute $\prod_{\vec{q}} |\langle m_{\vec{q}}|\mathcal{D}(\Lambda_{\vec{q}})|n_{\vec{q}}\rangle|^2$ by counting all possible combinations in which phonons are distributed along the modes. Suppose that $s + p$ modes, labeled by $l', l'', ..., l^{(s+p)}$ acquire one quantum while s modes, $r', r'', ..., r^{(s)}$, are lowered by one quantum each of them. Then we can separate the product into modes l and r,

$$\prod_{\vec{q}} |\langle m_{\vec{q}}|\tilde{n}_{\vec{q}}\rangle|^2 =$$

$$\prod_{\vec{j}} |\langle n_{\vec{j}}|\mathcal{D}(\Lambda_{\vec{j}})|n_{\vec{j}}\rangle|^2 \prod_{\vec{r}=\vec{r}'}^{\vec{r}^{(s)}} \frac{|\langle n_{\vec{r}} - 1|\mathcal{D}(\Lambda_{\vec{r}})|n_{\vec{r}}\rangle|^2}{|\langle n_{\vec{r}}|\mathcal{D}(\Lambda_{\vec{r}})|n_{\vec{r}}\rangle|^2} \prod_{\vec{l}=\vec{l}'}^{\vec{l}^{(s+p)}} \frac{|\langle n_{\vec{l}} + 1|\mathcal{D}(\Lambda_{\vec{l}})|n_{\vec{l}}\rangle|^2}{|\langle n_{\vec{l}}|\mathcal{D}(\Lambda_{\vec{l}})|n_{\vec{l}}\rangle|^2}, \tag{4.29}$$

where the denominators are inserted to let $\vec{j}$ span all modes. We now need to perform the sum over all possible combinations of distribution of quanta, as prescribed by $\sum_{\{m\}}$. The sum of products is rewritten as

$$
\sum_{\{m\}} \prod_{\vec{q}} |\langle m_{\vec{q}}|\tilde{n}_{\vec{q}}\rangle|^2 =
$$

$$
\sum_{p=-\infty}^{\infty} \sum_{s=0}^{\infty} \frac{1}{s!(s+p)!} \left(\sum_{\vec{l}} \frac{|\langle n_{\vec{l}}+1|\mathcal{D}(\Lambda_{\vec{l}})|n_{\vec{l}}\rangle|^2}{|\langle n_{\vec{l}}|\mathcal{D}(\Lambda_{\vec{l}})|n_{\vec{l}}\rangle|^2} \right)^{(s+p)} \left(\sum_{\vec{r}} \frac{|\langle n_{\vec{r}}-1|\mathcal{D}(\Lambda_{\vec{r}})|n_{\vec{r}}\rangle|^2}{|\langle n_{\vec{r}}|\mathcal{D}(\Lambda_{\vec{r}})|n_{\vec{r}}\rangle|^2} \right)^{s}
$$

$$
\times \prod_{\vec{j}} |\langle n_{\vec{j}}|\mathcal{D}(\Lambda_{\vec{j}})|n_{\vec{j}}\rangle|^2, \tag{4.30}
$$

where the terms $s!$ and $(s+p)!$ eliminate the excess of repetitions. While $|\Lambda_{\vec{q}}|^{2j} \propto \frac{1}{V^j}$, the above summation yields $\sum_{\vec{q}} \to \frac{V}{(2\pi)^3} \int d^3q$. So, terms containing two phonons in the same mode are proportional to $V/V^2 \to 0$ in the thermodynamic limit ($V \to \infty$), justifying the assumption of only zero- and one-phonon transitions in degenerate modes. Explicit calculation gives

$$
\frac{|\langle n_{\vec{q}}+1|\mathcal{D}(\Lambda_{\vec{q}})|n_{\vec{q}}\rangle|^2}{|\langle n_{\vec{q}}|\mathcal{D}(\Lambda_{\vec{q}})|n_{\vec{q}}\rangle|^2} = \Lambda_{\vec{q}}^2 \, (n_{\vec{q}}+1) \quad \text{and} \quad \frac{|\langle n_{\vec{q}}-1|\mathcal{D}(\Lambda_{\vec{q}})|n_{\vec{q}}\rangle|^2}{|\langle n_{\vec{q}}|\mathcal{D}(\Lambda_{\vec{q}})|n_{\vec{q}}\rangle|^2} = \Lambda_{\vec{q}}^2 \, n_{\vec{q}} \, . \tag{4.31}
$$

Defining $S_\uparrow \equiv \sum_{\vec{l}} \Lambda_{\vec{l}}^2 (n_{\vec{l}}+1)$ and $S_\downarrow \equiv \sum_{\vec{r}} \Lambda_{\vec{r}}^2 \, n_{\vec{r}}$, Eq.(4.30) is written

$$
\sum_{\{m\}} \prod_{\vec{q}} |\langle m_{\vec{q}}|\tilde{n}_{\vec{q}}\rangle|^2 = \sum_{p=-\infty}^{\infty} \left(\sum_{s=0}^{\infty} \frac{S_\uparrow^{(s+p)} S_\downarrow^{s}}{s!(s+p)!} \right) \prod_{\vec{j}} |\langle n_{\vec{j}}|\mathcal{D}(\Lambda_{\vec{j}})|n_{\vec{j}}\rangle|^2. \tag{4.32}
$$

The inner sum is solved using Bessel functions $I_p[z]$ of complex variable,

$$
\sum_{s=0}^{\infty} \frac{S_\uparrow^{(s+p)} S_\downarrow^{s}}{s!(s+p)!} = \left(\frac{S_\uparrow}{S_\downarrow} \right)^{\frac{1}{2}} I_p[2\sqrt{S_\downarrow S_\uparrow}]. \tag{4.33}
$$

The number of phonons $n_{\vec{q}}$ in each mode $\vec{q}$ of the initial state is determined by a thermal distribution $n_{\vec{q}} = N_q = [\exp(\beta\hbar\omega_q) - 1]^{-1}$. Thus,

$$
\frac{S_\uparrow}{S_\downarrow} = \frac{\sum_{\vec{l}} \Lambda_{\vec{l}}^2 (N_q+1)}{\sum_{\vec{r}} \Lambda_{\vec{r}}^2 N_q} = \frac{N_q+1}{N_q} \quad \text{and} \quad \sqrt{S_\downarrow S_\uparrow} = \sum_{\vec{q}} \Lambda_{\vec{q}}^2 \sqrt{N_q(N_q+1)}. \tag{4.34}
$$

The thermal equilibrium of the initial state also yields

$$\left| \prod_{\vec{q}} \sum_{n_{\vec{q}}} \frac{e^{-\beta n_{\vec{q}} \hbar \omega_q}}{\mathcal{Z}_{\vec{q}}} \langle n_{\vec{q}} | \mathcal{D}(\Lambda_{\vec{q}}) | n_{\vec{q}} \rangle \right|^2 = \left| \prod_{\vec{q}} \left(e^{-\frac{\Lambda_{\vec{q}}}{2}} \sum_{n_{\vec{q}}=0}^{\infty} \frac{(e^{-\beta \hbar \omega_q})^{n_{\vec{q}}}}{\mathcal{Z}_{\vec{q}}} \langle n_{\vec{q}} | e^{\Lambda_{\vec{q}} a_{\vec{q}}^{\dagger}} e^{-\Lambda_{\vec{q}} a_{\vec{q}}} | n_{\vec{q}} \rangle \right) \right|^2 ,$$
(4.35)

where we have used the Baker-Campbell-Hausdorff formula. The Laguerre polynomial $L_n(x)$ of order n is used to compute the matrix element

$$\langle n_{\vec{q}} | e^{\Lambda_{\vec{q}} a_{\vec{q}}^{\dagger}} e^{-\Lambda_{\vec{q}} a_{\vec{q}}} | n_{\vec{q}} \rangle = \sum_{l=0}^{n_{\vec{q}}} \frac{(\Lambda_{\vec{q}}^2)^l}{(l!)^2} \frac{n_{\vec{q}}!}{(n_{\vec{q}}-l)!} = L_{n_{\vec{q}}}(\Lambda_{\vec{q}}^2).$$
(4.36)

The sum over Laguerre polynomials is performed using that

$$e^{-\frac{z}{1-z} u^2} = (1-z) \sum_{n=0}^{\infty} L_n(u^2) z^n,$$
(4.37)

where we identify $z = e^{-\beta \hbar \omega_q}$, recalling that $\mathcal{Z}_{\vec{q}} = \sum_{\mu=0}^{\infty} (e^{-\beta \hbar \omega_q})^{\mu} = [1 - e^{-\beta \hbar \omega_q}]^{-1}$. This gives

$$\sum_{n_{\vec{q}}=0}^{\infty} \frac{(e^{-\beta \hbar \omega_q})^{n_{\vec{q}}}}{\mathcal{Z}_{\vec{q}}} \langle n_{\vec{q}} | e^{\Lambda_{\vec{q}} a_{\vec{q}}^{\dagger}} e^{-\Lambda_{\vec{q}} a_{\vec{q}}} | n_{\vec{q}} \rangle = e^{-\Lambda_{\vec{q}}^2 N_q}.$$
(4.38)

Inserting Eq.(4.38) into Eq.(4.35) and applying the result to Eqs.(4.32), (4.33) and (4.34) we finally obtain, for a constant frequency ω_q, the spectrum

$$\Gamma(\omega_k) = 2\pi g_k^2 \sum_{p=-\infty}^{\infty} W_p[\omega_q] \, \delta(\tilde{\omega}_0 - \omega_k - p \, \omega_q),$$
(4.39)

where

$$W_p[\omega_q] = \left(\frac{N_q + 1}{N_q} \right)^{\frac{p}{2}} e^{-(\sum_{\vec{q}} \Lambda_{\vec{q}}^2)(2N_q+1)} I_p \left(2 \left\{ \sum_{\vec{q}} \Lambda_{\vec{q}}^2 \right\} \sqrt{N_q(N_q+1)} \right)$$
(4.40)

and the sum is performed over all phonon modes $\vec{q}$ that have the same frequency $\omega_{\vec{q}} = \omega_q$.

Eqs.(4.39) and (4.40) are the result found by Huang and Rhys for a constant frequency. The frequency restriction is introduced in Huang-Rhys calculations because they intended to study longitudinal optical phonons, which have constant dispersion relation, $\omega_{\vec{q}} = \omega_{\text{LO}}$.

To reobtain Eqs.(4.26) and (4.27) from Eqs.(4.39) and (4.40), Huang-Rhys reasoning can be directly applied. One just has to notice that the continuum of phonon modes consists in an ensemble of concentric shells, each shell defined by a constant wavevector radius $|\vec{q}| = q$. Given that the wavevector radius is constant, so is the frequency, $\omega_{\vec{q}} = \omega_q$. The degeneracy inside each shell comes from all possible wavevector directions $\hat{q}$, such that $\vec{q} = |\vec{q}|\,\hat{q}$. So, for each shell, Huang-Rhys approach is valid, clearly providing the same result as in Eqs.(4.26) and (4.27).

We will be interested in the modeling of longitudinal acoustic phonons, which have linear dispersion relation, $\omega_{\vec{q}} = c_s|\vec{q}|$, being c_s the speed of sound in the material. Thus, acoustical phonons obey the condition we have imposed, $\omega_{\vec{q}} = \omega_{|\vec{q}|}$.

4.1.3 Free-space spontaneous emission at zero temperature

We study now a specific case of the general framework introduced above. We focus on the zero temperature regime. Our intention is to provide the most clear example of how phonons modify the spontaneous emission of a two-level system.

The initial quantum state of a phonon bath in equilibrium at temperature $T = 0\mathrm{K}$ is the vacuum state, $\prod_{\vec{q}}|\tilde{0}_{\vec{q}}\rangle$. Our spectrum is then given by

$$\Gamma(\omega_k) = 2\pi g_k^2 \sum_{\{m\}} \prod_{\vec{q}} |\langle m_{\vec{q}}|\tilde{0}_{\vec{q}}\rangle|^2\, \delta\left(\tilde{\omega}_0 - \omega_k - \sum_{\vec{q}} m_{\vec{q}}\,\omega_{\vec{q}}\right). \qquad (4.41)$$

Note that only phonon emission is allowed, given that no phonons are available for absorption.

As we have stated in Eq.(4.8), the displaced vacuum is a coherent state, whose components in Fock states are given by

$$\langle m_{\vec{q}}|\tilde{0}_{\vec{q}}\rangle = e^{-\frac{1}{2}|\Lambda_{\vec{q}}|^2} \frac{\Lambda_{\vec{q}}^{m_{\vec{q}}}}{\sqrt{m_{\vec{q}}!}}. \qquad (4.42)$$

This allows us to write Eq.(4.41) as a sum of the zero-phonon line (ZPL), one-phonon line (1PL) and so on. The ZPL contribution reads

$$\Gamma_{\mathrm{ZPL}}(\omega_k) = 2\pi g_k^2 e^{-S}\, \delta(\tilde{\omega}_0 - \omega_k), \qquad (4.43)$$

where $S = \sum_{\vec{q}} |\Lambda_{\vec{q}}|^2$. We introduce a finite lifetime for the QD phenomenologically, replacing the delta function by a normalized Lorentzian [93],

$$\delta(\omega_0 - \omega) \to \mathcal{L}(\omega) = \frac{1}{\pi} \frac{\frac{\gamma}{2}}{\left(\frac{\gamma}{2}\right)^2 + (\omega_0 - \omega)^2}, \tag{4.44}$$

where γ includes pure dephasing rate [90], as discussed at the beginning of this chapter.

The one-phonon line is given by

$$\Gamma_{1\text{PL}}(\omega_k) = 2\pi g_k^2 e^{-S} \sum_{\vec{q}} |\Lambda_{\vec{q}}|^2 \; \delta(\tilde{\omega}_0 - \omega_k - \omega_q). \tag{4.45}$$

Direct calculations show that, at zero temperature, transitions involving two or more phonons contribute much less (one order of magnitude) than the one-phonon transition and hence will be neglected.

The acoustic phonon coupling [91] depends on the wavefunctions of the electron $|\psi_e\rangle$ and the hole $|\psi_h\rangle$ through

$$\Lambda_{\vec{q}} = \frac{|D_e g_e(\vec{q}) + D_h g_h(\vec{q})|}{\hbar \omega_q} \sqrt{\frac{\hbar \omega_q}{2 c_s^2 \rho_m V}}, \tag{4.46}$$

where

$$g_{e,h}(\vec{q}) = \langle \psi_{e,h}| \; e^{i\vec{q}.\vec{r}} \; |\psi_{e,h}\rangle, \tag{4.47}$$

being $\vec{r}$ the particle coordinate operator, $D_{e,h}$ the deformation potentials for the electron (e) and the hole (h), c_s the speed of sound in the solid and ρ_m the bulk mass density.

The wave functions of both electron and hole can be approximated by Gaussians with extensions $\sigma_{e,h}$, $\psi_{e,h}(\vec{r}) = (4\pi\sigma_{e,h}^2)^{-\frac{3}{4}} \exp\left[-r^2/(8\sigma_{e,h}^2)\right]$, so the Fourier transform reads

$$g_{e,h}(\vec{q}) = e^{-\sigma_{e,h}^2 \; q^2}. \tag{4.48}$$

We use the acoustic phonon dispersion relation $\omega_q = c_s q$ and perform the integration in the continuum limit,

$$\sum_{\vec{q}} \to \frac{V}{(2\pi)^3} \int d^3 q,$$

finding

$$\Gamma_{1\mathrm{PL}}(\omega_k) = \frac{g_k^2\, e^{-S}}{2\pi\hbar\rho_m c_s^4}\left(\frac{\tilde{\omega}_0 - \omega_k}{c_s}\right)\left| D_e e^{-\left(\sigma_e\frac{\tilde{\omega}_0 - \omega_k}{c_s}\right)^2} + D_h e^{-\left(\sigma_h\frac{\tilde{\omega}_0 - \omega_k}{c_s}\right)^2}\right|^2 \Theta(\tilde{\omega}_0 - \omega_k),$$

$$(4.49)$$

where $S = \frac{1}{(2\pi)^2\hbar\rho_m c_s^3}\left(\frac{D_e^2}{4\sigma_e^2} + \frac{D_h^2}{4\sigma_h^2} + \frac{D_e D_h}{\sigma_e^2 + \sigma_h^2}\right)$ and $\Theta(x)$ is the Heaviside step function.

To finally obtain the spectrum, we still need to multiply the function $\Gamma(\omega) = \Gamma_{\mathrm{ZPL}}(\omega) + \Gamma_{1\mathrm{PL}}(\omega)$ by the density of states $\rho_{\mathrm{free}}(\omega)$ of the vacuum of electromagnetic fields in 3D space (see Eq.4.14),

$$\rho_{\mathrm{free}}(\omega) = \frac{V}{\pi^2 c^3}\,\omega^2, \qquad (4.50)$$

where c is the speed of light. The divergence of volume V is compensated by the coupling, $g_k^2 = \frac{d^2\omega_k}{2\hbar\epsilon_0 V}$, as defined in Chapter 1. Note that the function $g_k^2\rho_{\mathrm{free}}(\omega_k)$ is effectively flat in the region of optical frequencies, leaving no net contribution apart from a multiplicative constant $\approx g_0^2\rho_{\mathrm{free}}(\tilde{\omega}_0)$.

In Fig.4.6, we plot the spontaneous emission spectrum

$$S_{\mathrm{QD}}(\omega) = \rho_{\mathrm{free}}(\omega)\,[\Gamma_{\mathrm{ZPL}}(\omega) + \Gamma_{1\mathrm{PL}}(\omega)],$$
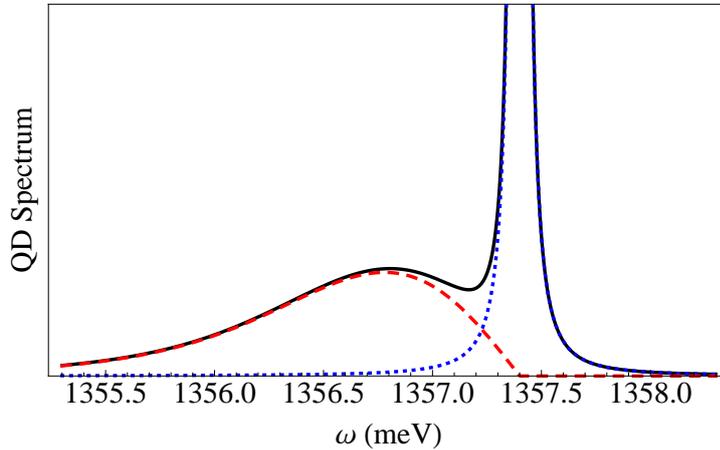

Figure 4.6: Spontaneous emission spectrum $S(\omega)$ of a quantum dot coupled to acoustic phonons at temperature $T = 0K$ (solid black curve). Dashed red: one-phonon emission contribution. Dotted blue: zero-phonon line lorentzian.

The dotted blue curve is the zero-phonon line, given by the standard Lorentzian found in the spontaneous emission spectrum of a two-level system [19]. The dashed red is the one-phonon emission contribution, governed by the inverse of the spatial extension of the quantum dot wavefunctions ($\sim 1/\sigma_{e,h}$). Only the low frequency contribution appears at zero temperature, given that only phonon emission is allowed. These are commonly called phonon wings, as they provide a wing-shaped pedestal that strongly modifies the usual Lorentzian profile. In the plot we used the parameters listed in Table 4.1, based on typical values for InAs/GaAs quantum dots [93, 95, 96].

$\tilde{\omega}_0$	1357.4	meV
γ	10	μeV
De	12.50	eV
Dh	6.25	eV
σ_e	3.0	nm
σ_h	1.5	nm
c_s	5000	m/s
ρ_m	5320	Kg/m^3

Table 4.1: Parameters of the quantum dot and its solid-state matrix.

4.1.4 The low temperature limit

Now we show how to extend the model to low (finite) temperatures. We define low temperature as $T \lesssim T_R$, where the reference temperature T_R is related to the population of the maximally coupled phonon mode (maximum of the phonon wing) of frequency ω_{m},

$$N_{\mathrm{m}}(T_R) = \frac{1}{e^{\frac{\hbar\omega_{\mathrm{m}}}{k_B T_R}} - 1} \lesssim 1. \tag{4.51}$$

The parameters here used give $\omega_{\mathrm{m}} \approx 600\mu$eV, so that $T_R \sim 10$K.

The expression for the low-temperature regime follows from intuitive considerations. We assume that phonon emission is enhanced (stimulated) by a factor $N_{\omega_{\mathrm{ph}}}(T) + 1$. We

also consider that phonon absorption is proportional to the average number of phonons $N_{\omega_{\text{ph}}}(T)$ available in a given mode ω_{ph}. The modified one-phonon line is then

$$\Gamma_{1\text{PL}}^T(\omega) = [N_{\omega_{\text{ph}}}(T) + 1]\, \Gamma_{1\text{PL}}(\omega) + [N_{\omega_{\text{ph}}}(T)]\, \tilde{\Gamma}_{1\text{PL}}(\omega), \qquad (4.52)$$

where $\tilde{\Gamma}_{1\text{PL}}(\omega)$ is the spectral component related to phonon-absorption, defined here as the mirror image of $\Gamma_{1\text{PL}}(\omega)$ around $\tilde{\omega}_0$, i.e., $\tilde{\Gamma}_{1\text{PL}}(\omega) \equiv \Gamma_{1\text{PL}}(2\tilde{\omega}_0 - \omega)$. Note that $\Gamma_{1\text{PL}}^{T=0}(\omega) = \Gamma_{1\text{PL}}(\omega)$.

The resulting spectrum from Eq.(4.52),

$$S_{\text{QD}}(\omega) = \rho_{\text{free}}(\omega)\, [\Gamma_{\text{ZPL}}(\omega) + \Gamma_{1\text{PL}}^T(\omega)], \qquad (4.53)$$

is plotted in Fig.4.7 for temperatures $T = 0$K (black), $T = 1$K (blue), $T = 3$K (red) and $T = 10$K (green). Our result for low temperatures is qualitatively similar to the experimental outcome from Ref.[95], by E. Peter and colleagues, obtained at $T = 7$K and $T = 15$K, which is consistent with the data from Ref.[93] (Fig.4.4). Both present asymmetric non-Lorentzian piedestals. The asymmetry occurs because phonon emission ($\propto N_q + 1$) is more likely than absorption ($\propto N_q$).
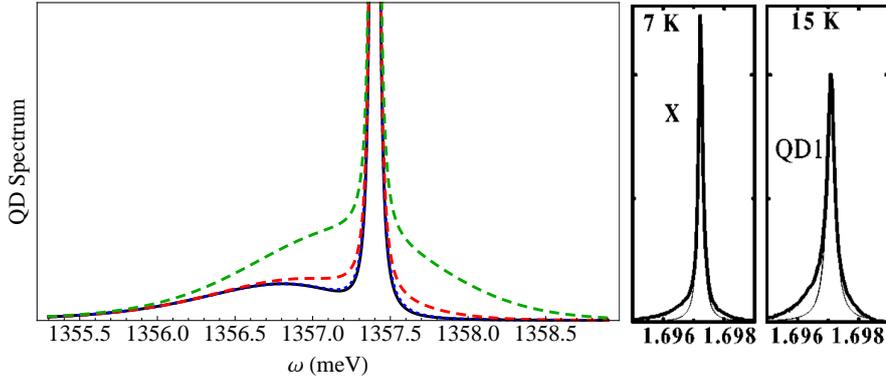

Figure 4.7: Left: Spontaneous emission spectrum $S_{\text{free}}(\omega)$ of a quantum dot coupled to acoustic phonons at low temperatures $T = 0$K (black), $T = 1$K (blue), $T = 3$K (red) and $T = 10$K (green). Right: QD emission spectra (μ-PL, thick lines) in the experiment from Ref.[95] at temperatures $T = 7$K and 15K. The thin lines represent Lorentzian profile.

We finish this subsection with a quantitative justification for Eq.(4.52), derived from the low temperature limit of Eqs.(4.26) and (4.27). The first step is expanding $\Gamma(\omega)$ in a sum of zero and one-phonon transitions,

$$
\begin{aligned}
\Gamma(\omega) &= \sum_{\{p\}} \prod_{\vec{q}} W_{p_{\vec{q}}}(\omega_q)\, \delta\!\left(\omega_0 - \omega - \sum_{\vec{q}} p_{\vec{q}}\omega_q\right) \\
&= \left(\prod_{\vec{q}'} W_0(\omega_{q'})\right) \delta(\omega_0 - \omega) + \\
&\quad + \left(\prod_{\vec{q}'} W_0(\omega_{q'})\right) \sum_{\vec{q}} \frac{W_1(\omega_q)}{W_0(\omega_q)}\delta(\omega_0 - \omega - \omega_q) \\
&\quad + \left(\prod_{\vec{q}'} W_0(\omega_{q'})\right) \sum_{\vec{q}} \frac{W_{-1}(\omega_q)}{W_0(\omega_q)}\delta(\omega_0 - \omega + \omega_q) \\
&\quad + \mathcal{O}(2\text{ phonons}),
\end{aligned} \tag{4.54}
$$

where the term containing $W_{-1}(\omega_q)$ represents phonon absorption. The denominator has been introduced so that the product spans all modes. The expression for $W_p(\omega)$, Eq.(4.27), involves modified Bessel functions $I_p(x)$, with integral representation, for $\mathrm{Re}[x] > 0$,

$$
I_p(x) = \frac{1}{\pi}\int_0^\pi e^{x\cos\theta}\cos(p\theta)d\theta - \frac{\sin(p\pi)}{\pi}\int_0^\pi e^{-x\cosh(t)-p\,t}dt, \tag{4.55}
$$

allowing us to compute the Taylor expansions

$$
I_0(x) = 1 + \mathcal{O}(x^2) \quad\text{and}\quad I_1(x) = \frac{x}{2} + \mathcal{O}(x^3). \tag{4.56}
$$

From Eqs.(4.46) and (4.27) it follows that $x \propto 1/V$, where V is the volume of quantization for the phonons. Assuming the thermodynamical limit $V \to \infty$ (i.e., $V \gg \sigma_e^3, \sigma_h^3$), the above expansion is justified. Then we have

$$
W_0(\omega_q) = e^{-\Lambda_{\vec{q}}^2(2N_q+1)}I_0(2\Lambda_{\vec{q}}^2\sqrt{N_q(N_q+1)}) \longrightarrow e^{-\Lambda_{\vec{q}}^2}, \tag{4.57}
$$

where both $V \to \infty$ and $N_q \ll 1$ limits have been applied, so that

$$
\prod_{\vec{q}} W_0(\omega_q) \to e^{-\sum_{\vec{q}}\Lambda_{\vec{q}}^2} = e^{-S}, \tag{4.58}
$$

where S has been defined in the previous subsection. By keeping the condition $V \to \infty$, the finite temperature case of Eq.(4.58) can be readily computed, yielding nothing but a different pre-factor in the spectrum. We also have, in the limit $V \to \infty$,

$$\frac{W_1(\omega_q)}{W_0(\omega_q)} \to \left(\frac{N_q+1}{N_q}\right)^{\frac{1}{2}} \frac{1}{2} \, 2\Lambda_{\vec{q}}^2 \sqrt{N_q(N_q+1)} = \Lambda_{\vec{q}}^2 \, (N_q+1) \qquad (4.59)$$

and

$$\frac{W_{-1}(\omega_q)}{W_0(\omega_q)} \to \left(\frac{N_q+1}{N_q}\right)^{-\frac{1}{2}} \frac{1}{2} \, 2\Lambda_{\vec{q}}^2 \sqrt{N_q(N_q+1)} = \Lambda_{\vec{q}}^2 \, N_q. \qquad (4.60)$$

Inserting the above expressions into Eq.(4.54), we get exactly what is obtained by using Eqs.(4.52), (4.43) and (4.45). This concludes the quantitative justification of Eq.(4.52).

4.2 Phonon-assisted off-resonance cavity feeding

In what follows, we model the spontaneous emission of a quantum dot weakly coupled to a dissipative single-mode cavity, in the presence of phonons. The cavity is introduced within the formalism developed in the previous sections. We present evidence that acoustic phonons can be responsible for cavity feeding, i.e., the efficient spontaneous emission of a photon at the frequency of a cavity that is very far from resonance.

Two-level system (no phonons) weakly coupled to a cavity: Purcell effect

A cavity weakly coupled to an emitter affects its electromagnetic environment by changing the density of modes [14],

$$\rho_{\text{free}}(\omega) = \frac{V}{\pi^2 c^3} \, \omega^2 \quad \longrightarrow \quad \rho_{\text{cav}}(\omega) = \frac{1}{\pi} \frac{\frac{\omega_c}{2Q}}{\left(\frac{\omega_c}{2Q}\right)^2 + (\omega_c - \omega)^2}, \qquad (4.61)$$

characterized by the central frequency ω_c and the quality factor $Q \equiv \omega_c/\kappa$, where κ is the cavity decay rate (linewidth).

Another difference introduced by a cavity is the finite volume V_c, in contrast to the infinite free-space volume V. The cavity volume V_c is obtaining by integrating the

modulus square of the spatial dependence of the electromagnetic field inside the cavity. The emitter-cavity coupling is given by $g_c^2(\omega) = \frac{d^2\omega}{2\hbar\epsilon_0 V_c}$.

We can now use Fermi's golde rule to compute the decay rate Γ_c of a two-level system under the influence of a cavity,

$$\Gamma_c = 2\pi\rho_{\text{cav}}(\omega_0)g_c^2(\omega_0). \tag{4.62}$$

We disregard phonons at this point.

Suppose, for instance, the resonant condition $\delta_c = \omega_c - \omega_0 = 0$. Let us call Γ_0 the decay rate in free space, $\Gamma_0 \equiv 2\pi\rho_{\text{free}}(\omega_0)g^2(\omega_0) = \frac{d^2\omega_0^3}{\pi\epsilon_0\hbar c^3}$. Then,

$$\Gamma_c = \eta_{\text{Purcell}}\ \Gamma_0, \tag{4.63}$$

where

$$\eta_{\text{Purcell}} \equiv \frac{\Gamma_c}{\Gamma_0} = \frac{\rho_{\text{cav}}(\omega_0)g_c^2(\omega_0)}{\rho_{\text{free}}(\omega_0)g^2(\omega_0)} = \frac{1}{4\pi^2}\ \frac{Q}{V_c}\ \lambda_c^3, \tag{4.64}$$

and $\lambda_c = 2\pi c/\omega_c$ is the wavelength of the cavity field. Parameter η_{Purcell} is the so called Purcell factor [15]. A small $(V_c < \lambda_c^3)$ and good $(Q > 4\pi^2)$ cavity yields $\eta_{\text{Purcell}} > 1$, increasing the emitter decay rate. On the other hand, if $\delta_c \gg \kappa$, the cavity can inhibit spontaneous emission. The Purcell effect is this modification of emission rate resulting from a structured electromagnetic vacuum with a given density of modes. Purcell effect plays a key role in cavity feeding.

4.2.1 Spectrum of the quantum-dot–cavity system in weak coupling regime

The formalism based on Fermi's golden rule, developed in the previous sections, allows us to compute the spectrum $S(\omega)$ of the composite system by simply introducing the cavity density of modes $\rho_{\text{cav}}(\omega) = S_{\text{cav}}(\omega)$,

$$S(\omega) = S_{\text{cav}}(\omega) \times S_{\text{QD}}(\omega), \tag{4.65}$$

where $S_{\text{QD}}(\omega) = \Gamma(\omega)$. At low temperatures, we have

$$S(\omega) = S_{\text{cav}}(\omega)\ [\Gamma_{\text{ZPL}}(\omega) + \Gamma_{\text{1PL}}^T(\omega)]. \tag{4.66}$$

Note that the zero-phonon contribution leads to the decay rate $\Gamma_c \, e^{-S}$. If phonon coupling is turned off ($\Lambda_{\vec{q}} = 0$), then $S = 0$ and the result from a two-level system is reobtained.

In the figures below we plot two superimposed curves:

- Black (solid): $S(\omega)$, asymmetric with cavity-QD detuning δ_c.

- Blue (dotted): $S_{\text{ZPL}}(\omega) \equiv S_{\text{cav}}(\omega)\Gamma_{\text{ZPL}}(\omega)$, representing the pure dephasing cavity feeding (no-phonon), symmetric with detuning.

In Fig.(4.8), we plot cavity-QD spectrum at $T = 0\text{K}$, for a cavity of $Q = 3000$ ($\kappa \approx 450\mu\text{eV}$) with two different detunings, $\delta_c = \mp 600\mu\text{eV}$ (resp. left/right frame). The QD parameters are the same as before, Tab.4.1. The influence of phonons in the cavity feeding process becomes evident.
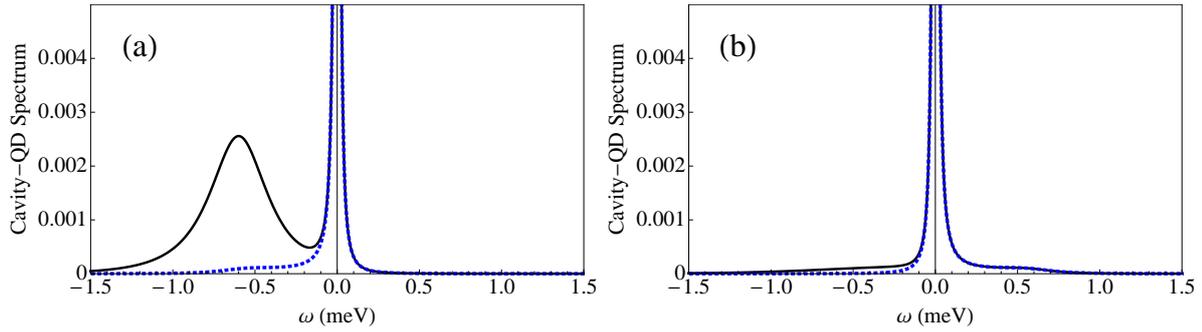
Figure 4.8: (a) $S(\omega)$ (solid black) and $S_{\text{ZPL}}(\omega)$ (dotted blue) at $\delta_c = -600\mu\text{eV}$. (b) the same for $\delta_c = 600\mu\text{eV}$. In both cases, $Q = 3000$ and $T = 0\text{K}$.

The cavity feeding mechanism can be understood in terms of Purcell effect. Phonons allow the emitter to create photons at the frequency of the cavity mode. Then, the efficiency of this process is dramatically enhanced by the cavity, which increases the density of electromagnetic modes in that frequency region. The ratio between the resonant cavity-phonon wing and the off-resonance cavity-phonon wing gives a Purcell factor for the feeding process. The visibility of the cavity-like peak increases, thus, with the quality factor.

In Fig.4.9 we do the same analysis as before (keeping $T = 0$K, $\delta_c = \mp 600\mu$eV), but for a huge quality factor of $Q = 30\ 000$ ($\kappa \approx 45\mu$eV).
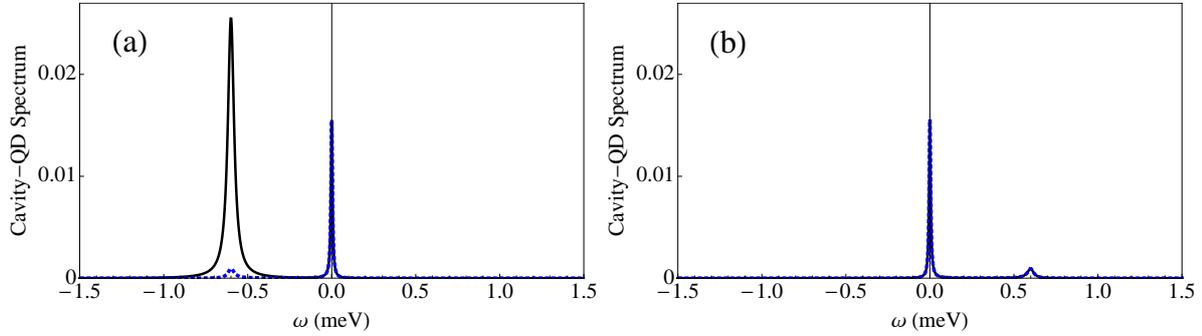
Figure 4.9: (a) $S(\omega)$ (solid black) and $S_{\text{ZPL}}(\omega)$ (dotted blue) at $\delta_c = -600\mu$eV. (b) the same for $\delta_c = 600\mu$eV. In both cases, $Q = 30\ 000$ and $T = 0$K

We now reobtain, in a qualitative manner, the result from Fig.4.2, taken from Ref.[89]. In that experiment, the cavity peak has a much higher frequency than the ZPL (smaller wavelength), giving $\delta_c \approx 2800\mu$eV. The experiment is performed for a Q factor between 12 000 and 30 000, with temperatures around 4.2K. We can only feed high-frequency cavities with a reasonable efficiency by increasing temperature. In Fig.4.10 we use $\delta_c = 2000\mu$eV, $Q = 30\ 000$ and $T = 10$K. The resulting cavity-like peak is broader and about three times shorter than the ZPL.

The role of phonons in cavity feeding has been the subject of other studies. Particular examples are an experiment by Ates and colleagues [97] and a theoretical work by Hughes and colleagues [98]. In what follows, we position our model with respect to the formalism developed by Hughes *et. al.*.
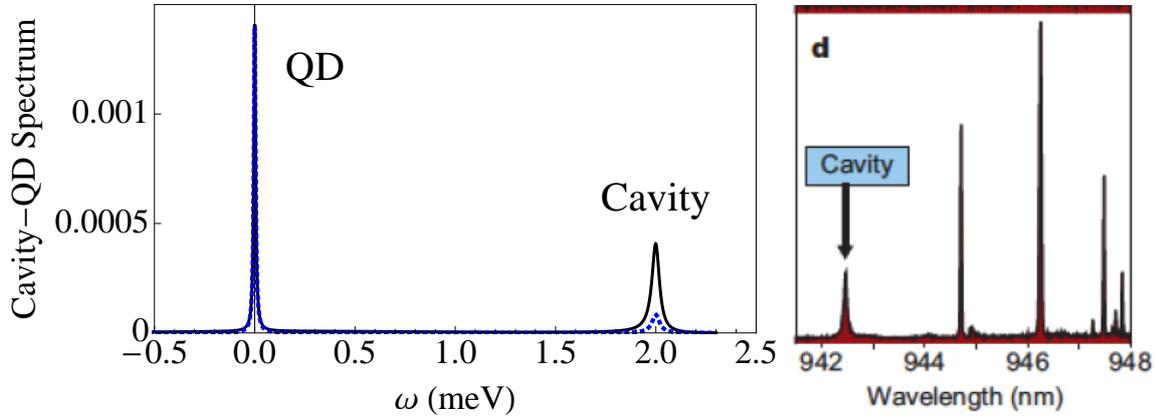
Figure 4.10: Left: $S(\omega)$ (solid black) and $S_{\mathrm{ZPL}}(\omega)$ (dotted blue) at $\delta_c = 2000\mu$eV, $T = 10$K and $Q = 30\,000$. Right: Experiment [89], wavelengths corresponding roughly to 943nm $\approx 1325, 56$ meV and 945nm $\approx 1322, 75$ meV, so that $\delta_c \approx 2800~\mu$eV; $Q \sim 12\,000$–$30\,000$ and $T \sim 4$K.

Link with the formalism for strong-coupling

A quantum dot in free space coupled to acoustic phonons exhibit non-Lorentzian spectral profile, due to phonon emission/absorption. This feature is preserved under the influence of a weakly coupled cavity and must remain so in the strong coupling regime. Many approaches to the modeling of strongly coupled cavity-quantum dot have been developed. In Ref.[99], for instance, the problem is treated under an approximation valid only when the coupling is much smaller than the maximal frequency of the phonon wings, which in our case means $g_c \ll \omega_{\mathrm{m}} \sim 1$meV. A solution for higher coupling strengths has been provided in Ref.[100]. While in Ref.[99] the non-Lorentzian aspect has been reproduced in the spectrum, this did not happen in Ref.[100], where the phonon-related asymmetry has appeared only in the decay rate. A complete solution for this problem has been provided by Hughes *et. al.* [98], which is valid for arbitrary coupling strengths and properly describes non-Lorentzian spectra.

The key point of the model by Hughes is the solution of the quantum field operators by Green's function, instead of using a master equation for the density matrix of the system. Without phonons, both approaches are equivalent, but the Green's function

formalism is directly extendable for phonons in a quite natural way.

From the Hamiltonian of the atom-cavity system (Eq.4.11), they derive the Heisenberg equations for the cavity fied $\hat{E}(t)$ and the atomic operator $\hat{\sigma}(t)$. Then a Fourier transform is applied, yielding $\hat{E}(\omega)$ and $\hat{\sigma}(\omega)$ which are solved by Green's function for the atom initially excited and the cavity in vacuum state. Note that this corresponds to the same initial state from our spontaneous emission spectrum. Their solution is valid for a low cavity excitation. Finally, normalized spectrum is obtained, $S(\omega) = \langle \hat{E}^\dagger(\omega)\hat{E}(\omega)\rangle$.

Their general procedure is particularized for the simplest case, namely, the spontaneous emission of a two-level system in free space, in the absence of phonons. Their normalized spectrum reads

$$S_{\text{QD}}(\omega) = \gamma \left| \frac{\omega_0 + \omega}{\omega_0^2 - \omega^2 - i\omega\gamma} \right|^2 = 2\pi \, \mathcal{L}_{\omega_0}(\omega), \qquad (4.67)$$

where we apply our notation. The rate γ is introduced phenomenologically, just as we do for the ZPL. The normalized Lorentzian, $\mathcal{L}_{\omega_0}(\omega) = \frac{1}{\pi}\frac{\gamma}{2}[(\frac{\gamma}{2})^2 + (\omega_0 - \omega)^2]^{-1}$, is explictly used here just to compare with our previous result: Eq.(4.67) corresponds to Eqs.(4.43) and (4.44) under proper normalization.

Still in the absence of a cavity, they show how phonons are introduced,

$$S_{\text{QD}}^{\text{ph}}(\omega) = \gamma \left| \frac{\omega_0 + \omega}{\omega_0^2 - \omega^2 - i\omega\gamma - \omega\Sigma_{\text{ph}}(\omega)} \right|^2, \qquad (4.68)$$

where $\Sigma_{\text{ph}}(\omega)$ is the phonon self-energy from the independent boson model. It is obtained as follows, in which we use Hughes' notations. The quantum-dot polarizability $\alpha_{\text{QD}}(t)$ is given by

$$\alpha_{\text{QD}}(t) = \alpha_{\text{QD}}(0) \, e^{-i\left(\tilde{\omega}_0 - i\frac{\gamma}{2}\right)t} \, e^{\phi_{\text{H}}(t)}, \qquad (4.69)$$

where

$$\phi_{\text{H}}(t) = \int_0^\infty d\omega \, \frac{J(\omega)}{\omega^2} \left[\coth\left(\frac{\beta\hbar\omega}{2}\right) \cos(\omega t) - i\sin(\omega t) \right], \qquad (4.70)$$

and the spectral function is defined as

$$J(\omega) = J_0 \, \omega^3 \exp(-\omega^2/2\omega_b^2), \qquad (4.71)$$

being J_0 a phenomenological constant and ω_b a cutoff frequency. The Fourier transform for $\alpha_{\mathrm{QD}}(t)$ is computed, yielding

$$\tilde{\alpha}_{\mathrm{QD}}(\omega) = \frac{d^2 2\tilde{\omega}_0/\hbar\epsilon_0}{\omega_0^2 - \omega^2 - i\omega\gamma - \omega\Sigma_{\mathrm{ph}}(\omega)}, \tag{4.72}$$

which is connected to spectrum, giving Eq.(4.68).

The model used by Hughes $et.$ $al.$ is the same we have been using, namely, the independent boson model. Therefore, the two results for spectrum must be equivalent. To map notations and clarify the equivalence we show that $\phi_{\mathrm{H}}(t) = -\sum_{\vec{q}} \phi_{\vec{q}}(t)$, where $\phi_{\vec{q}}(t)$ is given by Eq.(4.24), that we rewrite below:

$$\phi_{\vec{q}}(t) \;=\; \Lambda_{\vec{q}}^2 \left\{ 2N_{\vec{q}} + 1 - [N_{\vec{q}}(N_{\vec{q}}+1)]^{1/2} \left(e^{-i\omega_{\vec{q}}(t+i\hbar\beta/2)} + e^{i\omega_{\vec{q}}(t+i\hbar\beta/2)} \right) \right\}. \tag{4.73}$$

Simple algebra shows that

$$[N_{\vec{q}}(N_{\vec{q}}+1)]^{1/2} \left(e^{-i\omega_{\vec{q}}(t+i\hbar\beta/2)} + e^{i\omega_{\vec{q}}(t+i\hbar\beta/2)} \right) = \coth\left(\frac{\beta\hbar\omega}{2}\right) \cos(\omega t) - i\sin(\omega t). \tag{4.74}$$

Besides, using the continuum limit $\sum_{\vec{q}} \to \frac{V}{(2\pi)^3} \int d^3q$, the dispersion relation for acoustic phonons $\omega_q = c_s q$ and Eqs.(4.46), (4.47) and (4.48), we find

$$\sum_{\vec{q}} \Lambda_{\vec{q}}^2 \;\to\; \int_0^\infty d\omega\, \omega \left| D_e e^{-\frac{(\omega-\tilde{\omega}_0)^2}{(c_s/\sigma_e)^2}} + D_h e^{-\frac{(\omega-\tilde{\omega}_0)^2}{(c_s/\sigma_h)^2}} \right|^2$$

$$= J_0 \int_0^\infty d\omega\, \frac{\left(\omega^3\, e^{-\frac{\omega^2}{2(c_s/2\sigma_e)^2}} \right)}{\omega^2} = \int_0^\infty d\omega\, \frac{J(\omega)}{\omega^2}, \tag{4.75}$$

where it is assumed that $\sigma_e = \sigma_h$ and we identify the cutoff frequency $\omega_b = c_s/(2\sigma_e)$. Together, equations (4.74) and (4.75) show that our method gives identical results as the model by Hughes. That is, $S_{\mathrm{QD}}^{\mathrm{ph}}(\omega) = \mathcal{N}_{\mathrm{free}}\Gamma(\omega)$, given a normalization factor $\mathcal{N}_{\mathrm{free}}$.

Now the cavity is finally introduced in the modeling. For the coupled cavity-QD system of arbitrary coupling strengh g_c, the normalized spectrum writes

$$S(\omega) = \kappa \left| \frac{g_c\, 2\omega_c}{\omega_c^2 - \omega^2 - i\omega\kappa} \times \frac{\omega_0 + \omega}{\omega_0^2 - \omega^2 - i\omega\gamma - \frac{4g_c^2\omega_c\omega_0}{\omega_c^2-\omega^2-i\omega\kappa}} \right|^2. \tag{4.76}$$

Comparison between Eqs.(4.76) and (4.68) makes it straightforward to include phonons,

$$S^{\mathrm{ph}}(\omega) = \kappa \left| \frac{g_c \, 2\omega_c}{\omega_c^2 - \omega^2 - i\omega\kappa} \times \frac{\omega_0 + \omega}{\omega_0^2 - \omega^2 - i\omega\gamma - \omega\Sigma_{\mathrm{ph}}(\omega) - \frac{4g_c^2\omega_c\omega_0}{\omega_c^2 - \omega^2 - i\omega\kappa}} \right|^2. \qquad (4.77)$$

Eq.(4.77) is Hughes' general result, valid for all temperatures and coupling strenghs.

The weak-coupling limit, $g_c \ll \gamma$, is easily obtained, yielding

$$S^{\mathrm{ph}}(\omega; \ g_c \ll \gamma) \approx \kappa \left| \frac{g_c \, 2\omega_c}{\omega_c^2 - \omega^2 - i\omega\kappa} \right|^2 \left| \frac{\omega_0 + \omega}{\omega_0^2 - \omega^2 - i\omega\gamma - \omega\Sigma_{\mathrm{ph}}(\omega)} \right|^2. \qquad (4.78)$$

That is, the weak coupling limit is a product of the Lorentzian peak from a bare cavity and the non-Lorentzian peak from a quantum-dot coupled to phonons. Eq.(4.78) is nothing but $S^{\mathrm{ph}}(\omega; \ g_c \ll \gamma) = \mathcal{N}_{\mathrm{ph}} \, \rho_{\mathrm{cav}}(\omega) \, \Gamma(\omega) = \mathcal{N}_{\mathrm{ph}} \, S(\omega)$, under proper normalization $\mathcal{N}_{\mathrm{ph}}$. This clearly shows that our modeling for the cavity is consistent with the weak coupling limit from the general approach where strong coupling is allowed.

4.3 Exploring the spectral behaviour of the cavity

In this section we study intriguing effects that arise in the spectrum of the cavity mode [101]. Emission spectroscopy is often used to investigate the optical mode properties, measuring its frequency and quality factor. Nevertheless, the consequences of the solid-state environment on the measured emission spectra have been scarcely addressed [102]. Emission at the cavity mode energy is still considered as broad quantum dot (QD) emission "filtered" by the cavity, resulting in the idea that emission spectroscopy can be used to measure the cavity properties. Here we show that this image breaks down. The emission at the mode energy is just a mirage of the cavity mode, leading to mode narrowing or broadening, and mode pulling or hoping. So, it cannot be used to measure the cavity properties. These effects result from the competitive emission of a single photon in either the zero- or one-phonon line into the cavity mode.

4.3.1 Experimental evidences of the cavity mode distortion

This experiment is performed in a semiconducting micropillar cavity, as presented at the beginning of this chapter, Fig.4.1. The cavity quality factor is in the range of few thousands, so the QD-cavity system operates in the weak coupling regime. At spectral resonance with the cavity mode, the QD line experiences a Purcell factor between 5 and 10. The emission intensity as a function of temperature (detuning δ_c increases linearly with temperature) and energy is shown in Fig.4.11 (top). QD emission lines are spectrally narrow, with a strong energy dependence with temperature. The broad emission presenting a smaller energy variation with temperature corresponds to emission at the cavity mode energy. In Fig.4.11 (bottom), the strong increase of the QD emission at resonance with the cavity mode is the signature of the efficient light extraction resulting from the Purcell effect.

The central frequency of the mode is apparently pushed about $200\mu eV$ from the central QD peak when going towards resonance and shows an abrupt jump when it goes to the high energy side. The apparent linewidth of the mode also decreases by a factor of 2 along with intensity of emission and increases again at the high energy side. A comparison between deterministically matched and unmatched mode-QD is shown in Fig.4.12, evidencing the crucial importance of deterministic coupling in the experiment. More recently, another set of data has been extracted from similar yet cleaner samples and presents the same behaviour, as it can be seen in Fig.4.15 (a-f). Note that two types of materials have been used, namely, InAs/GaAs (III-V) and CdTe/ZnTe (II-VI) [101].

The fit procedure is based on a double-Lorentzian function, i.e., in a sum of two Lorentzians. However, as we have shown above, the spectrum is rather a product between the bare cavity, $S_{\mathrm{cav}}(\omega)$, and bare QD, $S_{\mathrm{QD}}(\omega)$, peaks, $S(\omega) = S_{\mathrm{cav}}(\omega) \times S_{\mathrm{QD}}(\omega)$. The QD contributes independently with the zero- and one-phonon lines, $S_{\mathrm{QD}}(\omega) = S_{ZPL}(\omega) + S_{1PL}(\omega)$. The 1PL contribution is usually considered much broader than the cavity. So, the cavity "filters" its own frequency, becoming predominant. On the other hand, the cavity is broader than the ZPL, so the ZPL "filters" the cavity and becomes predominant.

This reasoning yields the following approximation:

$$S_{\text{cav}}(\omega) \times S_{\text{QD}}(\omega) = S_{\text{cav}}(\omega) \times S_{\text{ZPL}}(\omega) + S_{\text{cav}}(\omega) \times S_{\text{1PL}}(\omega)$$

$$\approx S_{\text{ZPL}}(\omega) + S_{\text{cav}}(\omega). \tag{4.79}$$

This somehow justifies the common double-Lorentzian fitting. On the other hand, it displays the limitations of that procedure, evidencing that, if the cavity and the phonon wing have similar linewidths, deviations from the usual scenario should appear.
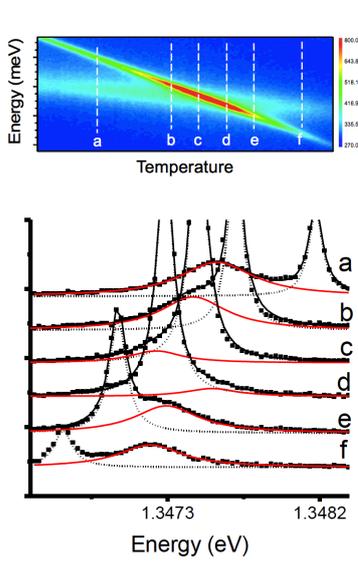
Figure 4.11: Top: Experimental Mode-QD spectra for varying detuning (temperature-tuning). Bottom: Double Lorentzian fit of the experimental data for representative cases a-f; the mode is in red (broad) and QD in black (narrow).
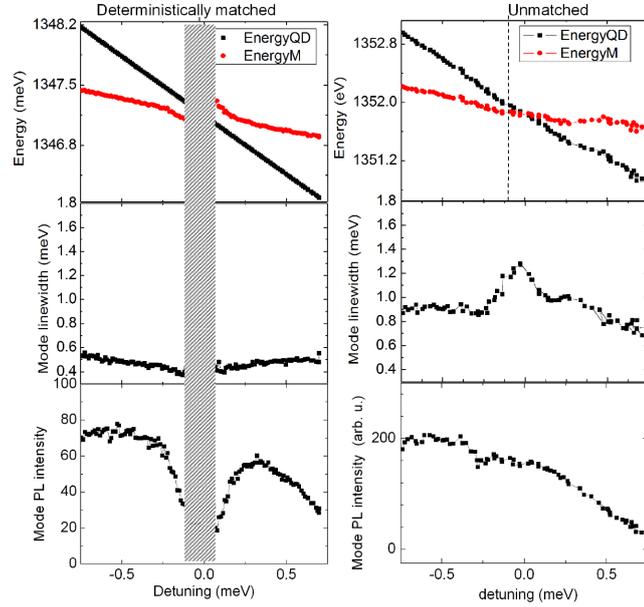
Figure 4.12: Left: Fitted results for a coupled mode-QD. The central energy of the mode is pushed from the ZPL around resonance. The cavity linewidth decreases when it approaches resonance. Intensity of emission also decreases. Right: unmatched mode-QD, showing the absence of those effects.

4.3.2 Theoretical analysis: "attractive phonon wings"

The problem described above is understood from the perspective of phonon wings in a rather intuitive manner. By feeding the cavity, the wings "attract" the mode towards its own frequency region. Consequently, the apparent center of the mode is shifted towards the maximum of the wing. The mode is also "stretched" or "squeezed" by the phonon wings, causing either apparent broadening when off-resonance and narrowing when close-to-resonance.

Fig.4.13 shows two contrasting situations: (a) close to resonance negative detuning, which experimentally represents the low-temperature regime (here, $T = 2$K) and (b) the off-resonant positive detuning, experimentally obtained for $T \sim 40$K. $S_{\mathrm{QD}}(\omega)$ is plotted in the dotted blue curve. The dashed red shows the bare-cavity spectrum $S_{\mathrm{cav}}(\omega)$. The dashed green curve represents the dressed mode obtained from a double-Lorentzian fit, as usually done experimentally. The mode pushing from the ZPL becomes clear as well as the narrowing effect. Figure 4.13 (b) shows mode attraction towards the phonon wings, as well as broadening. Fig. 4.14 shows the data from a recent experiment.
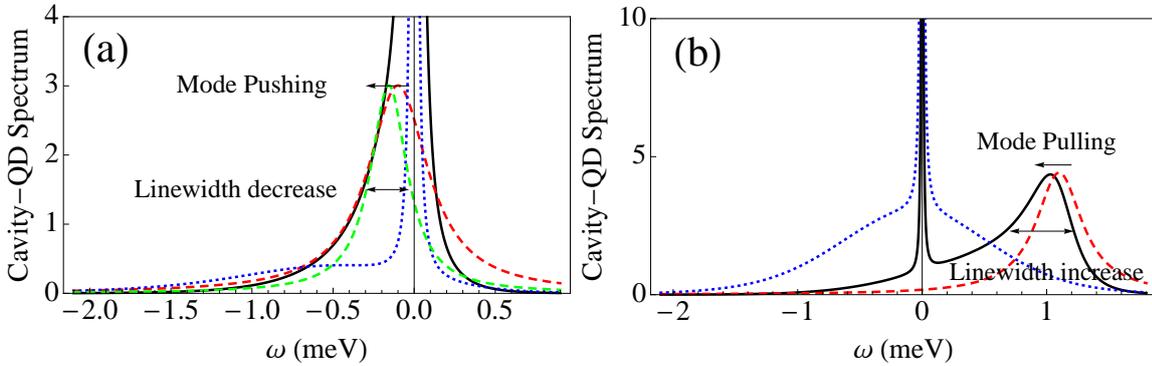
Figure 4.13: (a). Mode attracted by low-temperature phonon wing, close-to-resonance $\delta_c = -100\mu$eV, causing mode pushing from ZPL (red-shift) and linewidth narrowing. Solid black: $S(\omega)$. Dotted blue: $S_{\mathrm{QD}}(\omega)$ at $T = 2$K. Dashed red: $S_{\mathrm{cav}}(\omega)$. Dashed green: fitted cavity. (b) Mode attracted by moderate-temperature phonon wing, far-off-resonance $\delta_c = 1100\mu$eV, causing mode pulling by the ZPL (red-shift) and linewidth broadening. Solid black: $S(\omega)$. Dotted blue: $S_{\mathrm{QD}}(\omega)$ at $T = 37$K. Dashed red: $S_{\mathrm{cav}}(\omega)$.

Fig.4.15 presents a quantitative analysis of the double-Lorentzian fit from the theoretical curves, comparing to the fitting of the data from Fig.4.14. To be consistent with experiment, we assume a detuning-dependent temperature $T(\delta_c) = A\ \delta_c + B$. In the plots, we use $T(-200\mu eV) = 0K$ and $T(500\mu eV) = 20K$. Fig.4.15 (g) shows the central position of the fitted mode, plotted in blue, for a maximum phonon wing around $600\mu eV$ (large QD: $\sigma_e = 3nm$ and $\sigma_h = 1.5nm$). In black we plot a phonon wing put further apart, around $900\mu eV$ (small QD: $\sigma_e = 2nm$ and $\sigma_h = 1nm$). The red line is the bare mode frequency. Note the cavity hopping around resonance, of the order of $200\mu eV$. The difference between the blue and black curves simply comes from the relative position between the cavity and the maximum of the phonon wings. Fig.4.15 (h) shows the relative intensity, defined by the ratio between the integrated Lorentzian peak of the mode and the integrated sum of Lorentzians. The asymmetry evidences the role of phonons in the cavity feeding. In Fig.4.15 (i) the linewidth of the fitted cavity is shown to decrease up to $\kappa \sim 200\mu eV$, at $\delta_c = -100\mu eV$. At smaller absolute detunings, the mode peak is ill-defined. Higher positive detunings show larger effective linewidths, $\kappa = 600\mu eV$ at $\delta_c = 1100\mu eV$. The bare cavity quality factor is $Q = 3000$, i.e., $\kappa = 450\mu eV$.
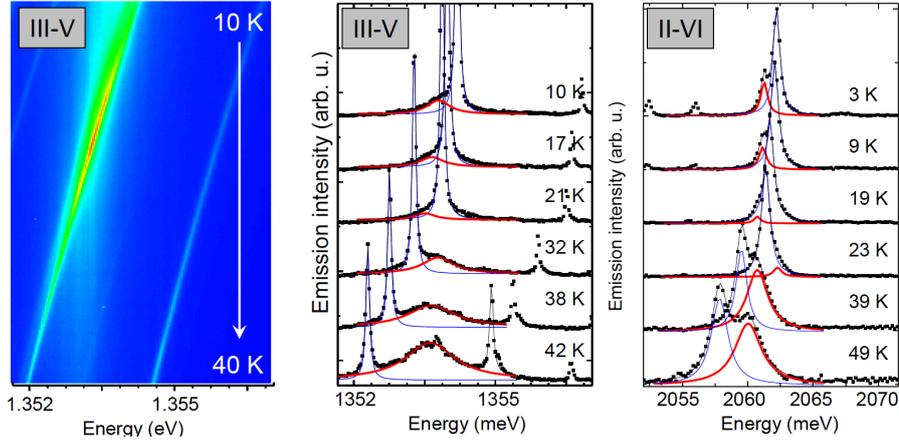

Figure 4.14: Spectra recently obtained from III-V (InGaAs) and II-VI (CdTeZn) samples [101].
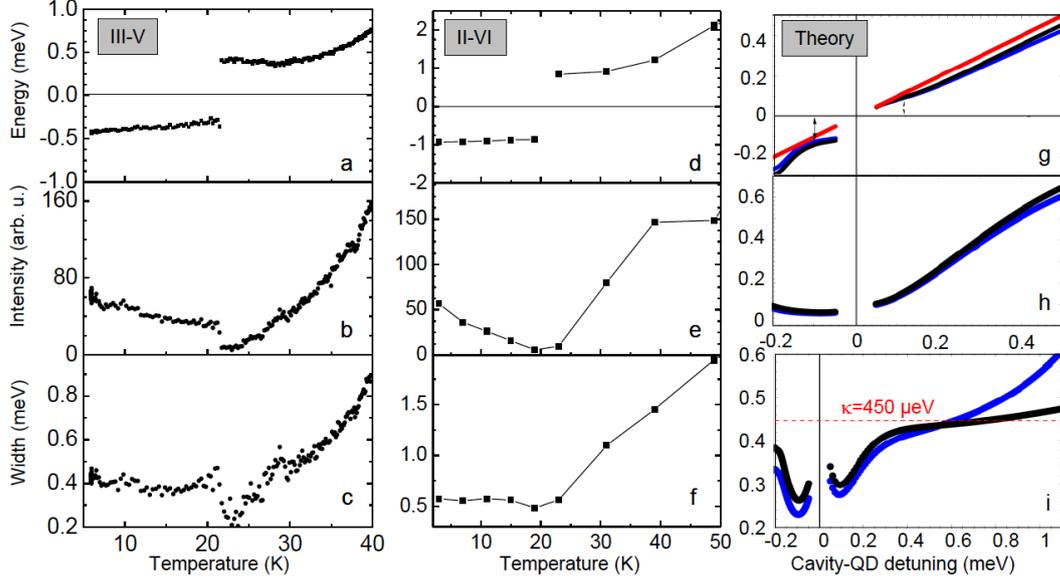
Figure 4.15: Double-Lorentzian fit of recent experimental results, showing respectively mode pushing (hopping) around resonance, asymmetric cavity feeding intensity and mode narrowing/broadening dependent on detuning (temperature). (a, b, c): InGaAs, (d, e, f): CdTeZn. (g, h, i): Double-Lorentzian fit of theoretical curves, qualitatively reproducing experimental features. Black: small QD ($\sigma_e = 2$nm, $\sigma_h = 1$nm); Blue: large QD ($\sigma_e = 3$nm, $\sigma_h = 1.5$nm).

4.4   Conclusions

In this chapter we have modeled the spontaneous emission of a quantum dot under the influence of phonons. We have developed a formalism to compute spectra based on a Fermi's golden rule approach. We have shown that our formalism describes well the emission both in free space and in a leaky cavity and that phonons allow far-off-resonance cavity feeding. We have also shown that this feeding mechanism modifies the apparent spectral properties of the cavity, leading to hopping and narrowing/broadening effects when passing through resonance with the quantum dot. These effects must be taken into account in photoluminescence experiments aiming at measuring optical mode properties.

Conclusions and perspectives

In the first part of this thesis we presented the one-dimensional atom. We have shown the dipole induced reflection that arises through destructive interference between incoming and emitted fields. We have also demonstrated the giant optical nonlinearity of 1D atoms, at the single-photon level. In the second part, we have evidenced signatures of stimulated emission at the single-photon level that arises through constructive interference between incoming and emitted fields. This is potentially observable with state-of-the-art solid-state atomic devices interacting with 1D light fields. In particular, we propose an experiment to probe the stimulated (optical) transition, based on the monitoring of an ancillary transition.

We have shown the influence of the incoming photon on the atom decay as a function of the packet shape. An irreversible and optimal stimulated emission occurs for the broadband mode-matching condition where the incoming photon is three times shorter than the spontaneously emitted one. We have also studied the influence of stimulation on the output field two-photon correlation function, which shows optimal photon bunching. Application of that effect to amplification has been discussed both in the classical and quantum cases.

By further exploring the optimal irreversible stimulation effect, we have presented a unique versatile device that can realize either universal optimal cloning or maximal entanglement in photon polarization. The choice depends only on the spectral shape of the incoming photon. For a highly monochromatic photon, a π-phase shift has been responsible for adiabatic transfer of population, redirecting the spontaneous atom-photon

entanglement to photon-photon entanglement. A realistic single-photon pulse shape has been considered, yielding maximal efficiencies on both processes.

In the last chapter we have modeled the spontaneous emission of a quantum dot under the influence of phonons. We have developed a formalism that describes well the role of phonons in far-off-resonance cavity feeding. We have also shown that this feeding mechanism distorts the apparent spectral properties of the cavity.

Our work suggests that 1D atoms are promising candidates for photodetectors, based on an avalanche of stimulated emission. This study starts at treating two atoms separated by a varying distance and initially excited. If by increasing the number of input excitations the transmission channel is correspondingly favored, then the effect would be of practical interest.

1D atoms have been studied as a resource for creation of correlated photons. It is of fundamental interest to understand the influence of correlated input two-photon packets on the transmission/reflection probabilities. In particular, it is an open question whether temporal correlation of photons affect stimulated emission of a single atom.

The role of phonons in the dynamics of a cavity-quantum dot system is still an open field of research. Modeling the solid-state induced dephasing during particular quantum information protocols is an important step towards practical applications of nanophotonic devices in future quantum technologies.

Bibliography

[1] L. Davidovich, *Sub-poissonian processes in quantum optics*, Rev. Mod. Phys. **68** 127 (1996);

[2] M. Planck, On an Improvement of Wien's Equation for the Spectrum, Verhandl. Dtsch. phys. Ges., 2, 202 (1900); M. Planck, *On the Theory of the Energy Distribution Law of the Normal Spectrum*, Verhandl. Dtsch. phys. Ges., 2, 237 (1900);

[3] A. Einstein, *On the present status of the radiation problem*, Phys. Z. 10, 185 (1909); A. Einstein, *On the development of our views concerning the nature and constitution of radiation*, Phys. Z. 10, 817 (1909);

[4] A. Einstein, *Zur Quantentheorie der Strahlung – On the quantum theory of radiation*, Phys. Z. **18**, 121 (1917);

[5] T. H. Maiman, *Stimulated Optical Radiation in Ruby*, Nature 187, 493 (1960);

[6] R. J. Glauber, *The Quantum Theory of Optical Coherence*, Phys. Rev. **130**, 2529 (1963);

[7] R. J. Glauber, *Coherent and Incoherent States of the Radiation Field*, Phys. Rev. **131**, 2766 (1963);

[8] R. J. Glauber, *Photon Correlations*, Phys. Rev. Lett. **10**, 84 (1963);

[9] E. C. G. Sudarshan, *Equivalence of Semiclassical and Quantum Mechanical Descriptions of Statistical Light Beams*, Phys. Rev. Lett. **10**, 277 (1963);

[10] L. Mandel, and E. Wolf, *Coherence Properties of Optical Fields*, Rev. Mod. Phys. **37**, 231 (1965).

[11] H. J. Carmichael, and D. Walls, *Proposal for the measurement of the resonant Stark effect by photon correlation techniques*, J. Phys. B 9, L43 (1976); H. J. Carmichael, and D. Walls, *A quantum-mechanical master equation treatment of the dynamical Stark effect*, J. Phys. B 9, 1199 (1976);

[12] Cohen-Tannoudji, C., 1977, in Frontiers in Laser Spectroscopy, Les Houches, Session XXVII (1975), edited by R. Balian, S. Haroche, and S. Liberman (North-Holland, Amsterdam), p.4;

[13] Kimble, H. J., and L. Mandel, *Theory of resonance fluorescence*, Phys. Rev. A 13, 2123 (1976);

[14] S. Haroche and J.-M. Raimond, *Exploring the quantum – Atoms, Cavities, and Photons*, 1st ed. (Oxford University Press, Oxford, 2006);

[15] E. M. Purcell, *Spontaneous emission probabilities at radio frequencies*, Phys. Rev. **69**, 681 (1946).

[16] A. L. Schawlow and C. H. Townes, *Infrared and Optical Masers*, Phys. Rev. 112, 1940â1949 (1958);

[17] A. Javan, *Possibility of Production of Negative Temperature in Gas Discharges*, Phys. Rev. Letters, 3, 87 (1959);

[18] J. H. Sanders, *Optical Maser Design*, Phys. Rev. Lett., 3, 86 (1959);

[19] H. Carmichael, *An Open System Approach to Quantum Optics*, 1st ed (Springer-Verlag, Berling, 2000);

[20] U. Weiss, *Quantum Dissipative Systems*, 2nd ed (World Scientific, Singapore, 2001);

[21] A. O. Caldeira, and A. J. Leggett, *Quantum tunnelling in a dissipative system*, Annals of Physics, 149, 374 (1983);

[22] A. O. Caldeira and A. J. Leggett, *Influence of damping on quantum interference: an exactly soluble model*, Phys. Rev. A 31, 1059 (1985);

[23] D. M. Valente and A. O. Caldeira, *Thermal equilibrium of two quantum Brownian particles*, Phys. Rev. A 81, 012117 (2010);

[24] E. Mascarenhas, B. Marques, D. Cavalcanti, M. T. Cunha, and M. F. Santos, *Protection of quantum information and optimal singlet conversion through higher-dimensional quantum systems and environment monitoring*, Phys. Rev. A 81, 032310 (2010);

[25] J. L. O'Brien, A. Furusawa and J. Vuckovic, *Photonic quantum technologies*, Nature Photonics, **3**, 687 (2009);

[26] A. Faraon, A. Majumdar, D. Englund, E. Kim, M. Bajcsy and J. Vuckovic, *Integrated quantum optical networks based on quantum dots and photonic crystals*, New J. Phys. 13, 055025 (2011);

[27] J.-M. Gérard, *Solid-State Cavity-Quantum Electrodynamics with Self-Assembled Quantum Dots*, Topics Appl. Phys. 90, 283 (2003), P. Michler (Ed.): Single Quantum Dots, (Springer-Verlag, Berlin, Heidelberg, 2003);

[28] A. J Shields, *Review: Semiconductor Quantum Light Sources*, Nature Photonics 1, 215 (2007);

[29] J. Kasprzak, S. Reitzenstein, E. A. Muljarov, C. Kistner, C. Schneider, M. Strauss, S. Höfling, A.Forchel and W.Langbein, *Up on the Jaynes-Cummings ladder of a quantum-dot/microcavity system*, Nature Mater. 9, 304 (2010);

[30] G. Ctistis, E. Yuce, A. Hartsuiker, J. Claudon, M. Bazin, J-M. Gérard, and W. L. Vos, *Ultimate fast optical switching of a planar microcavity in the telecom wavelength range*, Appl. Phys. Lett. 98, 161114 (2011);

[31] Research Highlights, Nature Photonics 5, 383 (2011);

[32] T. Shi, S. Fan, and C. P. Sun, *Two-photon transport in a waveguide coupled to a cavity in a two-level system*, Phys. Rev. A 84, 063803 (2011); T. Shi and C. P. Sun, *Lehmann-Symanzik-Zimmermann reduction approach to multiphoton scattering in coupled-resonator arrays*, Phys. Rev. B 79, 205111 (2009);

[33] J. Claudon, J. Bleuse, N. S. Malik, M. Bazin, P. Jaffrennou, N. Gregersen, C. Sauvan, P. Lalanne, and J.-M. Gérard, *A highly efficient single-photon source based on a quantum dot in a photonic nanowire*, Nature Photonics **4**, 174 (2010);

[34] News and Views, Nature Photonics 4, 132 (2010);

[35] M.Brune, F.Schmidt-Kaler, A.Maali, J.Dreyer, E.Hagley, J.M.Raimond and S.Haroche, *Quantum Rabi Oscillation: A direct test of Field Quantization in a cavity*, Phys.Rev.Lett **76**, 1800 (1996);

[36] R. J. Thompson, G. Rempe, and H. J. Kimble, *Observation of normal-mode splitting for an atom in an optical cavity*, Phys. Rev. Lett. **68**, 1132 (1992);

[37] Q. A. Turchette, R. J. Thompson, and H. J. Kimble, *One-dimensional atoms*, Appl. Phys. B **60**, S1 (1995);

[38] Q. A. Turchette, C. J. Hood, W. Lange, H. Mabuchi, and H. J. Kimble, *Measurement of Conditional Phase Shifts for Quantum Logic*, Phys. Rev. Lett. **75**, 4710 (1995);

[39] S. A. Aljunid, M. K. Tey, B. Chng, T. Liew, G. Maslennikov, V. Scarani, and C. Kurtsiefer, *Phase Shift of a Weak Coherent Beam Induced by a Single Atom*, Phys. Rev. Lett. **103**, 153601 (2009); M. Stobinska, G. Alber, and G. Leuchs, *Perfect*

excitation of a matter qubit by a single photon in free space, Europhys. Lett. **86**, 14007 (2009);

[40] G. Wrigge, I. Gerhardt, J. Hwang, G. Zumofen, and V. Sandoghdar, *Efficient coupling of photons to a single molecule and the observation of its resonance fluorescence*, Nat. Phys. **4**, 60 (2008); J. Hwang, M. Pototschnig, R. Lettow, G. Zumofen, A. Renn, S. Götzinger, and V. Sandoghdar, *A single-molecule optical transistor*, Nature (London) **460**, 76 (2009);

[41] D. Englund, A. Faraon, I. Fushman, N. Stoltz, P. Petroff and J. Vuckovic, *Controlling cavity reflectivity with a single quantum dot*, Nature **450**, 857 (2007);

[42] D. E. Chang, A. S. Sorensen, E A. Demler and M. D. Lukin, *A single-photon transistor using nanoscale surface plasmons*, Nat. Phys. **3** 807, (2007);

[43] R. J. Schoelkopf and S. M. Girvin, *Wiring up quantum systems*, Nature **451**, 664 (2008);

[44] O. Astafiev, A. M. Zagoskin, A. A. Abdumalikov Jr., Yu. A. Pashkin, T. Yamamoto, K. Inomata, Y. Nakamura, and J. S. Tsai, *Resonance Fluorescence of a Single Artificial Atom*, Science **327**, 840 (2010);

[45] A. Auffèves-Garnier, C. Simon, J.-M. Gérard, and J.-P. Poizat, *Giant optical nonlinearity induced by a single two-level system interacting with a cavity in the Purcell regime*, Phys. Rev. A **75**, 053823 (2007);

[46] K. Kojima, H. F. Hofmann, S. Takeuchi, and K. Sasaki, *Efficiencies for the single-mode operation of a quantum optical nonlinear shift gate*, Phys. Rev. A **70**, 013810 (2004);

[47] H. F. Hofmann, K. Kojima, S. Takeuchi, and K. Sasaki, *Optimized phase switching using a single atom nonlinearity*, J. Opt. B: Quantum Semiclassical Opt. **5**, 218 (2003);

[48] P. Domokos, P. Horak, and H. Ritsch, *Quantum description of light-pulse scattering on a single atom in waveguides*, Phys. Rev. A **65**, 033832 (2002);

[49] C. Cohen-Tannoudji, J. Dupont-Roc, and G. Grynberg, *Atom-Photon Interactions: Basic Processes and Applications*, 2nd ed. (Wiley, New York, 2004);

[50] B. R. Mollow, *Pure-state analysis of resonant light scattering: Radiative damping, saturation, and multiphoton effects*, Phys. Rev. **12**, 1919 (1975);

[51] R. Hanbury-Brown and R. W. Twiss, *Correlation between photons in two coherent beams of light*, Nature **177**, 27 (1956);

[52] H. Zheng, D. J. Gauthier, and H. U. Baranger, *Waveguide QED: Many-body bound-state effects in coherent and Fock-state scattering from a two-level system*, Phys. Rev. A **82**, 063816 (2010);

[53] A. E. Siegman, *Lasers* (University Science Books, Mill Valley, CA, 1986); B. E. A. Saleh and M. C. Teich, *Fundamentals of Photonics* (Wiley, New York, 1991), Vol. 5;

[54] B. R. Mollow, *Stimulated Emission and Absorption near Resonance for Driven Systems*, Phys. Rev. A **5**, 2217 (1972);

[55] D. Valente, S. Portolan, G. Nogues, J.-P. Poizat, M. Richard, J.-M. Gérard, M. F. Santos, and A. Auffèves, *Monitoring stimulated emission at the single-photon level in one-dimensional atoms*, Phys. Rev. A, **85**, 023811 (2012);

[56] A. Auffèves, J. M. Gérard, and J. P. Poizat, *Pure emitter dephasing: a resource for advanced solid-state single-photon sources*, Phys. Rev. A **79**, 053838 (2009);

[57] A. Dousse, J. Suffczyński, A. Beveratos, O. Krebs, A. Lemaître, I. Sagnes, J. Bloch, P. Voisin and P. Senellart, *Ultrabright source of entangled photon pairs*, Nature **466**, 217 (2010);

[58] M. Brune, J. M. Raimond, and S. Haroche, *Theory of the Rydberg-atom two-photon micromaser*, Phys. Rev. A **35**, 154 (1987); E. del Valle, S. Zippilli, F. P. Laussy, A. Gonzalez-Tudela, G. Morigi, and C. Tejedor, *Two-photon lasing by a single quantum dot in a high-Q microcavity*, Phys. Rev. B **81**, 035302 (2010);

[59] S. H. Autler and C. H. Townes, *Stark Effect in Rapidly Varying Fields*, Phys. Rev. **100**, 703 (1955);

[60] K. Brunner, G. Abstreiter, G. Bohm, G. Trankle, and G. Weimann *Sharp-Line Photoluminescence and Two-Photon Absorption of Zero-Dimensional Biexcitons in a GaAs/AlGaAs Structure*, Phys. Rev. Lett. **73**, 1138 (1994); M. Winger, T. Volz, G. Tarel, S. Portolan, A. Badolato, K. J. Hennessy, E. L. Hu, A. Beveratos, J. Finley, V. Savona, and A. Imamoglu, *Explanation of Photon Correlations in the Far-Off-Resonance Optical Emission from a Quantum-Dot-Cavity System*, ibid. **103**, 207403 (2009);

[61] T. Flissikowski, A. Betke, I. A. Akimov, and F. Henneberger, *Two-Photon Coherent Control of a Single Quantum Dot*, Phys. Rev. Lett. **92**, 227401 (2004);

[62] A. R. R. Carvalho and M. F. Santos, *Distant entanglement protected through artificially increased local temperature*, New J. Phys. **13**, 013010 (2011).

[63] D. Englund, A. Faraon, I. Fushman, N. Stoltz, P. Petroff and J. Vuckovic, *Controlling cavity reflectivity with a single quantum dot*, Nature **450**, 857 (2007);

[64] K. Kojima, H. F. Hofmann, S. Takeuchi, and K. Sasaki, *Nonlinear interaction of two photons with a one-dimensional atom: spatiotemporal quantum coherence in the emitted field*, Phys. Rev. A **70**, 013810 (2004);

[65] I. Friedler, P. Lalanne, J. P. Hugonin, J. Claudon, J. M. Gérard, A. Beveratos, and I. Robert-Philip, *Efficient photonic mirrors for semiconductor nanowires*, Opt Lett 33, 2635 (2008);

[66] D. Witthaut and A. S. Sorensen, *Photon scattering by a three-level emitter in a one-dimensional waveguide*, New J. Phys. **12**, 043052 (2010);

[67] M. O. Scully and M. S. Zubairy, *Quantum Optics*, 2nd ed. (Cambridge University Press, Cambridge, 2001); V. Weisskopf and E. Wigner, *Berechnung der natürlichen Linienbreite auf Grund der Diracschen Lichttheorie*, Z. Phys. **63**, 54 (1930);

[68] J. T. Shen and S. Fan, *Coherent photon transport from spontaneous emission in one-dimensional waveguides*, Opt. Express **30**, 2001 (2005);

[69] D. Valente, Y. Li, J. P. Poizat, J. M. Gérard, L. C. Kwek, M. F. Santos, and A. Auffèves, *Optimal irreversible stimulated emission*, New J. Phys. **14**, 083029 (2012);

[70] E. Rephaeli and S. Fan, *Stimulated emission from a single excited atom in a waveguide*, Phys. Rev. Lett. **108**, 143602 (2012);

[71] D. Valente, Y. Li, J. P. Poizat, J. M. Gérard, L. C. Kwek, M. F. Santos, and A. Auffèves, *Universal optimal broadband photon cloning and entanglement creation in one-dimensional atoms*, Phys. Rev. A **86**, 022333 (2012);

[72] J. Hwang, M. Pototschnig, R. Lettow, G. Zumofen, A. Renn, S. Gotzinger and V. Sandoghdar *A single-molecule optical transistor*, Nature **460**, 76 (2009);

[73] D. Bruss, A. Ekert, and C. Macchiavello, *Optimal universal quantum cloning and state estimation*, Phys. Rev. Lett. **81**, 2598 (1998);

[74] W. K. Wootters and W. H. Zurek, A single quantum cannot be cloned, Nature (London) **299**, 802 (1982);

[75] V. Scarani, S. Iblisdir, N. Gisin, and A. Acín, *Quantum cloning*, Rev. Mod. Phys. **77**, 1225 (2005);

[76] N. Gisin, *Quantum cloning without signaling*, Phys. Lett. A 242, 1 (1998);

[77] V. Vedral, M. B. Plenio, M. A. Rippin, and P. L. Knight, *Quantifying entanglement*, Phys. Rev. Lett. **78**, 2275 (1997); L. Amico, R. Fazio, A. Osterloh, and V. Vedral, *Entanglement in many-body systems*, Rev. Mod. Phys. **80**, 517 (2008);

[78] V. Buzek and M. Hillery, *Quantum copying: beyond the no-cloning theorem*, Phys. Rev. A **54**, 1844 (1996);

[79] N. Gisin and S. Massar, *Optimal quantum cloning machines*, Phys. Rev. Lett. **79** 2153;

[80] P.W. Milonni and M. L. Hardies, Photons cannot always be replicated, Phys. Lett. 92A, 321 (1982);

[81] C. Simon, G. Weihs, and A. Zeilinger, *Optimal quantum cloning via stimulated emission*, Phys. Rev. Lett. **84**, 2993 (2000);

[82] A. Lamas-Linares, C. Simon, J. C. Howell, D. Bouwmeester, *Experimental quantum cloning of single photons*, Science **296**, 712 (2002);

[83] E. Viasnoff-Schwoob, C. Weisbuch, H. Benisty, S. Olivier, S. Varoutsis, I. Robert-Philip, R. Houdré, and C. J. M. Smith, *Spontaneous emission enhancement of quantum dots in a photonic crystal wire*, Phys. Rev. Lett. **95**, 183901 (2005); T. Lund-Hansen, S. Stobbe, B. Julsgaard, H. Thyrrestrup, T. Sünner, M. Kamp, A. Forchel, and P. Lodahl, *Experimental realization of highly efficient broadband coupling of single quantum dots to a photonic crystal waveguide*, Phys. Rev. Lett. **101**, 113903 (2008);

[84] A. A. Abdumalikov Jr., O. Astafiev, A. M. Zagoskin, Yu. A. Pashkin, Y.Nakamura, and J. S.Tsai, *Electromagnetically induced transparency on a single artificial atom*, Phys. Rev. Lett. **104**, 193601 (2010);

[85] W. Langbein, P. Borri, U. Woggon, V. Stavarache, D. Reuter, and A. D. Wieck, *Radiatively limited dephasing in InAs quantum dots*, Phys. Rev. B **70**, 033301 (2004);

[86] *Handbook of Self Assembled Semiconductor Nanostructures for Novel Devices in Photonics and Electronics*, edited by M. Henini (Elsevier, New York, 2008);

[87] J. P. Reithmaier, G. Sek, A. Löffler, C. Hofmann, S. Kuhn, S. Reitzenstein, L. V. Keldysh, V. D. Kulakovskii, T. L. Reinecke and A. Forchel, *Strong coupling in a single quantum dot-semiconductor microcavity system* Nature **432**, 197 (2004);

[88] A. Dousse, L. Lanco, J. Suffczynski, E. Semenova, A. Miard, A. Lemaître, I. Sagnes, C. Roblin, J. Bloch, and P. Senellart, *Controlled Light-Matter Coupling for a Single Quantum Dot Embedded in a Pillar Microcavity Using Far-Field Optical Lithography*, Phys. Rev. Lett. **101**, 267404 (2008);

[89] K. Hennessy, A. Badolato, M. Winger, D. Gerace, M. Atatüre, S. Gulde, S. Fält, E. L. Hu and A. Imamoglu, *Quantum nature of a strongly coupled single quantum dot-cavity system*, Nature **445**, 896 (2007);

[90] A. Auffèves, J.-M. Gérard, and J.-P. Poizat, *Pure emitter dephasing: A resource for advanced solid-state single-photon sources*, Phys. Rev. A **79**, 053838 (2009);

[91] C. Kittel, *Quantum Theory of Solids* (John Wiley & sons, New York, 1963);

[92] G. D. Mahan, *Many-Particle Physics* (Plenum, New York, 1990);

[93] L. Besombes, K. Kheng, L. Marsal and H. Mariette, *Acoustic phonon broadening mechanism in single quantum dot emission*, Phys. Rev. B **63**, 155307 (2001);

[94] K. Huang and A. Rhys, *Theory of Light Absorption and Non-Radiative Transitions in F-Centres*, Proc. R. Soc. Lond. A, **204**, 406 (1950);

[95] E. Peter, J. Hours, P. Senellart, A. Vasanelli, A. Cavanna, J. Bloch, and J. M. Gérard, *Phonon sidebands in exciton and biexciton emission from single GaAs quantum dots*, Phys. Rev. B **69**, 041307(R) (2004);

[96] O. Verzelen, *Interaction électron-phonon LO dans les boîtes quantiques d'InAs/GaAs*, PhD thesis - Université de Paris VI, ENS (2002).

[97] S. Ates, S. M. Ulrich, A. Ulhaq, S. Reitzenstein, A. Löffler, S. Höfling, A. Forchel and P. Michler, *Non-resonant dot-cavity coupling and its potential for resonant single-quantum-dot spectroscopy*, Nature Photonics **215**, 1 (2009);

[98] S. Hughes, P. Yao, F. Milde, A. Knorr, D. Dalacu, K. Mnaymneh, V. Sazonova, P. J. Poole, G. C. Aers, J. Lapointe, R. Cheriton, and R. L. Williams, *Influence of electron-acoustic phonon scattering on off-resonant cavity feeding within a strongly coupled quantum-dot cavity system*, Phys. Rev. B **83**, 165313 (2011);

[99] I. Wilson-Rae and A. Imamoglu, *Quantum dot cavity-QED in the presence of strong electron-phonon interactions*, Phys. Rev. B **65**, 235311 (2002);

[100] U. Hohenester, *Cavity quantum electrodynamics with semiconductor quantum dots: Role of phonon-assisted cavity feeding*, Phys. Rev. B **81**, 155303 (2010);

[101] D. Valente, J. Suffczynskii, T. Jakubczyk, A. Dousse, A. Lemaitre, I. Sagnes, W. Pacuski, C. Kruse, D. Hommel, L. Lanco, J. Bloch, P. Kossacki, A. Auffèves and P. Senellart, *Distortion of cavity mode in the emission of coupled quantum dot-cavity devices*, submitted.

[102] T. Tawara, H. Kamada, T. Tanabe, T. Sogawa, H. Okamoto, P. Yao, P. K. Pathak, and S. Hughes, *Cavity-QED assisted attraction between a cavity mode and an exciton mode in a planar photonic-crystal cavity*, Opt. Express **18**, 2719 (2010);